ABSTRACT

PEARCE, RYAN CHRISTOPHER. DC Plasma Synthesis of Carbon Nanofibers for Biointerfacing. (Under the direction of Anatoli Melechko).

Vertically aligned carbon nanofibers (VACNFs) are a class of materials whose nanoscale dimensions and physical properties makes them uniquely suitable as functional elements in many applications for biodetection and biointerfacing on a cellular level. Control of VACNF synthesis by catalytic plasma enhanced chemical vapor deposition (PECVD) presents many challenges in integration into devices and structures designed for biointerfacing, such as transparent or flexible substrates. This dissertation addresses ways to overcome many of these issues in addition to deepening the fundamental understanding of nano-synthesis in catalytic PECVD.

First, a survey of the field of VACNF synthesis and biointerfacing is presented, identifying the present challenges and greatest experimental applications. It is followed by experimental observations that elucidate the underlying mechanism to fiber alignment during synthesis, a critical step for deterministic control of fiber growth. Using a grid of electrodes patterned by photolithography on an insulating substrate, it was found that the alignment of the fibers is controlled by the anisotropic etching provided by ions during dc-PECVD synthesis. The VACNFs that have been utilized for many cellular interfacing experiments have unique mechanical and fluorescent properties due to a SiNx coating. The mechanism for SiN_x deposition to VACNF sidewalls during synthesis is explored in addition to a detailed study of the optical properties of the coating. To explain the optical properties of this coating it is proposed that the source of photoluminescence for the SiN_x coated VACNFs is quantum confinement effects due to the presence of silicon nanoclusters embedded in a Si_3N_4 matrix.

These luminescent fibers have proven useful as registry markers in cell impalefection studies. To realize VACNF arrays used as an inflatable angioplasty balloon with embedded fibers to deliver drugs across the blood-brain barrier, a method for transferring fibers to flexible polydimethylesiloxane (PDMS) is presented. A process has been developed that involves synthesizing fibers on aluminum, followed by spin coating a thin layer of PDMS and then dissolving the underlying aluminum with KOH. Finally, a method of fiber synthesis using just air and acetone as the process gases is presented, enabling the possibility of in-atmosphere, large scale VACNF synthesis.

It is envisioned that these advancements should assist the viability of large scale VACNF related technologies and will help to bridge the gap between experimental applications and industrial adoption.

DC Plasma Synthesis of Vertically Aligned Carbon Nanofibers for Biointerfacing

by
Ryan Christopher Pearce

A dissertation submitted to the Graduate Faculty of
North Carolina State University
in partial fulfillment of the
requirements for the degree of
Doctor of Philosophy

Material Science and Engineering

Raleigh, North Carolina

2013

APPROVED BY:

_____	_____
Dr. Anatoli Melechko Committee Chair	Dr. Joseph Tracy
_____	_____
Dr. Yaroslava Yingling	Dr. Nagiza Samatova

Dedication

I dedicate this work to the future that I am striving for.

Biography

Ryan Christopher Pearce was born in Oak Ridge, Tennessee on November 14, 1987. His parents were both involved with Oak Ridge National Laboratories and got him involved with science and technology from a very early age. He attended Woodland Elementary School, Jefferson Middle School, and Oak Ridge High School. During high school he participated heavily in orchestra, where he played the viola, tennis, and chess. He attended University of Tennessee, Knoxville, starting in 2006 where he studied materials science and engineering. He interned with Oak Ridge National Laboratory at the Center for Nanophase Materials Science under Dr. Anatoli Melechko the summer after his freshman year. After that summer, he continued working at the CNMS on a part time basis during the school year and full time during breaks. While he was there, he performed research on vertically aligned carbon nanofibers in addition to a variety of user projects. After his junior year, Dr. Melechko moved to North Carolina to be a professor at North Carolina State University. Ryan graduated in 2010 and began his graduate studies that fall under his former advisor, Dr. Melechko. While at NCSU, Ryan studied for a Ph.D. in materials science and engineering, performing research on the synthesis and bioapplications of vertically aligned carbon nanofibers. His hobbies include video games, reading, tennis, beer, electronic music, anime, film, body building, Reddit, cats, board games, and politics.

Acknowledgments

I would like to acknowledge everyone who made my graduate life bearable and not completely devoid of social interaction. I especially want to thank my advisor, Tolik, for being such a great counselor, friend, and overall positive influence. My family is marvelous and supportive as well for which I thank them, especially Mom for always providing advice when it was needed, whether or not I asked for it. My warmest regards go out to my collaborators, coworkers, and sponsors including: Dr. Samatova, Dale Hensley, Dr. Tracy, Dr. Simpson, Dr. Yingling, Alex Vasenkov, Mehmet, and Bryan. I am also very appreciative of all my lab mates and RB1 friends: Marc, Lindsay, Tony, Milena, Christer, Zach, Isaac, Justin, and Wei. We had a pretty good time for the most part, didn't we? I am most thankful to Jessica, who has always been there for me, and without whom these last few years would have been utterly unbearable. I love you. Finally, thanks to my committee who have been wonderful, helpful, and very attractive.

Table of Contents

List of Tables

List of Figures

Chapter 1 - Introduction

1.1 Aim of Dissertation

The aim of this thesis is to provide clear insight into the role of DC plasma in the synthesis of vertically aligned carbon nanofibers (VACNFs) for biointerfacing applications. First, a survey of the state of the technology has been carried out to identify the main challenges in synthesis and integration of VACNFs into devices as well as the most impactful experimental research directions. These surveys are presented in **Chapter 2** and **Chapter 3**. The main research focuses that have been pursued in this dissertation fill several gaps in the current understanding of how the fibers are synthesized and integrated into devices.

The first topic is the lack of an alignment mechanism for freestanding VACNFs that fit all of the experimental data. We noticed that the impact of edge effects on the alignment of VACNFs varied as a function of pressure as well as a function of distance from a patterned electrode. This data, presented in **Chapter 4**, led us to the conclusion that anisotropic etching from the ionic flux is the underlying mechanism for fiber alignment. Our new understanding of this phenomenon allowed us for the first time to synthesize VACNFs on a transparent, insulating substrate with DC plasma enhanced chemical vapor deposition (PECVD). The ability to synthesize VACNFs on transparent substrates is critical for cellular imaging with differential contrast microscopy. Using the ability to synthesize fibers on optically transparent substrates, we demonstrated differential contrast microscopy of human osteosarcoma cells cultured on a VACNF array that was synthesized on fused silica.

It has been known for a decade that during synthesis of VACNFs at certain regimes a SiN_x coating will form in-situ on the sidewalls of the fibers, depending on the synthesis parameters. It was thought this coating enhanced the mechanical properties of the fibers; however, there was no speculation into the mechanism of deposition or study of the coating's optical properties. **Chapter 5** provides insight into both the deposition mechanism and the optical properties of the SiN_x coating. We notice a strong photoluminescent response from SiN_x coated fiber that is similar to the response from a SiN_x thin film deposited using PECVD. A deposition mechanism is proposed, combining aspects of both sputter deposition and CVD-like deposition. Furthermore, strong evidence for the presence of silicon nanoclusters embedded in the SiN_x matrix is presented, suggesting that a portion of the luminescence is due to quantum confinement effects from the nanoclusters. The usefulness of these luminescent fibers is then demonstrated as registry markers in fluorescent microscopy of cellular mitosis, showing no signs of loss of luminescence, also known as photo bleaching.

One large obstacle for VACNF device integration is the ability to transfer the fibers to a substrate different from the one they've been synthesized. Additionally, the capability to have fibers on a flexible, stretching substrate has not previously existed. In **Chapter 6**, we present a technique to transfer fibers from an aluminum substrate to polydimethylsiloxane (PDMS), which is highly flexible and biocompatible. This feat was achieved by growing fibers on aluminum that had Si microparticles dropcast onto it to be redposited onto the sidewalls of the VACNFs as discussed in **Chapter 5.** After fiber synthesis, a thin PDMS

layer was deposited by spinning, leaving the fibers above film. The aluminum was then selectively etched away using KOH, leaving a flexible membrane with vertical fibers sticking out. These embedded fibers were successfully used to transfect cells. This work represents the first step towards inflatable angioplasty balloons with the capability to pierce the blood-brain barrier to deliver drugs or genes.

Finally, a large challenge facing adoption of many nanostructures is the difficulty and expense of large scale synthesis. We feel that our efforts have made the first strides towards alleviating this issue with VACNF synthesis. We detail in **Chapter 7** a method by which fibers are grown using only acetone and air as the process gases; considerably cheaper and less harmful than the traditional acetylene and ammonia. This advance opens the possibility of large scale in-atmosphere synthesis of VACNFs, a critical requirement for large surface area VACNF coatings.

1.2 Vertically Aligned Carbon Nanofibers

1.2.1 Definition

Vertically aligned carbon nanofibers are a unique allotrope of carbon that is similar yet distinct from multi-walled and single-walled carbon nanotubes (MWCNT and SWCNT respectively). A single graphene layer is composed of a hexagonal network of covalently bonded carbon atoms. VACNFs are composed of stacked, curved graphene "cones" or "cups" as opposed to the hollow cylinders of a MWCNT which are composed of a single graphene sheet with the ends brought together.[1] **Figure 1.1** shows a schematic as well as a

high resolution transmission electron microscopy (HRTEM) image of a VACNF. **Figure 1.2** shows schematic as well as HRTEM images of MWCNTs. In literature, VACNFs are frequently misreported as CNTs or MWCNTs but are in fact separate entities with entirely different structures, properties, and synthesis mechanisms which will be discussed in more detail in the following sections. The reason for this conflation is unclear, though some have speculated it may be due to greater name recognition of carbon nanotubes.[2] For the purposes of this thesis, carbon nanotubes and multi-walled carbon nanotubes will only be used for structures that are cylindrical and therefore hollow, whereas vertically aligned carbon nanofibers will refer to any carbon nanostructure that has the aforementioned graphitic cups or cones.

1.2.2 Synthesis

VACNFs are synthesized by catalytic plasma-enhanced chemical vapor deposition (c-PECVD). Synthesis is composed of four basic steps: substrate and catalyst selection, substrate patterning/preparation, fiber growth, and post-processing/device integration. There are many excellent articles covering each of these steps in great detail, but the basics will be reviewed here.[2, 3, 4] Silicon is most commonly used as the substrate for VACNF synthesis, and it does not seem to make a difference whether or not it is p-type or n-type silicon. The most frequently used catalysts, in order of increasing rareness, are nickel, iron, and cobalt. Nickel is by far the most used catalyst for VACNF growth due to its high carbon solubility at moderate temperatures.[5] VACNFs grown from nickel catalysts result in herringbone-type fibers, as shown in **Figure 1.1b**. Iron and cobalt catalyst yield fibers with bamboo-type

structures like those shown in **Figure 1.3**. The exact mechanism for the difference in fiber structure between these catalysts remains unclear, though it could be due to crystal orientation of the catalyst particle or carbon solubility/mobility in the catalyst.[2, 6]

After substrate and catalyst selection, the catalyst must be placed onto the substrate. A thin film of catalyst can be deposited onto the substrate using techniques such as electron beam evaporation or magnetron sputtering. Alternatively, lithography can be used to create an array of catalyst dots which will result in patterned arrays of sparse VACNFs which are frequently used in cellular transfection studies.[7, 8, 9, 10, 11] The size of the catalyst dot strongly influences the final fiber. Larger dots result in multiple fibers from a single dot, while smaller dots yield fewer fibers. At a sufficiently small dot size (~500nm diameter) a singular fiber can be obtained from a single dot.[2]

Synthesis is performed by plasma enhanced chemical vapor deposition (PECVD). Though many power sources have been used for PECVD synthesis of VACNFs, direct current (dc) PECVD is the simplest and most common for VACNFs. The operating principle of dc-PECVD is that process gases introduced into the chamber will decompose into ions, electrons, neutrals, and excited species that become re-deposited onto the substrate. The plasma is maintained by the induced bias accelerating ions towards the cathode, colliding with neutrals and the substrate to produce secondary electrons which further collide with species in the gas phase. Growth is carried out at elevated temperature (typically around 700°C) to ease plasma initiation and to dewet the catalyst film or dot. VACNF synthesis requires two process gases: an etchant and a carbon source. The gases most commonly used

are acetylene (C_2H_2) and ammonia (NH_3). During growth, the acetylene decomposes over the metal catalyst particle. The decomposed carbon then diffuses through the catalyst particle or along the particle step edges to become incorporated into the growing graphitic structure. The processes occurring at the nanoparticle surface are shown in **Figure 1.4**. Should a carbon film completely cover the catalyst nanoparticle, growth is terminated. To prevent the covering of the particle, the ratio of process gases has to be controlled to ensure a sufficient etching rate of carbon build-up. By controlling the C_2H_2/NH_3 ratio (R) the growth can be moved towards a carbon deposition regime or an etching regime. The effect of R on growth rate is depicted in **Figure 1.5**. Etching rate can also be controlled by the current, with increasing current moving more towards etching regimes. In fact, current can be used to compensate for R, meaning a high R can be moved away from the deposition regime by increasing current. Pressure is another key variable of fiber growth, with higher pressures resulting monotonically in greater growth rates; however plasma cannot be maintained in most dc-PECVD systems with pressure greater than 20 or 30 Torr. The final controllable parameter is temperature. For nickel, growth is rate limited up to 700°C, meaning the energy provided by the temperature directly increases the rate of incorporation of carbon atoms into the graphitic cones. Above 700°C however, the sticking coefficient of carbon on nickel is reduced, so the growth rate actually decreases.[3] By controlling these parameters, the growth of fibers is nearly entirely deterministic; meaning complete control of the final products is possible.

After fibers are synthesized, there are a number of post-processing steps that can be undertaken to incorporate the fibers into a device or change their function. The most common post-processing step for VACNFs is chemical functionalization, where some target chemical is affixed to the VACNF. Functionalization can be achieved a number of ways, using a variety of chemistries. One of the most common is to coat the VACNFs with a thin gold film via electron beam deposition and then use alkane-thiol chemistry to attach the desired molecule.[12] Functionalization will be covered more in depth later in this thesis. As has already been mentioned, fibers can also be coated with metal layers using standard deposition techniques such as magnetron sputtering and e-beam evaporation. Insulating coatings can be formed as well, such as Si_3N_4 using PECVD as a post-processing technique. The VACNFs can then serve as a sacrificial template for "nano-pipes" after a wet chemical etch to remove the nanoparticle followed by an oxygen plasma etch to remove the carbon structure, leaving behind the Si_3N_4 walls.[13] A wide variety of techniques are available to post-process fibers, a matter which will be discussed more later, but which also includes transfer of fibers to a different substrate, functionalization, coating, etching, and deposition of polymeric material by spinning.

1.2.3 Applications

Vertically aligned carbon nanofibers have properties which lend themselves extremely well to a wide variety of potential applications. Primarily, they have very high aspect ratios coupled with good mechanical properties that allow them to undergo a great deal of compressive stress. Therefore, they are frequently used as scanning probe tips and

gene/drug delivery arrays.[14] Their mechanical strength coupled with their conductivity has also enabled them to be used as neuronal interfaces, where hippocampal slices have been pressed onto the fibers repeatedly without the fibers being damaged.[9, 15, 16] In these studies, arrays of VACNFs were able to both record and stimulate electrophysiological signals from brain tissue. The ability to deterministically synthesize VACNFs has allowed for nanofluidic structures to be created, making "zoo pens" from walls of fibers.[17, 18] Much more of VACNFs varied applications will be discussed in further detail later.

1.3 History of Vertically Aligned Carbon Nanofibers

Carbon nanostructures have become subject to an immense amount of research after the discovery and observation of a new allotrope of carbon, buckminster fullerene or C_{60}, by Kroto *et al.* in 1985.[19] Iijima *et al.* followed this observation with the discovery that carbon nanotubes (CNTs) could be formed through arc discharge synthesis of C_{60} and other fullerenes.[20] These nanotubes had amazing electrical, mechanical, and optical properties and were heralded as the material of the future. In the 1990's pioneering work of catalytic plasma enhanced chemical vapor deposition (C-PECVD) allowed for increased determinism in the synthesis of carbon nanostructures. It was noted that carbon fibers grew alongside CNTs using these methods, the two being differentiated by carbon fibers having a grain size that is small compared to its circumference and the perfect single crystalline structure of CNTs.[21, 22] In 1997 Chen et al. used C-PECVD to grow aligned carbon nanofibers, work which was further supplemented by a study performed by Ren *et al.* in 1998 which suggested that the growth mechanism of fibers was different from that of carbon nanotubes.[23, 24] Then,

in 1999 Ren *et al.* developed a C-PECVD process that allowed growth of individual free standing vertically aligned carbon nanofibers, which sidestepped all the laborious post-synthesis processing required to create devices from carbon nanotube or nanofibers bundles.[25] The work done by Ren *et al.* serves as the basis for all modern research into vertically aligned carbon nanofibers.

Over the years there have been several influential groups in the field of VACNFs. Dr. Zhifeng Ren's group started at SUNY at Buffalo and is currently located at Boston College. Dr. Bill Milne's group at Cambridge in the UK has had a splinter group form under former graduate student Dr. Manish Chhowalla at Rutgers University. Dr. Meyya Meyyappan leads a group at NASA Ames center. Dr. Kostya Ostrikov leads efforts at CSIRO in Australia. A large and very good looking group has also been active at Oak Ridge National Labs in Tennessee under Dr. Michael L. Simpson, Dr. Anatoli Melechko, and Dr. Vladimir Merkulov. Dr. Melechko has since formed his own group at NCSU in North Carolina.

1.4 References

(1) Merkulov, V. I.; Hensley, D. K.; Melechko, A. V.; Guillorn, M. A.; Lowndes, D. H.; Simpson, M. L. *Journal of Physical Chemistry B* **2002,** *106,* 10570-10577.

(2) Melechko, A. V.; Merkulov, V. I.; McKnight, T. E.; Guillorn, M. A.; Klein, K. L.; Lowndes, D. H.; Simpson, M. L. *Journal of Applied Physics* **2005,** *97,* Artn 041301.

(3) Chhowalla, M.; Teo, K. B. K.; Ducati, C.; Rupesinghe, N. L.; Amaratunga, G. A. J.; Ferrari, A. C.; Roy, D.; Robertson, J.; Milne, W. I. *Journal of Applied Physics* **2001,** *90,* 5308-5317.

(4) Meyyappan, M.; Delzeit, L.; Cassell, A.; Hash, D. *Plasma Sources Science & Technology* **2003,** *12,* 205-216.

(5) Lander, J.; Kern, H.; Beach, A. *Journal of Applied Physics* **1952,** *23,* 1305-1309.

(6) Melechko, A. V.; Klein, K. L.; Fowlkes, J. D.; Hensley, D. K.; Merkulov, I. A.; McKnight, T. E.; Rack, P. D.; Horton, J. A.; Simpson, M. L. *Journal of Applied Physics* **2007,** *102,* 074314-7.

(7) Fletcher, B. L.; Hullander, E. D.; Melechko, A. V.; McKnight, T. E.; Klein, K. L.; Hensley, D. K.; Morrell, J. L.; Simpson, M. L.; Doktycz, M. J. *Nano Letters* **2004,** *4,* 1809-1814.

(8) McKnight, T. E.; Melechko, A. V.; Austin, D. W.; Sims, T.; Guillorn, M. A.; Simpson, M. L. *Journal of Physical Chemistry B* **2004,** *108,* 7115-7125.

(9) McKnight, T. E.; Melechko, A. V.; Fletcher, B. L.; Jones, S. W.; Hensley, D. K.; Peckys, D. B.; Griffin, G. D.; Simpson, M. L.; Ericson, M. N. *Journal of Physical Chemistry B* **2006,** *110,* 15317-15327.

(10) McKnight, T. E.; Melechko, A. V.; Griffin, G. D.; Guillorn, M. A.; Merkulov, V. I.; Serna, F.; Hensley, D. K.; Doktycz, M. J.; Lowndes, D. H.; Simpson, M. L. *Nanotechnology* **2003,** *14,* 551-556.

(11) Pearce, R. C.; Railsback, J. G.; Anderson, B. D.; Sarac, M. F.; McKnight, T. E.; Tracy, J. B.; Melechko, A. V. *ACS Appl. Mater. Interfaces* **2013**.

(12) Wang, X.; Landis, E. C.; Franking, R.; Hamers, R. J. *Accounts of Chemical Research* **2010,** *43,* 1205-1215.

(13) Melechko, A. V.; McKnight, T. E.; Guillorn, M. A.; Merkulov, V. I.; Ilic, B.; Doktycz, M. J.; Lowndes, D. H.; Simpson, M. L. *Applied Physics Letters* **2003,** *82,* 976-978.

(14) McKnight, T. E.; Melechko, A. V.; Hensley, D. K.; Mann, D. G. J.; Griffin, G. D.; Simpson, M. L. *Nano Letters* **2004,** *4,* 1213-1219.

(15) Yu, Z.; McKnight, T. E.; Ericson, M. N.; Melechko, A. V.; Simpson, M. L.; Morrison, B. *Nano Letters* **2007,** *7,* 2188-2195.

(16) Yu, Z.; McKnight, T. E.; Ericson, M. N.; Melechko, A. V.; Simpson, M. L.; Morrison, B. *J Neurotraum* **2007,** *24,* 1235-1235.

(17) Doktycz, M. J.; Fletcher, B. L.; Hullander, E. D.; Fowlkes, J. D.; Retterer, S. T.; McKnight, T. E.; Melechko, A. V.; Simpson, M. L. *2006 Bio- Micro- and Nanosystems Conference* **2006,** 13-13, 107.

(18) Doktycz, M. J.; Zhang, L.; Melechko, A. V.; Klein, K.; McKnight, T. E.; Britt, P. F.; Guillorn, M. A.; Merkulov, V. I.; Lowndes, D. H.; Simpson, M. L. *Nanotech 2003, Vol 3* **2003,** 420-423, 561.

(19) Kroto, H. W.; Heath, J. R.; Obrien, S. C.; Curl, R. F.; Smalley, R. E. *Nature* **1985,** *318,* 162-163.

(20) Iijima, S. *Nature* **1991,** *354,* 56-58.

(21) Ebbesen, T. W., *Carbon Nanotubes: Preparation and Properties*. CRC Press: 1997.

(22) Merkulov, V. I.; Lowndes, D. H.; Wei, Y. Y.; Eres, G.; Voelkl, E. *Applied Physics Letters* **2000,** *76,* 3555-3557.

(23) Chen, Y.; Lin Wang, Z.; Song Yin, J.; Johnson, D. J.; Prince, R. H. *Chemical Physics Letters* **1997,** *272,* 178-182.

(24) Ren, Z. F.; Huang, Z. P.; Xu, J. W.; Wang, J. H.; Bush, P.; Siegal, M. P.; Provencio, P. N. *Science* **1998,** *282,* 1105-1107.

(25) Ren, Z. F.; Huang, Z. P.; Wang, D. Z.; Wen, J. G.; Xu, J. W.; Wang, J. H.; Calvet, L. E.; Chen, J.; Klemic, J. F.; Reed, M. A. *Applied Physics Letters* **1999,** *75,* 1086-1088.

(26) Endo, M.; Kim, Y. A.; Hayashi, T.; Fukai, Y.; Oshida, K.; Terrones, M.; Yanagisawa, T.; Higaki, S.; Dresselhaus, M. S. *Applied Physics Letters* **2002,** *80,* 1267-1269.

(27) Klein, K. L.; Melechko, A. V.; McKnight, T. E.; Retterer, S. T.; Rack, P. D.; Fowlkes, J. D.; Joy, D. C.; Simpson, M. L. *Journal of Applied Physics* **2008,** *103,* -.

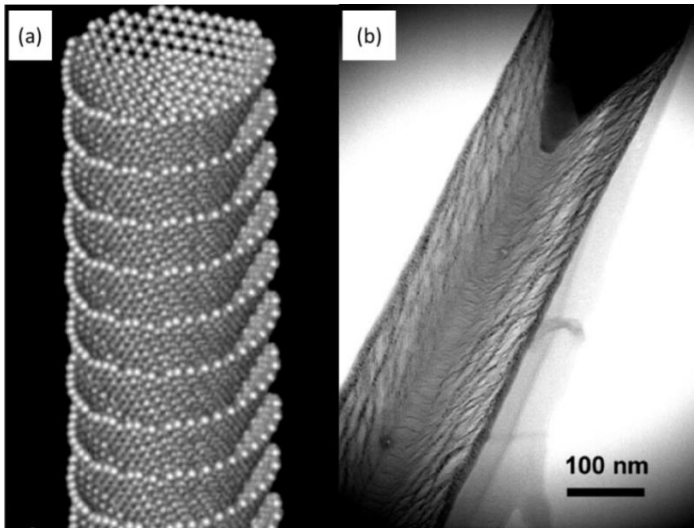

Figure 1.1: (a) Schematic of atomic structure in a vertically aligned carbon nanofibers without a catalyst particle at tip. (b) HRTEM image of a VACNF that has been knocked over onto a TEM grid. The cross sectional pattern is frequently referred to as herringbone, as it appears similar to a fish skeleton. Adapted from [26] and [2] respectively.

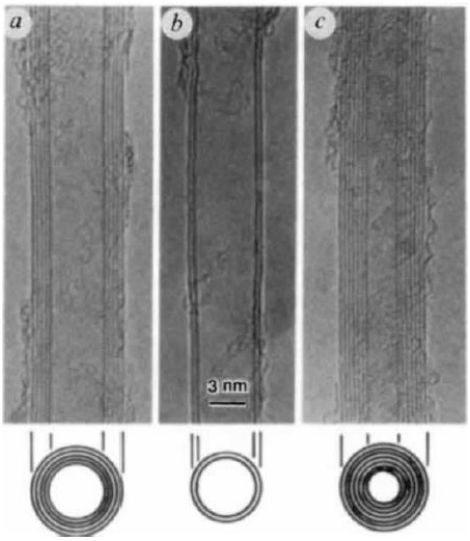

Figure 1.2: Electron micrographs of several MWCNTs composed of (a) 5 (b) 2 (c) 7 graphitic sheets. One important difference between CNTs and CNFs is that true CNTs are hollow like a pipe, while CNFs are not. Adapted from [20]

Figure 1.3: TEM image of bamboo type nanofibers with the catalyst nanoparticles at the tip of the fibers. The internal structure is reminiscent of bamboo with hollow areas separated by cross struts. Adapted from.[27]

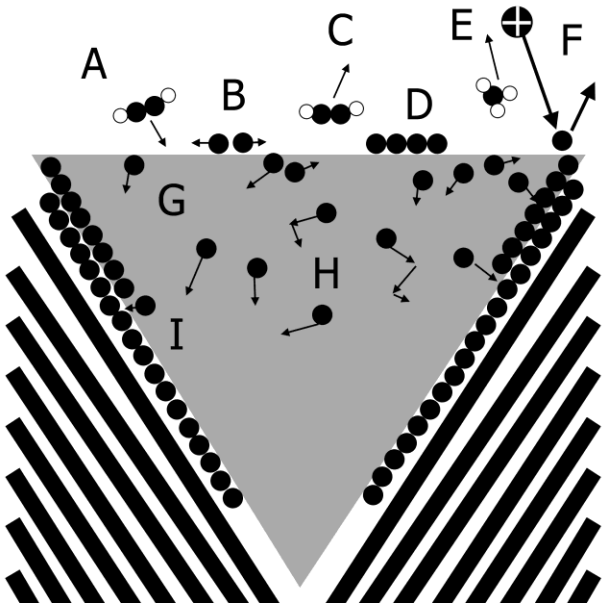

Figure 1.4: Diagram of interactions occurring on catalyst nanoparticle during PECVD synthesis of VACNFs. (A) Arrival of excited species to the surface of the catalyst (B) Catalytic dissociation of carbonaceous species (C) Departure of any undissociated molecules (D) Formation of a carbon film on the catalyst surface (E) Isotropic chemical etching (F) Sputtering from ionic bombardment (G) Solution of carbon into the catalyst particle (H) Diffusion of carbon through and/or around the catalyst particle (I) Incorporation of carbon atoms into a growing graphene layer. Adapted from [1].

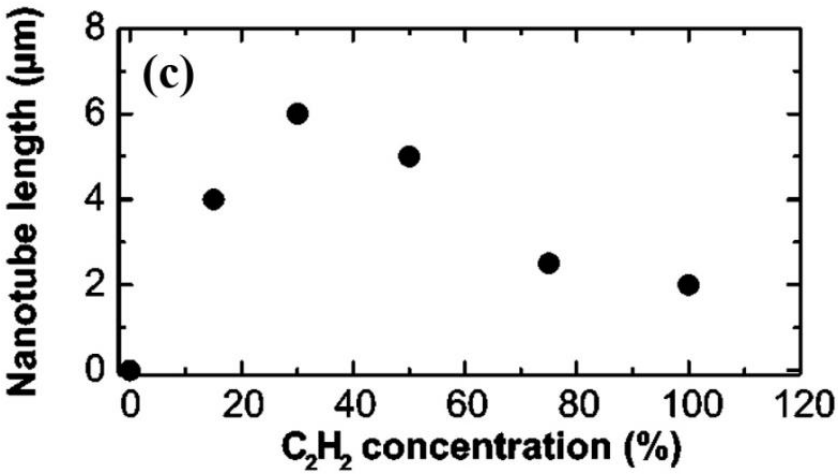

Figure 1.5: Chart showing the effect of C_2H_2/NH_3 ratio on the growth rate of VACNFs. Adapted from [3].

Chapter 2 - Challenges in process integration of catalytic DC plasma synthesis of vertically aligned carbon nanofibers

This work has previously appeared in Melechko, A.V., R.C. Pearce, D.K. Hensley, et al., *Challenges in process integration of catalytic DC plasma synthesis of vertically aligned carbon nanofibres.* Journal of Physics D-Applied Physics, 2011. **44**(17).

The ability to synthesize free-standing, individual carbon nanofibers aligned perpendicular to a substrate has enabled fabrication of a large array of devices with nanoscale functional elements, including electron field emission sources, electrochemical probes, neural interface arrays, scanning probes, gene delivery arrays and many others. This was made possible by development of a catalytic plasma process, with DC bias directing the alignment of nanofibers. Successful implementation of prototypical devices has uncovered numerous challenges in the integration of this synthesis process as one of the steps in device fabrication. This chapter is dedicated to these engineering and fundamental difficulties that hinder further device development. Relatively high temperature for catalytic synthesis, electrical conductivity of the substrate to maintain DC discharge and other difficulties place restrictions on substrate material. Balancing non-catalytic carbon film deposition and substrate etching, non-uniformity of plasma due to growth of the high aspect ratio structures, plasma instabilities and other factors lead to challenges in controlling the plasma. Ultimately,

controlling the atomistic processes at the catalyst nanoparticle and the behavior of the nanoparticle is the central challenge of plasma nanosynthesis of vertically aligned carbon nanofibers. This chapter represents my research into the current state of the field and poses some of the fundamental issues in fiber synthesis and device incorporation.

2.1 Introduction

Carbon nanostructures are an important class of materials because of their high degree of chemical, electrochemical and thermal stability and exceptional mechanical properties. Because carbon has many possible bonding arrangements [1], a rich variety of nanostructured materials (*e.g.* fullerenes[2], carbon nanotubes (CNTs)[3], carbon nanofibers (CNFs)[4], and graphene[5]) can be formed. Metal nanoparticles (NPs), especially, Ni, Co, and Fe, catalytically rearrange atoms from carbon precursors to produce graphitic nanostructures. The controlled synthesis of carbon nanostructures by methods that permit their assembly as functional nanoscale components is a crucial challenge in nanoscale science and technology.

The use of direct current (DC) plasma synthesis, first introduced by Ren et al in 1998 [6], has made possible the devices discussed in this article. The most remarkable aspect of this process is that even individually free-standing nanofibers could maintain their orientation after growth [7, 8]. This is in contrast to thermal chemical vapor deposition in which carbon nanotubes or nanofibers grow in random uncontrolled directions if there are no neighbors to provide such orientation via crowding [9, 10]. The reason for using *DC* plasma is in its ability to establish growth direction of vertically aligned carbon nanofibers. The alignment mechanism proposed, based on stress-controlled carbon diffusion, is frequently referenced [9]. However,

up to this day it remains merely a proposed hypothesis and experimental and theoretical understanding is still needed. DC plasma processing has many challenges. Substrates have to be electrically conductive and able to dissipate significant currents. DC discharges are notoriously unstable and arcs and other plasma instabilities occur frequently. Non–uniformity in substrate material, such as a wafer with prefabricated devices or patterns, create additional challenges in maintaining a stable DC discharge.

There are many applications of carbon nanofibers that require the integration of PECVD synthesis into the overall device microfabrication process. Very often synthesis is not the first or the last step, which requires compatibility of the processes and materials. First of all, the integration of the VACNF growth process requires use of large-scale reactors for substrates compatible with microelectronic device manufacturing equipment (e.g., Si and quartz wafer diameters of 100 mm or larger). Secondly, multilevel processing requires the ability to synthesize high-quality VACNFs in precisely defined locations, as subsequent fabrication processes need to be performed in registry with defined patterns. This can be achieved by the deposition of catalyst in areas defined by lithography. Thirdly, the nanofibers must be able to withstand various conditions to which they are exposed during standard microfabrication processing used in the production of integrated circuits and microelectromechanical systems (MEMS). Fortunately, in many cases this compatibility has been demonstrated as summarized briefly below.

Carbon nanofibers are a class of materials that consist of curved graphene layers stacked to form a filament.[7] Despite the distinct difference between nanotubes and

nanofibers, nanofibers are often called nanotubes, as they have the same cylindrical morphology.[11] However the physical and chemical properties of nanofibers drastically differ from nanotubes. Since single wall carbon nanotubes are made out of a continuous covalently bonded carbon network, they are endowed with diamond-like tensile strength. In contrast, the bonding of carbon nanofibers along their axes is similar to bonding of graphene layers in graphite. Similarly, since the sidewalls of carbon nanotubes expose the basal plane of graphene, nanotube chemistry and electrochemistry is significantly different from graphene edge presenting sidewalls of carbon nanofibers [12]. VACNFs are synthesized by catalytic plasma-enhanced chemical vapor deposition. First, resist is patterned (by optical or electron beam lithography), and a Ni metal film is deposited by physical vapor deposition. The metal outside the pattern is lifted off by a solvent that dissolves the resist. Prior to nanofiber growth, the substrate is heated, and pretreated with ammonia plasma to facilitate the formation of catalyst NPs. This process, usually solid-state dewetting, leads to the formation of arrays of catalyst nanoparticles.[13,14,15,16] Films below a few hundred nanometers in thickness are thermodynamically unstable. The NP surface density and their size distribution depend on the film thickness and the surface energies. It is possible to design the patterned film to produce single particles at each location.[7, 8] Thin film dewetting provides additional control over NP formation and a path to potentially control the internal structure of carbon nanofibers.[17] For many applications, however, such control is not necessary, and dewetting is an expensive method. Deposition of pre-synthesized NPs is an attractive alternative that is poorly understood and underutilized.[18, 19, 20] The next stage in the synthesis of VACNFs is to administer acetylene into DC glow discharge plasma to initiate nanofiber growth. At this

stage, graphitic carbon forms under the catalytic NPs and elevates them off the surface.[21]. The growth process takes place at high temperature (700 °C). Low temperature growth has been reported to produce catalytically grown carbon structures with amorphous internal structure.[22, 23, 24, 25] Throughout this DC plasma process, the substrate serves as a cathode and the showerhead as an anode. Typically, VACNF growth is performed in a mixture of acetylene and ammonia gas at several Torr total pressure. Many aspects of VACNF controlled synthesis and VACNF functionalization and characterization have been reviewed in other works.[26, 27]

The ability to grow individual aligned fibers has distinguished VACNFs from dense arrays (or mats) of vertically aligned carbon nanotubes that require van der Waals interaction with neighboring nanotubes to maintain alignment. There are few reports on mechanical properties of vertically aligned carbon nanofibers.[28, 29, 30] In device fabrication, it has been observed that VACNFs are able to maintain their vertical alignment even during post-synthesis processing. Spin casting photoresist over the nanofiber, handling in liquids, or even physical pressing into cellular matrices are examples of procedures that surprisingly do not destroy VACNF arrays.[31, 32, 33, 34, 35, 36, 37, 38, 39, 40, 41] This mechanical robustness along with the ability to withstand different material coating and removal processes has allowed for the integration of VACNFs into a number of microfabrication processes. This has resulted in VACNF incorporation into micro- and nano-scale devices that include electron field emitters [31, 35, 42], active microfluidic structures [43, 44, 45, 46], biosensors [47, 48, 49, 50], gene delivery arrays [37,

[41, 51, 52], electrochemical probes [36, 53, 54], electrodes for neuronal interfacing [39, 55], and scanning probe microscopy tips [56, 57].

The VACNFs in **Figure 2.1** are grown on a silicon wafer with 1 μm of silicon dioxide coated with a Ti/W/Ti/Si stack metallization. This metal layer ultimately is patterned and etched into electrical leads that would provide individual addressability for each of the nanofibers. While considered a successful outcome of the synthesis process, this array illustrates multiple challenges that remain unresolved. The heights of these nanofibers vary by hundreds of nanometers. Their shape has multiple deviations from a straight line. There is a depression in the substrate surrounding each nanofiber. The diameter of the tips varies from fiber to fiber. The nanofiber positions are also shifted slightly from their lithographically defined locations. These challenges present further difficulties in manufacturing consistently functional devices with predictable uniform characteristics. The underlying causes of these issues are fundamental problems in plasma nanoscience. Understanding how to use plasma to control processes at a catalyst nanoparticle and its surrounding should provide solutions to these challenges.

Catalytic chemical vapor deposition (CVD) routes provide a means for the synthesis of CNTs and CNFs and it will be seen that only catalytic PECVD on supported catalysts allows for truly deterministic synthesis.[7, 8, 27, 58] By deterministic synthesis we imply the ability to grow individual nanostructures with *precisely* defined characteristics, such as size, location, chemical composition, internal structure, etc., all by varying the starting materials or plasma conditions during growth. Thus for the purpose of attaining this level of controlled synthesis,

the focus of this review will only be on the catalytic PECVD growth process used to produce VACNFs.

In general, the location of the VACNF is defined by patterning the catalyst material lithographically with the size of the catalyst nanoparticle controlling the resultant nanofiber diameter. The nanofiber length is controlled by the growth rate and duration of the growth process while the nanofiber shape and sidewall chemical composition are tailored by the ratio of gases used during synthesis. The alignment of the fibers is directed by the electric field present in the plasma sheath and most recently, control over the internal crystalline structure of the VACNF has been achieved by catalyst preparation and the total gas pressure. [17, 59]

While a variety of plasma power sources have been used for CNF synthesis (e.g. radio frequency, inductively coupled, microwave, etc.)[27], direct current systems are the simplest of the PECVD reactors. In a direct current PECVD (DC-PECVD) process the substrate heater also acts as the cathode, requiring conductivity of the substrate. The showerhead located above the heater similarly serves a dual purpose by distributing gases evenly over the sample as well as functioning as the anode.

From this overview, it can be seen that plasma excitation introduces an additional level of process complexity over the basic diffusion/precipitation model applicable to standard CVD. However, this complexity simultaneously provides additional aspects of control over the shape and alignment of the carbon nanofibers. Unlike CVD synthesis where temperature, total gas pressure and flow govern the growth process, PECVD synthesis also includes parameters specific to the glow discharge. These parameters include the voltage,

current, power, and electric field distributions within the discharge, which all play a critical role in shaping the resultant carbon nanofibers. Since the plasma can produce both etching and deposition of conformal films (depending on the conditions), care must be taken to balance the two regimes in order to deposit only catalytic graphitic carbon and avoid thin film formation of non-catalytic amorphous carbon that can ultimately halt VACNF growth [60].

The substrate also plays a crucial role in carbon nanostructure synthesis, especially in PECVD processes. The substrate not only acts as a support but it also interacts with the catalyst and the plasma growth environment. Silicon and silicon dioxide are two of the most commonly used substrates for obvious reasons of application in silicon-based processing. In reality, the choice of substrate is practically unlimited (for extensive list see [27]); however there are several issues that should be considered. First, typical PECVD substrate temperatures are between 500-800°C. However, there are several reports of low temperature or even room temperature growth whereby nanofibers are synthesized with no direct heat applied to the substrate [45-46]. It should be realized, however, that in DC plasma a thin metal film is still inevitably heated by possibly hundreds of degrees by joule heating in addition to plasma heating [61, 62]. For applications where the growth temperature is a concern, arrays of VACNFs can be transferred post-synthesis to temperature sensitive substrates [63]. Many of the challenges involved in the synthesis of VACNFs are due to the high temperatures involved, both from substrate heating to dewet the nickel catalyst particles and from plasma heating. If synthesis were to occur at lower temperatures many of these problems would be obviated.[22, 64, 65] A method to selectively heat the catalyst particles would

remove a great many of the challenges currently presented to synthesis. Only the nanoparticle needs to be hot to fuel catalytic growth. [22, 23, 24]

2.2 Substrate

As previously stated, in DC-PECVD systems, the substrate is placed on the cathode. To sustain glow discharge at the catalyst location, the underlying electrically conductive substrate can be simply connected to the cathode. However in fabrication of devices with VACNF elements it is often necessary to provide isolation between the nanofibers or their groups. To grow VACNFs on insulating substrates, like SiO_2, in one approach the whole surface of a wafer is coated by a metal layer, which is removed after growth at the areas outside of the nanofibers and the connecting electrodes [53]. In another approach, metal micropads are patterned prior to growth of VACNFs.[49, 66, 67, 68, 69, 70] Alternatively, radio frequency sources can be used to sustain plasma with generated self-bias to provide vertical alignment.[71]

Substrate choice also contributes to variation of the secondary electron yield and subsequently the plasma current and the density of ion/radical species in the plasma. Yet another issue in PECVD synthesis is removal and re-deposition of substrate material. For instance, during PECVD growth on Si substrates, silicon species can be etched or sputtered, and re-deposited onto the sidewalls of the fibers, creating an insulating SiN_x sheath[26, 52], which may or may not be desirable. To avoid Si incorporation on the fiber sidewalls, a typically refractory metal overlayer can be deposited to cover the silicon substrate. Additional incompatibilities of the substrate with catalyst materials and the growth

environment have prompted the use of buffer layers or adhesion layers *underneath* the catalyst. Buffer layers including Ti, W, and SiO_2 are often used to prevent diffusion or intermixing of catalyst and substrate, such as the formation of silicides [58]. The underlayer material's effect on the actual carbon growth is mostly attributed to catalyst wetting and particle formation, which in turn can affect the growth mode if strong catalyst-substrate interactions exist.

2.3 Catalyst nanoparticle

VACNF location is directly defined by the catalyst material deposition. If catalyst patterning is required, i.e. for VACNF arrays, it can be done before or after the catalyst film is deposited. Most commonly, the pattern is defined beforehand using photo- or electron beam lithography and metal lift-off is subsequently employed. Conversely, the film can also be patterned following catalyst deposition by applying a patterned resist and removing the peripheral metal via wet etching, ion beam sputtering or reactive ion etching.

If a periodic array of individual VACNFs is desired, first an array of lithographically defined catalyst "dots" is deposited. Each dot is essentially a disk of metal that remains after removing the surrounding catalyst film. The amount of material (diameter and thickness) deposited for each patterned dot is crucial to determining whether single or multiple fibers form at the growth site. Merkulov *et al* found that there was a critical dot diameter resulting in single nanofibers. This critical dot diameter of course would depend upon several parameters including the choice of underlayer, substrate, and type and thickness of catalyst used [7]. Subsequent work by Melechko *et. al.* with larger, photo-lithographically defined dot

arrays, also determined that there is a critical dot thickness for obtaining a single nanofiber from each dot [52]. These two results underline that there is interplay between thickness and area when considering relevant dewetting instabilities, which will result in either single or multiple catalyst nanoparticles.

The VACNF tip diameter is approximately equal to the diameter of the catalyst nanoparticle. It has been observed that the size of the catalyst particle decreases continually during the PECVD synthesis process [72], eventually disappearing altogether. The loss of the catalyst material is likely due to ion beam sputtering or possibly incorporation of Ni along the nanofiber body (**Figure 2.2**). Since particle size correlates to fiber diameter, particle size reduction results in fiber diameter reduction during growth. This trend can be used to sharpen the tips of the nanofibers for use in such applications as field emission and probes for cell and tissue interfacing. However, the constant tip size reduction simultaneously creates a limitation on the maximum obtainable length of the free standing isolated nanofiber. In order to achieve the desired final length, the amount of metal contained in the catalyst particle must be sufficient to last the duration of the growth process, which may reintroduce issues with formation of single nanofibers. The catalyst particle, in addition to facilitating growth, also protects the nanostructure from physical and chemical etching. Should the nanoparticle disappear before the nanofiber achieves the targeted length, the nanofiber is no longer protected and will be etched back with continued plasma exposure [72]. In some ways this phenomenon of "survival of the fittest" (or largest particle) has proven useful as a strategy to grow high-quality, tall arrays of VACNFs, where the smaller extraneous nanofibers are

etched back and disappear. The mechanisms that lead the to distribution of nanoparticle catalyst along the nanofiber interior require further study.

Another mysterious type of catalyst loss is illustrated in **Figure 2.3**. In this image the nanofibers that grew between lithographically defined locations indicate that catalyst film has been redistributed as large nanoparticles to very large distances outside the original location, sometimes tens of microns. This cannot be accounted by diffusion or mobility of the nanoparticles formed at the origin. It's been hypothesized that metal gets "spluttered" by microdischarges. This phenomenon significantly reduces yield of functional devices and remains an unresolved issue in process integration of VACNF synthesis by catalytic DC PECVD into microfabrication.

2.4 Growth conditions

The catalytic PECVD process entails a host of parameters that are variable over a multidimensional space,[27] leading to difficulties controlling the growth rate, morphology, and composition of the resulting deposit. The main factors governing this multidimensional parameter space include: total pressure, total gas flow rate, carbon source to etchant gas flow ratio (e.g. C_2H_2/NH_3,CH_4/H_2, etc.), substrate temperature, and plasma power [current and voltage, coupled in DC plasma]. It should be mentioned that while plasma current and plasma voltage can have quite different effects on the growth of VACNFs, in a DC glow discharge these two parameters are coupled and cannot be changed independently [58, 73] as in RF plasmas [71].

The selection of parameters used for VACNF growth is dependent upon the combination of catalysts, substrates, carbon source and etchant gases, and most importantly, the catalyst pattern, where the density of packing affects all aspects of growth [74]. Therefore, the recipe must be tailored to suit each different application. General parameter space trends facilitate navigating to the optimal growth conditions and are thus enumerated briefly below.

To begin with, the growth rate of VACNFs by PECVD has been shown experimentally to be linked to several parameters, namely total pressure *P*, gas flow ratio *R*, and temperature *T*, as well as total gas flow rate *F*. It is encouraging to realize that the growth rate remains fairly constant over time.[58, 72] As a result, VACNFs can be grown to very precise average lengths just by monitoring the growth time. With respect to adjusting this rate, Chhowalla *et. al*. found that the nanofiber growth rate increases almost linearly with *P*, at least up to 10 Torr.[58] By increasing *P*, a faster supply of carbon source material arrives at the catalyst. The relationship with the gas ratio *R* is not so straightforward. A peak is observed with the maximal growth rate occurring at about the mid-range of *R*.[58, 73] At ratios above this optimum, increased C_2H_2 causes a buildup of non-catalytic carbon on the catalyst surface, decreasing its activity. Likewise, if C_2H_2 is replaced by too much NH_3, etching processes are increased and insufficient quantities of carbon species arrive to the catalyst, leading to decreased growth rates. Temperature also exhibits a peaked relationship, with a maximum around 700°C.[58] This can be explained by the competing mechanisms of an increase in carbon diffusion rate with temperature and concurrent decrease in sticking coefficient of carbon species to the catalyst surface with temperature. Lastly, the total gas flow rate has also

been found to have a considerable impact on the growth rate. Increasing *F* by using a gas inlet nozzle of variable orifice has shown that a smaller orifice, hence higher local flows, can drastically increase the VACNF growth rate.[73]

Controlling the shape or morphology of the VACNF structures as well as the elemental composition of the sidewalls mainly involves adjusting the gas flow ratio in order to affect the same etching and deposition mechanisms that influenced the growth rate. In PECVD, various species are present in the glow discharge, including C neutrals, C ions, and reactive etchant species (H^+, N^+, etc.) that are formed during the decomposition of acetylene and ammonia. By increasing the C_2H_2 flow relative to the NH_3, the number of C species exceeds etchant species and condensation of amorphous carbon occurs on the surface. [60, 75, 76] While the neutrals randomly move about sticking to any surface, the electric field lines govern the direction travelled by the ions, thus creating a directional disparity in amorphous carbon accumulation. The result is the formation of conical nanostructures [74].

Thus by changing the source/etchant gas ratio, the cone angle of individually patterned nanostructures could be controlled.[74, 75] VACNFs can change from cylindrical to highly conical with increasing *R*; however when *R* becomes too high, an amorphous carbon film forms [77], which halts growth altogether. Therefore the flow ratio can be used to tailor the conicity of the CNF along its length. A second type of sidewall deposition that occurs on low-density arrays in an etching regime (higher NH_3 flow), in which amorphous carbon is prevented from condensing. In this regime, the substrate, unprotected by carbon film, is etched by the plasma species and the etch products redeposit on the sidewalls of growing

carbon nanofibers. In the case of CNF growth on silicon substrates using a C_2H_2/NH_3 mixture, the Si reacts with the N from the ammonia etchant gas to form $Si_xN_y(C,O)$ compounds on the VACNF surface [52, 78, 79, 80]. Thus there is a delicate balance to the gas ratios used in regard the desired sidewall composition. For VACNFs without an amorphous carbon coating, a C_2H_2:NH_3 ratio of 20% or below must be used [60]. However, for ratios lower than this, sidewall deposition of Si_xN_y material becomes more favorable. The balanced C_2H_2/NH_3 gas flow ratio depends strongly on the substrate material. For example, above W this ratio could be 40/80 sccm/sccm while above Si it would be 65/80 at all other parameters, especially current, kept constant. **Figure 2.4** displays variation of dark field space from above W to above Si. The nonuniformity in substrate material leads to variation of the carbon film etch rate often resulting in undesirable carbon film deposits on a wafer that makes it unusable for subsequent fabrication steps (e.g. SiO_2 deposition).

One other challenge is that plasma does not stay unchanged during nanofiber growth. If a high density nanofiber array starts growing, the glow discharge above this area changes (becomes similar to the area above W in Fig. 4). This leads to a shift in optimal acetylene to ammonia ratio towards the regime of carbon film deposition and nanofibers become coated with this film (**Figure 2.5**). The effect of changing synthesis parameters during growth has not been well explored. Whether one set of parameters is optimal for the beginning of growth and another set for various other stages of growth is unknown.

2.5 Alignment

In PECVD, alignment can be achieved regardless of the density the CNF array. A strong correlation has been observed between the carbon nanofiber growth axis and the direction of the electric field in the plasma.[81, 82] In the PECVD growth system usually the electric field is perpendicular to the conductive planar substrate located on the sample holder, producing vertically aligned CNFs. However, the field direction can be changed by placing the substrate close to the edge of the sample holder to produce angled alignment of CNF forests where the tilt angle varies with distance from the edge. [82]

There is also a direct correlation between alignment in PECVD and the growth mode.[81] Alignment with the electric field only occurs in tip-type growth and not with base-type growth. In tip-type growth, the catalyst particle is lifted up from the substrate and follows the path of the electric field lines in the plasma sheath. In contrast, when growth proceeds from the catalyst remaining at the nanofiber base, random growth orientation transpires. This control of the nanofiber alignment during growth is a remarkable phenomenon that is quite useful for many applications. However, there are fluctuations in the growth direction that can be quite substantial (**Figure 2.6**). The underlying mechanism of this phenomenon is not understood. One potential cause is that electrical field is modified by the presence of the neighboring fibers. In **Figure 2.6**, the fibers that are bent toward the neighbors switch their direction to vertical when they reach the neighboring site. However, there are fluctuations in growth direction even in singular fibers. The key to this phenomenon lies in understanding the behavior of the nanoparticle during growth. The in situ imaging by

Helveg et al showed a frequent change of growth direction in a plasma (and field) free experiment.[83]

They performed time-resolved, atomic-resolution *in situ* TEM observations of the formation of carbon nanofibers from methane decomposition over supported nickel nanocrystals at ~500°C. Carbon nanofibers were observed to develop through a reaction-induced *reshaping* of the nickel nanoparticles, as shown by the series of frames extracted from captured movies. The nucleation and growth of graphene layers were found to be assisted by a dynamic, repetitive formation and restructuring of mono-atomic step edges at the nickel surface.

The dynamic behavior of nanoparticles during growth observed by *in situ* microscopy also suggests a possibility of internal structure control. From the video sequences presented by Helveg *et al* it is clear that in-plane graphitic growth is about an order of magnitude faster than growth perpendicular to the layers.[83] Such a difference should be reflected in the dependence between growth rate and the internal structure of the nanofiber. Indeed, it has been shown that nanofibers grown at different growth rates can have distinctly different internal structure.[17] This high growth rate and structural change was achieved at much higher pressure, temperature, and plasma current than has previously been reported in the literature. The "fast" growth rate (8000 nm/min) exceeded the "slow" growth rate (80 nm/min) by two orders of magnitude. The particle morphology also changed from a teardrop shape to an elongated rectangle. One of the important implications of this result is that the internal structure can be modulated along the nanofiber by switching growth conditions during the

synthesis process. Despite these advances, the fact that true carbon nanotubes cannot be produced in this process remains mostly unexplained.

Since the synthesis process occurs completely at the catalytic nanoparticle, the central goal of the future should be to control local environment at the nanoparticle separately from the substrate. For example, if it were possible to heat the nanoparticle separately from the substrate, then it would be possible to grow VACNF with minimal load on the devices prefabricated on the wafer. Possibilities of such localized heating have been recently explored. [62, 84]

The complexity of VACNF synthesis process integration into microfabrication can be illustrated by the fabrication of electrically addressable arrays. In this case, there are two approaches: growth *before* or *after* the definition of electrode interconnects. The former approach was designed to fabricate nanoscale electrochemical probes. First, alignment marks for subsequent projection and contact photolithography steps are patterned onto 100mm diameter silicon wafers with 1 μm thick thermal silicon oxide. These patterns are then etched into the oxide layer using a CHF_3/O_2 based reactive ion etch. The wafers are then coated with 10nm of Ti, 100 nm of W, 10 nm of Ti, and 10 nm of Si using electron-beam physical vapor deposition. In the next procedure, the sites for fiber growth are defined photolithographically into a photoresist layer as 500 nm diameter circular patterns and 40 nm of nickel is deposited using electron-beam physical vapor deposition followed by lift-off. Fiber synthesis is conducted using a dc PECVD process. During this growth, the underlying metallization serves as the cathode for the dc-plasma. Following fiber growth, electrode interconnects are

patterned with photoresist that is used as an etch mask during RIE removal of the metal outside interconnects. First, a CF_4- based silicon etch removes the surface layer of Si, followed by a $SF_6/CF_4/O_2$-based refractory metal etch to remove the underlying Ti, W, and Ti. A passivation layer of ~100 nm of PECVD silicon dioxide is coated conformally on all surfaces (interconnects, substrate, and fibers), and a subsequent passivation layer of 2 □m of SU-8 is spun onto the wafer to further bury the underyling interconnects. Contact pads are lithographically defined in the SU-8 photoresist layer. A second layer of SU-8 resist is then spun on at a thickness greater than the length of the nanofibers, typically 15-20 μm. Fiber regions and contact pads are cleared of this SU-8 layer using contact photolithography. An oxygen-based SU-8 dry etch process is then used to remove (ash) residual SU-8 resist and to emancipate the oxide-coated nanofiber tips from any SU-8 residual that has accumulated on the fiber surface. Finally, a CHF_3/O_2-based silicon dioxide reactive ion etch process is used to emancipate the nanofiber tips from the silicon dioxide and to open the peripheral contact pads.[36] **Figure 2.7** bottom left-to-right shows: a low magnification SEM image of the carbon nanofiber microelectrode arrays after silicon oxide deposition and before SU-8 passivation; a higher magnification image of a 4-element carbon nanofiber array; SEM image of the 4-element carbon nanofibers after SU-U passivation; and a high magnification of a single carbon nanofiber illustrating the very tip of the oxide-coated carbon nanofiber has successfully been locally etched thus creating a nanoscale electrochemical probe.

2.6 Plasma instabilities and plasma damage

Plasma instabilities pose a tremendous challenge in using DC plasma for VACNF synthesis integration, particularly in multilevel device fabrication whereby earlier processing steps can impact the success or failure of the plasma synthesis step. One of the most frequent causes of failure is due to development of running arcs across the device. Typical damage due to running arcs is shown in **Figure 2.8**. An arc between anode and a substrate is initiated, possibly, at a defect site. The metal film at this location heats up, which increases the current at this arc by enhancing electron emission. When the temperature reaches critical point the film melts and explodes, splashing molten droplets across the wafer. A metal film new edge is then produced, which then is heated and the location of the arc shifts. The arc could run across large regions of the device substrate. If multiple arcs develop simultaneously, the surface of the whole wafer can be damaged and every die rendered useless in under a second. With growth time required to achieve necessary length in tens of minutes, even low probability of such events drops the device yield significantly. Microcracks due to stress induced by thermal expansion mismatch are suspected to be such an initializing defect.

Yet another challenge of incorporating VACNFs into a device is determining at what point of the fabrication process to synthesize the VACNFs. In one study the nanofibers were synthesized inside a well of SiO2 coated with metal [34]. However, this process was highly unreliable due to the challenge of microexplosions. Even with top metallization present, discharges directed toward electrically insulated areas with accumulated charge would cause damage to the SiO_2 substrate hundreds of microns in diameter, splashing molten SiO_2 over

the entire wafer. As a work around, the growth of the nanofibers was performed prior to the microfabrication of the rest of the device. However, other groups were successful in engineering proper electrode geometry in a post-fabrication synthesis approach. To make individually addressable electrodes Guillorn et al designed a process where VACNFs were grown first and metal was removed post growth, while Mosier et al approached the issue by growing nanofibers on prepatterned electrodes [53, 85]

Many of the applications that could benefit from VACNF integration require that the placement of the nanofibers be precisely controlled. The locations of the nanofibers are determined by two factors: the initial placement of the nanoparticle and subsequent movement of the nanoparticle along the substrate surface. First of all, during dewetting nanoparticles form approximately within the boundaries of the catalyst film, e.g. 100 nm diameter disk defined by electron beam lithography. This process is initiated by dewetting of the film by raising the temperature of the film via conduction through the substrate, laser irradiation, or ion irradiation. It is believed that dewetting is facilitated by exposure to a reducing atmosphere of hydrogen (gas or plasma), which presumably removes the thin oxide film from the catalyst metal. When the film is dewetted, metal droplets are mobile and can migrate from the intended position.[86] Second, the nanoparticle frequently moves away from its site of origin by hundreds of nanometers. It remains an unresolved challenge to fix the location of the catalyst nanoparticle, essential for such devices as focused electron field emitters.[35]

PECVD synthesis of VACNFs results in significant substrate heating. It has been shown that with a DC plasma being the only heat source, substrate temperatures can reach up to 700°C.[61] Significant heating may have deleterious effects on the underlying substrates such as interdiffusion between metal layers, stress failure due to dissimilar thermal expansion of device layers, and/or the dewetting and consequent destruction of thin films.

There are some methods used to circumvent substrate heating. One method used is transferal of the nanofibers post synthesis to a new substrate. Fletcher et al transferred fibers after growth by embedding them in a UV hardened epoxy membrane which was subsequently peeled from the original substrate and then aligned and placed onto the new substrate [63]. This technique has its own challenges such as how the fibers are removed from the substrate without causing significant damage to the fibers. Alignment and bonding with the new substrate also present challenges. .Another approach to this problem is using substrate materials that are specifically designed to withstand the environment of PECVD growth.

While growth conditions are optimal for catalytic synthesis of a vertically aligned carbon nanofiber, the same conditions could be used for reactive ion etching of the substrate. For example tens of nanometers of Si are removed during growth of 20 μm long nanofibers in a sparse array. Moreover DC plasma synthesis of VACNFs on micromachined structures presents additional challenges. Field enhancement due to structures such as cantilevers can increase the substrate etch rate to the point of failure (**Figure 2.9**). Search for the proper

balance of carbon film removal, nanofiber growth, and limiting the damage to the Si substrate could be a very difficult and exhausting process.

Some metals, such as Cu or Au enhance Si substrate etch rate after dewetting into nanoparticles at the same conditions that would produce catalytic growth of VACNFs.[87] This nanoparticle masked etch leads to creation of an array of very sharp "etch grass" (**Figure 2.10**). While such sharp vertical nanostructures can provide similar utility as VACNFs at some applications, e.g. field emission, gene delivery, they would be a source of failure where only VACNFs were supposed to be grown. Thus careful selection of materials that are compatible with VACNF growth conditions have to be.

The interface between nanofiber and the substrate present yet another challenging area. In case of Si, for example SiC formation has been observed.[78] Metal properties are altered by the environment of CNF growth to the extent that the etch resistance is increased. For example if the nanofiber growth is followed by resist patterning and then attempted removal of deposited tungsten by $SF_{6,}$ the metal will often not etch due to surface contaminants. Occasionally an oxygen etch helps to alleviate problem – but not always.

2.7 Postsynthesis processing

Several challenges lie in microfabrication steps following nanofiber synthesis. It is a challenge well familiar to MEMS developers. High aspect ratio 3D structure creates difficulties to all planar processing. For example, photoresist, spun to define leads to carbon nanofibers, would inevitably contain dips which result in photolithography defects as in

Figure 2.11. Exposing VACNF studded substrates to further plasma processing such as reactive ion etching or PECVD of silicon dioxide influences processes in the vicinity of a nanofiber, leading to higher etch rates, or high deposition rates due electrical field enhancement at the nanofiber tip. For example, at certain conditions a ball of SiO_2 could develop instead of a conformal coating desired for electrical insulation of a nanofiber along its length. The non-uniformity of thin film deposition over VACNFs could be used in self-aligned microfabrication [33]. Prior many of the processing steps deposition and removal of a protection later is required to preserve VACNF [57].

2.8 Conclusions

Many of the challenges in process integration of catalytic DC plasma synthesis of vertically aligned carbon nanofibers still remain, perhaps manageable only on a level of a device proof-of-principle demonstration of a few functional dies. Some of these challenges require answers to fundamental questions, some require clever process engineering. Would it be possible to develop a plasma process in which only catalyst nanoparticles, and not substrate is heated to high temperatures? Is it possible to make the nanofiber grow exactly at the defined position with nanometer precision? What mechanism could be used to pin the nanoparticle location at elevated temperatures? What is necessary to make a VACNF grow without any deviations from a desired direction? What is the mechanism that allows plasma-influenced processes at the nanoparticle to control this growth direction? Is it possible to eliminate catalyst loss during VACNF growth? What strategies could be used to monitor and adjust plasma parameters during growth? What is the mechanism preventing formation of

true nanotubes at the nanoparticle in DC plasma? How to control the shape and crystallographic orientation of a nanoparticle by plasma? How to exert this level of control in nanofiber synthesis without detrimentally impacting a substrate? How does substrate material affect plasma at the catalytic synthesis site – a nanoparticle? How to control growth rate simultaneously at all nanoparticles to produce VACNFs with nanometer uniformity on wafer scale? These questions focused on manipulating the nanoworld of catalytic nanoparticles by plasma need to be answered in order to tackle nanomanufacturing towards realization of VACNF integrated devices on an industrial scale.

2.9 References

(1) Dresselhaus, M. S., Carbon: bonding. In *Encyclopedia of Materials: Science and Thechnology*, Elsevier Science Ltd.: 2001.

(2) Kroto, H. W.; Heath, J. R.; Obrien, S. C.; Curl, R. F.; Smalley, R. E. *Nature* **1985,** *318*, 162-163.

(3) Iijima, S. *Nature* **1991,** *354*, 56-58.

(4) Baker, R. T. K. *Carbon* **1989,** *27*, 315-323.

(5) Geim, A. K.; Novoselov, K. S. *Nature Materials* **2007,** *6*, 183-191.

(6) Ren, Z. F.; Huang, Z. P.; Xu, J. W.; Wang, J. H.; Bush, P.; Siegal, M. P.; Provencio, P. N. *Science* **1998,** *282*, 1105-1107.

(7) Merkulov, V. I.; Lowndes, D. H.; Wei, Y. Y.; Eres, G.; Voelkl, E. *Applied Physics Letters* **2000,** *76*, 3555-3557.

(8) Ren, Z. F.; Huang, Z. P.; Wang, D. Z.; Wen, J. G.; Xu, J. W.; Wang, J. H.; Calvet, L. E.; Chen, J.; Klemic, J. F.; Reed, M. A. *Applied Physics Letters* **1999,** *75*, 1086-1088.

(9) Merkulov, V. I.; Melechko, A. V.; Guillorn, M. A.; Lowndes, D. H.; Simpson, M. L. *Applied Physics Letters* **2001,** *79*, 2970-2972.

(10) Fan, S. S.; Chapline, M. G.; Franklin, N. R.; Tombler, T. W.; Cassell, A. M.; Dai, H. J. *Science* **1999,** *283*, 512-514.

(11) Melechko, A. V.; Merkulov, V. I.; McKnight, T. E.; Guillorn, M. A.; Klein, K. L.; Lowndes, D. H.; Simpson, M. L. *Journal of Applied Physics* **2005,** *97*, Artn 041301.

(12) Landis, E. C.; Klein, K. L.; Liao, A.; Pop, E.; Hensley, D. K.; Melechko, A. V.; Hamers, R. J. *Chemistry of Materials* **2010,** *22*, 2357-2366.

(13) Becker, J.; Grun, G.; Seemann, R.; Mantz, H.; Jacobs, K.; Mecke, K. R.; Blossey, R. *Nature Materials* **2003,** *2,* 59-63.

(14) Bischof, J.; Scherer, D.; Herminghaus, S.; Leiderer, P. *Physical Review Letters* **1996,** *77,* 1536-1539.

(15) Giermann, A. L.; Thompson, C. V. *Appl. Phys. Lett.* **2005,** *86*.

(16) Herminghaus, S.; Jacobs, K.; Mecke, K.; Bischof, J.; Fery, A.; Ibn-Elhaj, M.; Schlagowski, S. *Science* **1998,** *282,* 916-919.

(17) Melechko, A. V.; Klein, K. L.; Fowlkes, J. D.; Hensley, D. K.; Merkulov, I. A.; McKnight, T. E.; Rack, P. D.; Horton, J. A.; Simpson, M. L. *Journal of Applied Physics* **2007,** *102,* 074314-7.

(18) Murray, C. B.; Kagan, C. R.; Bawendi, M. G. *Annual Review of Materials Science* **2000,** *30,* 545-610.

(19) Puntes, V. F.; Krishnan, K. M.; Alivisatos, A. P. *Science* **2001,** *291,* 2115-2117.

(20) Dong, L.; Jiao, J.; Pan, C.; Tuggle, D. W. *Applied Physics a-Materials Science & Processing* **2004,** *78*, 9-14.

(21) Cui, H. T.; Yang, X. J.; Simpson, M. L.; Lowndes, D. H.; Varela, M. *Appl. Phys. Lett.* **2004,** *84,* 4077-4079.

(22) Hofmann, S.; Ducati, C.; Robertson, J.; Kleinsorge, B. *Applied Physics Letters* **2003,** *83,* 135-137.

(23) Hofmann, S.; Kleinsorge, B.; Ducati, C.; Ferrari, A. C.; Robertson, J. *Diamond and Related Materials* **2004,** *13,* 1171-1176.

(24) Hofmann, S.; Kleinsorge, B.; Ducati, C.; Robertson, J. *New Journal of Physics* **2003,** *5*.

(25) Boskovic, B. O.; Golovko, V. B.; Cantoro, M.; Kleinsorge, B.; Chuang, A. T. H.; Ducati, C.; Hofmann, S.; Robertson, J.; Johnson, B. F. G. *Carbon* **2005,** *43,* 2643-2648.

(26) Klein, K. L.; Melechko, A. V.; McKnight, T. E.; Retterer, S. T.; Rack, P. D.; Fowlkes, J. D.; Joy, D. C.; Simpson, M. L. *Journal of Applied Physics* **2008,** *103*.

(27) Melechko, A. V.; Merkulov, V. I.; McKnight, T. E.; Guillorn, M. A.; Klein, K. L.; Lowndes, D. H.; Simpson, M. L. *Journal of Applied Physics* **2005,** *97,* Art. No. 041301.

(28) Tan, E. P. S.; Goh, C. N.; Sow, C. H.; Lim, C. T. *Appl. Phys. Lett.* **2005,** *86,* -.

(29) Tan, E. P. S.; Lim, C. T. *Composites Science and Technology* **2006,** *66,* 1102-1111.

(30) Qi, H. J.; Teo, K. B. K.; Lau, K. K. S.; Boyce, M. C.; Milne, W. I.; Robertson, J.; Gleason, K. K. *Journal of the Mechanics and Physics of Solids* **2003,** *51,* 2213-2237.

(31) Guillorn, M. A.; Melechko, A. V.; Merkulov, V. I.; Ellis, E. D.; Britton, C. L.; Simpson, M. L.; Lowndes, D. H.; Baylor, L. R. *Applied Physics Letters* **2001,** *79,* 3506-3508.

(32) Guillorn, M. A.; Melechko, A. V.; Merkulov, V. I.; Ellis, E. D.; Simpson, M. L.; Baylor, L. R.; Bordonaro, G. J. In *Microfabricated field emission devices using carbon nanofibers as cathode elements*, Washington, D.C., May 29-Jun 01; Washington, D.C., 2001; pp 2598-2601.

(33) Guillorn, M. A.; Melechko, A. V.; Merkulov, V. I.; Hensley, D. K.; Simpson, M. L.; Lowndes, D. H. *Applied Physics Letters* **2002,** *81,* 3660-3662.

(34) Guillorn, M. A.; Simpson, M. L.; Bordonaro, G. J.; Merkulov, V. I.; Baylor, L. R.; Lowndes, D. H. *Journal of Vacuum Science & Technology B* **2001,** *19,* 573-578.

(35) Guillorn, M. A.; Yang, X.; Melechko, A. V.; Hensley, D. K.; Hale, M. D.; Merkulov, V. I.; Simpson, M. L.; Baylor, L. R.; Gardner, W. L.; Lowndes, D. H. *Journal of Vacuum Science & Technology B* **2004,** *22,* 35-39.

(36) McKnight, T. E.; Melechko, A. V.; Austin, D. W.; Sims, T.; Guillorn, M. A.; Simpson, M. L. *Journal of Physical Chemistry B* **2004,** *108,* 7115-7125.

(37) McKnight, T. E.; Melechko, A. V.; Griffin, G. D.; Guillorn, M. A.; Merkulov, V. I.; Serna, F.; Hensley, D. K.; Doktycz, M. J.; Lowndes, D. H.; Simpson, M. L. *Nanotechnology* **2003,** *14,* 551-556.

(38) McKnight, T. E.; Melechko, A. V.; Fletcher, B. L.; Jones, S. W.; Hensley, D. K.; Peckys, D. B.; Griffin, G. D.; Simpson, M. L.; Ericson, M. N. *Journal of Physical Chemistry B* **2006,** *110,* 15317-15327.

(39) Yu, Z.; McKnight, T. E.; Ericson, M. N.; Melechko, A. V.; Simpson, M. L.; Morrison, B. *Nano Letters* **2007,** *7,* 2188-2195.

(40) McKnight, T. E.; Melechko, A. V.; Griffin, G. D.; Simpson, M. L. *In Vitro Cellular & Developmental Biology-Animal* **2006,** *42,* 17a-17a.

(41) McKnight, T. E.; Melechko, A. V.; Hensley, D. K.; Mann, D. G. J.; Griffin, G. D.; Simpson, M. L. *Nano Letters* **2004,** *4,* 1213-1219.

(42) Baylor, L. R.; Lowndes, D. H.; Simpson, M. L.; Thomas, C. E.; Guillorn, M. A.; Merkulov, V. I.; Whealton, J. H.; Ellis, E. D.; Hensley, D. K.; Melechko, A. V. *Journal of Vacuum Science & Technology B* **2002,** *20,* 2646-2650.

(43) Dhindsa, M. S.; Smith, N. R.; Heikenfeld, J.; Rack, P. D.; Fowlkes, J. D.; Doktycz, M. J.; Melechko, A. V.; Simpson, M. L. *Langmuir* **2006,** *22,* 9030-9034.

(44) Fletcher, B. L.; McKnight, T. E.; Fowlkes, J. D.; Allison, D. P.; Simpson, M. L.; Doktycz, M. J. *Synthetic Metals* **2007,** *157,* 282-289.

(45) Fletcher, B. L.; Hullander, E. D.; Melechko, A. V.; McKnight, T. E.; Klein, K. L.; Hensley, D. K.; Morrell, J. L.; Simpson, M. L.; Doktycz, M. J. *Nano Letters* **2004,** *4,* 1809-1814.

(46) Zhang, L.; Melechko, A. V.; Merkulov, V. I.; Guillorn, M. A.; Simpson, M. L.; Lowndes, D. H.; Doktycz, M. J. *Appl. Phys. Lett.* **2002,** *81,* 135-137.

(47) Baker, S. E.; Tse, K. Y.; Hindin, E.; Nichols, B. M.; Clare, T. L.; Hamers, R. J. *Chemistry of Materials* **2005,** *17,* 4971-4978.

(48) Baker, S. E.; Tse, K. Y.; Lee, C. S.; Hamers, R. J. *Diam Relat Mater* **2006,** *15,* 433-439.

(49) Li, J.; Ng, H. T.; Cassell, A.; Fan, W.; Chen, H.; Ye, Q.; Koehne, J.; Han, J.; Meyyappan, M. *Nano Letters* **2003,** *3,* 597-602.

(50) Baker, S. E.; Colavita, P. E.; Tse, K. Y.; Hamers, R. J. *Chem Mater* **2006,** *18,* 4415-4422.

(51) Mann, D. G. J.; McKnight, T. E.; Melechko, A. V.; Simpson, M. L.; Sayler, G. S. *Biotechnology and Bioengineering* **2007,** *97,* 680-688.

(52) Melechko, A. V.; McKnight, T. E.; Hensley, D. K.; Guillorn, M. A.; Borisevich, A. Y.; Merkulov, V. I.; Lowndes, D. H.; Simpson, M. L. *Nanotechnology* **2003,** *14,* 1029-1035.

(53) Guillorn, M. A.; McKnight, T. E.; Melechko, A.; Merkulov, V. I.; Britt, P. F.; Austin, D. W.; Lowndes, D. H.; Simpson, M. L. *Journal of Applied Physics* **2002,** *91,* 3824-3828.

(54) McKnight, T. E.; Melechko, A. V.; Guillorn, M. A.; Merkulov, V. I.; Doktycz, M. J.; Culbertson, C. T.; Jacobson, S. C.; Lowndes, D. H.; Simpson, M. L. *Journal of Physical Chemistry B* **2003,** *107,* 10722-10728.

(55) Nguyen-Vu, T. D. B.; Chen, H.; Cassell, A. M.; Andrews, R. J.; Meyyappan, M.; Li, J. *Ieee Transactions on Biomedical Engineering* **2007,** *54,* 1121-1128.

(56) Cui, H.; Kalinin, S. V.; Yang, X.; Lowndes, D. H. *Nano Letters* **2004,** *4,* 2157-2161.

(57) Ye, Q.; Cassell, A.; Liu, H.; Chao, K.-J.; Han, J.; Meyyappan, M. *Nano Letters* **2004,** *4,* 1301-1305.

(58) Chhowalla, M.; Teo, K. B. K.; Ducati, C.; Rupesinghe, N. L.; Amaratunga, G. A. J.; Ferrari, A. C.; Roy, D.; Robertson, J.; Milne, W. I. *Journal of Applied Physics* **2001,** *90,* 5308-5317.

(59) Fowlkes, J. D.; Melechko, A. V.; Klein, K. L.; Rack, P. D.; Smith, D. A.; Hensley, D. K.; Doktycz, M. J.; Simpson, M. L. *Carbon* **2006,** *44,* 1503-1510.

(60) Teo, K. B. K.; Chhowalla, M.; Amaratunga, G. A. J.; Milne, W. I.; Pirio, G.; Legagneux, P.; Wyczisk, F.; Olivier, J.; Pribat, D. *Journal of Vacuum Science & Technology B* **2002,** *20,* 116-121.

(61) Teo, K. B. K.; Hash, D. B.; Lacerda, R. G.; Rupesinghe, N. L.; Bell, M. S.; Dalal, S. H.; Bose, D.; Govindan, T. R.; Cruden, B. A.; Chhowalla, M.; Amaratunga, G. A. J.; Meyyappan, J. M.; Milne, W. I. *Nano Letters* **2004,** *4,* 921-926.

(62) Denysenko, I.; Ostrikov, K. *J. Phys. D-Appl. Phys.* **2009,** *42,* 12.

(63) Fletcher, B. L.; McKnight, T. E.; Melechko, A. V.; Hensley, D. K.; Thomas, D. K.; Ericson, M. N.; Simpson, M. L. *Advanced Materials* **2006,** *18,* 1689-+.

(64) Boskovic, B. O.; Stolojan, V.; Khan, R. U. A.; Haq, S.; Silva, S. R. P. *Nature Materials* **2002,** *1,* 165-168.

(65) Hofmann, S.; Ducati, C.; Kleinsorge, B.; Robertson, J. *Applied Physics Letters* **2003,** *83,* 4661-4663.

(66) Arumugam, P. U.; Chen, H.; Siddiqui, S.; Weinrich, J. A. P.; Jejelowo, A.; Li, J.; Meyyappan, M. *Biosensors and Bioelectronics* **2009,** *24,* 2818-2824.

(67) Siddiqui, S.; Arumugam, P. U.; Chen, H.; Li, J.; Meyyappan, M. *ACS Nano* **2010,** *4,* 955-961.

(68) Koehne, J. E.; Chen, H.; Cassell, A. M.; Ye, Q.; Han, J.; Meyyappan, M.; Li, J. *Clin Chem* **2004,** *50,* 1886-1893.

(69) Cassell, A. M.; Li, J.; Stevens, R. M. D.; Koehne, J. E.; Delzeit, L.; Ng, H. T.; Ye, Q.; Han, J.; Meyyappan, M. *Applied Physics Letters* **2004,** *85,* 2364-2366.

(70) de Asis, E.; Nguyen-Vu, T.; Arumugam, P.; Chen, H.; Cassell, A.; Andrews, R.; Yang, C.; Li, J. *Biomedical Microdevices* **2009,** *11,* 801-808.

(71) Caughman, J. B. O.; Baylor, L. R.; Guillorn, M. A.; Merkulov, V. I.; Lowndes, D. H.; Allard, L. F. *Applied Physics Letters* **2003,** *83,* 1207-1209.

(72) Merkulov, V. I.; Melechko, A. V.; Guillorn, M. A.; Lowndes, D. H.; Simpson, M. L. *Chemical Physics Letters* **2001,** *350,* 381-385.

(73) Merkulov, V.; Melechko, A. V.; Guillorn, M. A.; Lowndes, D. H.; Simpson, M. L. *Chemical Physics Letters* **2002,** *361,* 492-498.

(74) Merkulov, V. I.; Hensley, D. K.; Melechko, A. V.; Guillorn, M. A.; Lowndes, D. H.; Simpson, M. L. *Journal of Physical Chemistry B* **2002,** *106,* 10570-10577.

(75) Guillorn, M. A.; Melechko, A. V.; Merkulov, V. I.; Ellis, E. D.; Simpson, M. L.; Baylor, L. R.; Bordonaro, G. J. *Journal of Vacuum Science & Technology B* **2001,** *19,* 2598-2601.

(76) Merkulov, V. I.; Melechko, A. V.; Guillorn, M. A.; Lowndes, D. H.; Simpson, M. L. *Applied Physics Letters* **2002,** *80,* 476-478.

(77) Teo, K. B. K.; Chhowalla, M.; Amaratunga, G. A. J.; Milne, W. I.; Hasko, D. G.; Pirio, G.; Legagneux, P.; Wyczisk, F.; Pribat, D. *Applied Physics Letters* **2001,** *79,* 1534-1536.

(78) Yang, X. J.; Guillorn, M. A.; Austin, D.; Melechko, A. V.; Cui, H. T.; Meyer, H. M.; Merkulov, V. I.; Caughman, J. B. O.; Lowndes, D. H.; Simpson, M. L. *Nano Letters* **2003,** *3,* 1751-1755.

(79) Cui, H.; Yang, X.; Meyer, H. M.; Baylor, L. R.; Simpson, M. L.; Gardner, W. L.; Lowndes, D. H.; An, L.; Lui, J. *Journal of Materials Research* **2005,** *20*.

(80) Klein, K. L.; Melechko, A. V.; Rack, P. D.; Fowlkes, J. D.; Meyer, H. M.; Simpson, M. L. *Carbon* **2005,** *43*, 1857-1863.

(81) Merkulov, V. I.; Melechko, A. V.; Guillorn, M. A.; Lowndes, D. H.; Simpson, M. L. *Appl. Phys. Lett.* **2001,** *79*, 2970-2972.

(82) Merkulov, V. I.; Melechko, A. V.; Guillorn, M. A.; Simpson, M. L.; Lowndes, D. H.; Whealton, J. H.; Raridon, R. J. *Applied Physics Letters* **2002,** *80*, 4816-4818.

(83) Helveg, S.; Lopez-Cartes, C.; Sehested, J.; Hansen, P. L.; Clausen, B. S.; Rostrup-Nielsen, J. R.; Abild-Pedersen, F.; Norskov, J. K. *Nature* **2004,** *427*, 426-429.

(84) Vasenkov, A. V. *Journal of Computational and Theoretical Nanoscience* **2008,** *5*, 48-55.

(85) Moser, J.; Panepucci, R.; Huang, Z. P.; Li, W. Z.; Ren, Z. F.; Usheva, A.; Naughton, M. J. *Journal of Vacuum Science & Technology B* **2003,** *21*, 1004-1007.

(86) Retterer, S. T.; Melechko, A.; Hensley, D. K.; Simpson, M. L.; Doktycz, M. J. *Carbon* **2008,** *46*, 1378-1383.

(87) Klein, K. L.; Melechko, A. V.; Fowlkes, J. D.; Rack, P. D.; Hensley, D. K.; Meyer, H. M.; Allard, L. F.; McKnight, T. E.; Simpson, M. L. *Journal of Physical Chemistry B* **2006,** *110*, 4766-4771.

(88) Guillorn, M. A.; Ilic, B.; Melechko, A. V.; Merkulov, V. I.; Lowndes, D. H.; Simpson, M. L. Cantilever structure e.g. chemical force microscope tip, fabricating method for use in scanning probe microscope, involves transferring outline of relieved volume from

mask layer into substrate to remove volume from substrate. US2005103993-A1; US7151256-B2, US2005103993-A1 19 May 2005 G12B-021/02 200541.

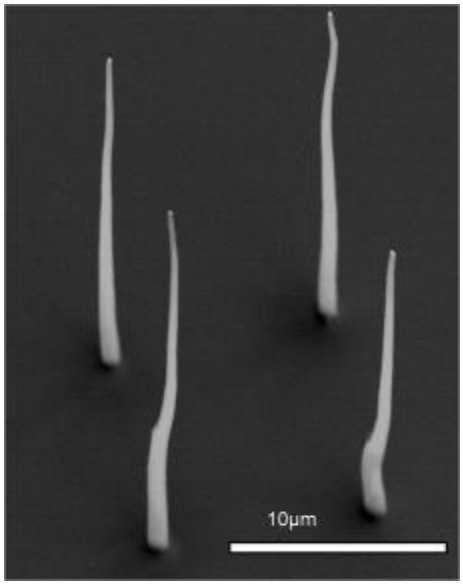

Figure 2.1: SEM micrograph of vertically aligned carbon nanofibers synthesized by catalytic DC PECVD on thin metal film coating 1 μm thin SiO_2. [36]

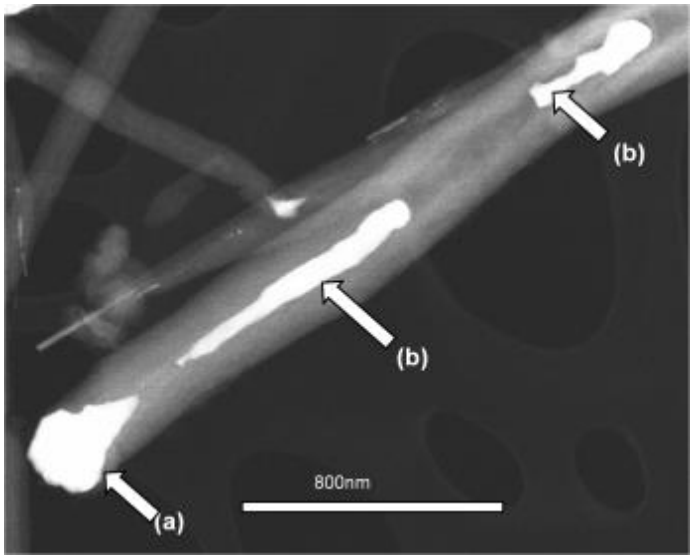

Figure 2.2: Scanning transmission electron micrograph (Z-contrast mode) of VACNFs with Ni nanoparticle distributed along the length during growth. Arrows point to Ni (a) catalyst nanoparticle directing nanofiber growth, (b) portions of catalyst nanoparticle that got detached from the nanoparticle. [17]

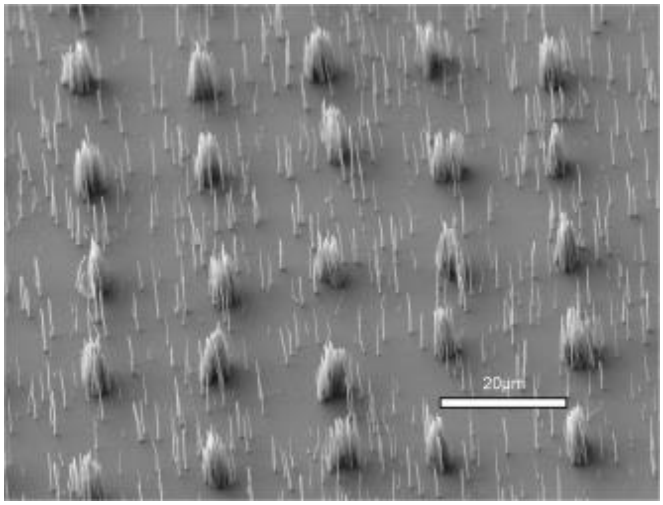

Figure 2.3: SEM image of VACNFs at the lighthraphically defined sites (dense bunches) and in between produced by catalyst material redistributed by plasma ("spluttered").

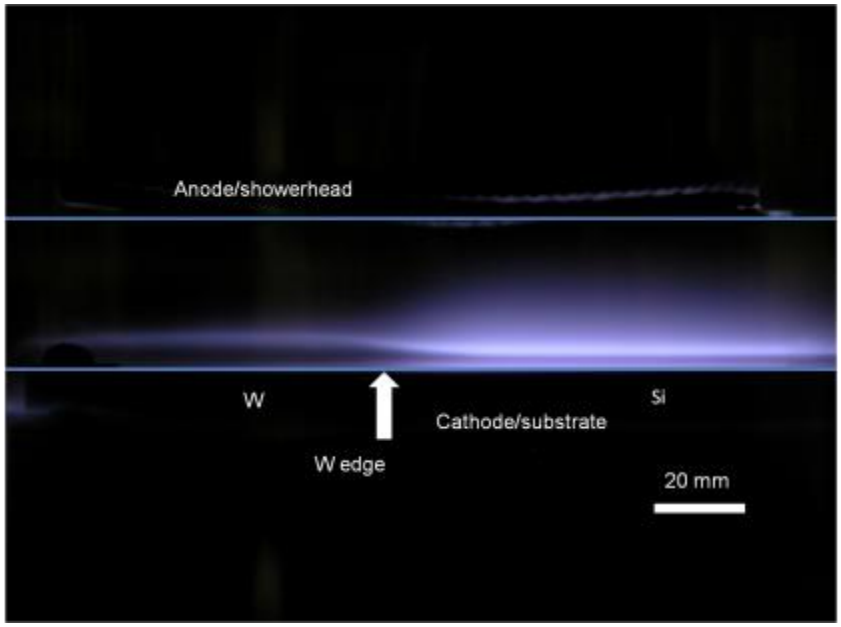

Figure 2.4: A photograph of the glow discharge over a 100 mm diameter Si wafer with a half (left side) coated by 100 nm W. The difference in a size of dark field and glow intensity above W (left) and Si (right) is notable.

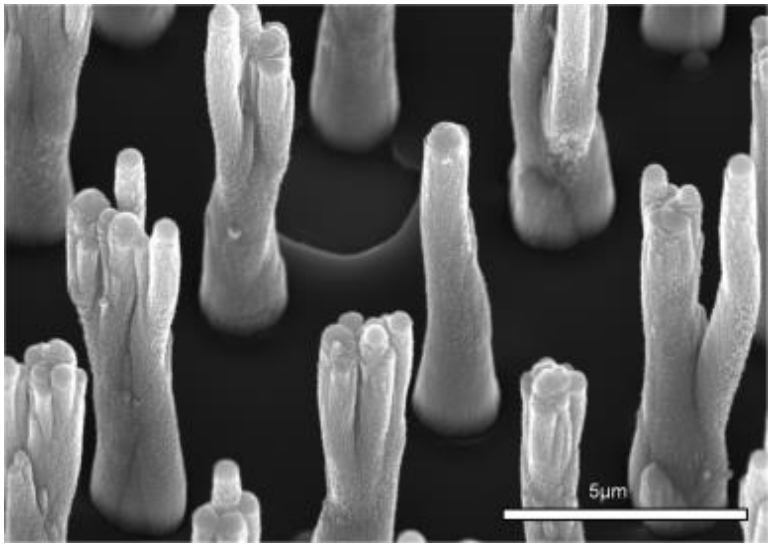

Figure 2.5: SEM micrograph of an array of VACNF coated by a thick non catalytic carbon due to change in plasma chemistry produced by growth of the VACNFs.

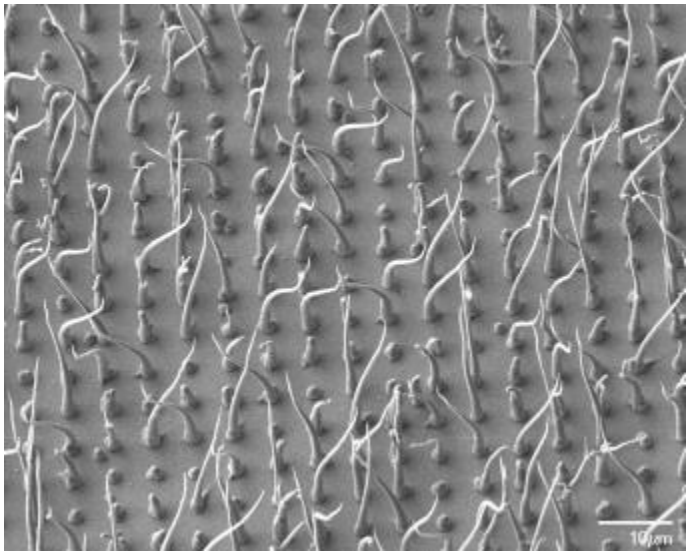

Figure 2.6: SEM micrograph of VACNFs grown on Si substrate. The cause of the loss of alignment is unknown.

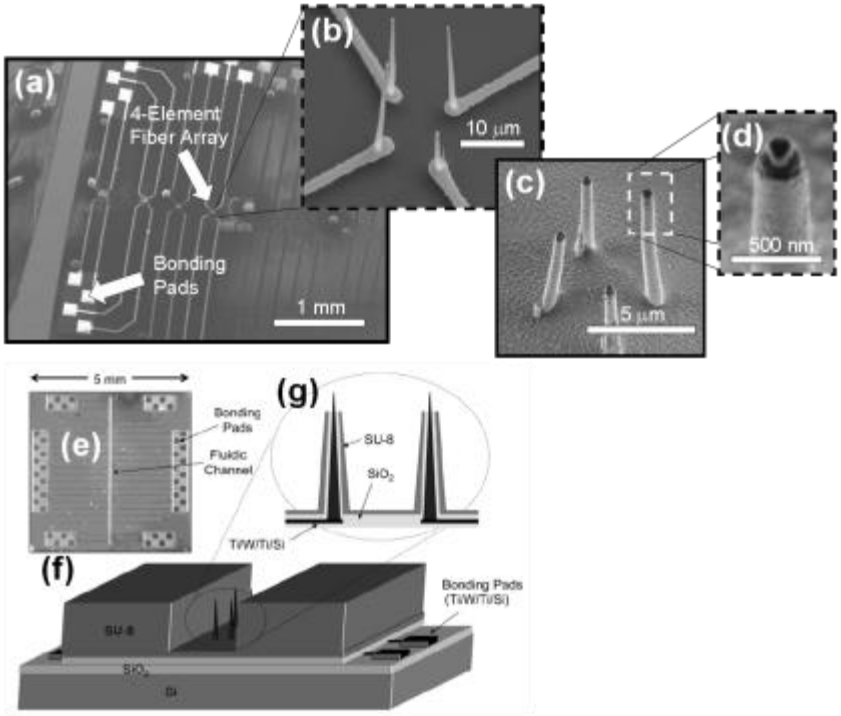

Figure 2.7: A series of SEM micrographs and a schematic illustrating some of the critical aspects of a VACNF intracellular probe array (see text for details). Reproduced with permission from [36]. Copyright 2004, American Chemical Society.

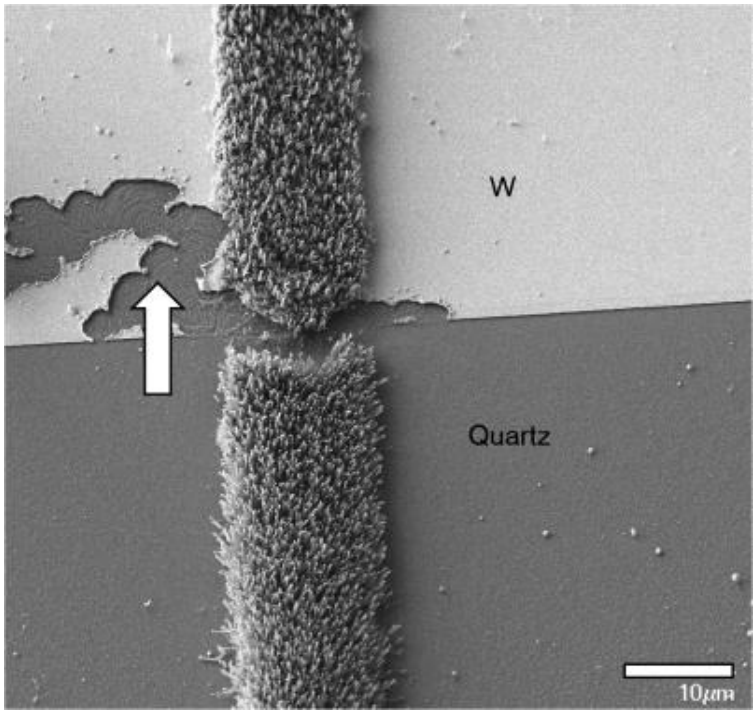

Figure 2.8: SEM micrograph (viewed at 30° of normal) of a damaged to thin film metallization (W on quartz) caused by a running electrical arc indicated by an arrow. A stripe of VACNFs traverses the image vertically.

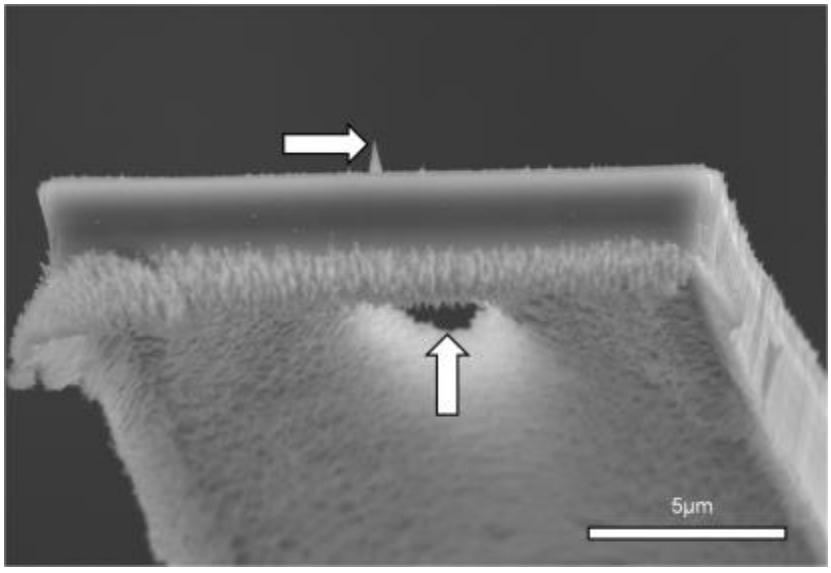

Figure 2.9: SEM micrograph of a cantilever with a VACNF tip (arrow at the top) for high aspect ratio atomic force microscopy. While growth conditions are near optimal for VACNF growth, the silicon cantilever gets an etch through (bottom arrow pointing the hole through). Higher electrical fields at the cantilever surface compared to flat substrates and higher thermal load due to cantilever isolation lead to this damage. [88]

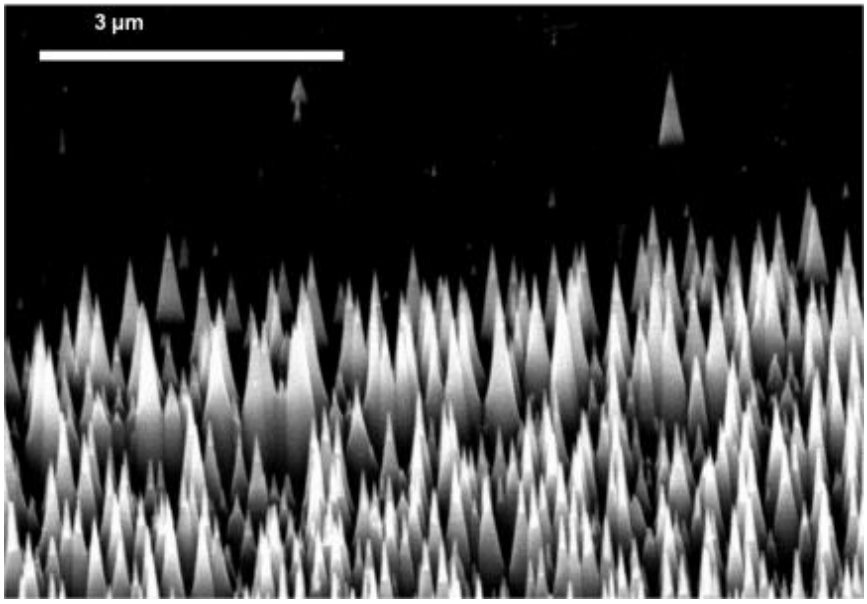

Figure 2.10: SEM micrograph of silicon nanocones created by DC plasma of acetylene/ammonia mixture. Copper film covering a lower portion of this image got dewetting into nanoparticles that assembled in to etch mask. Copper presence enhanced Si removal rate by orders of magnitude leaving Si cones at the conditions that would only remove a few tens of nanometers.

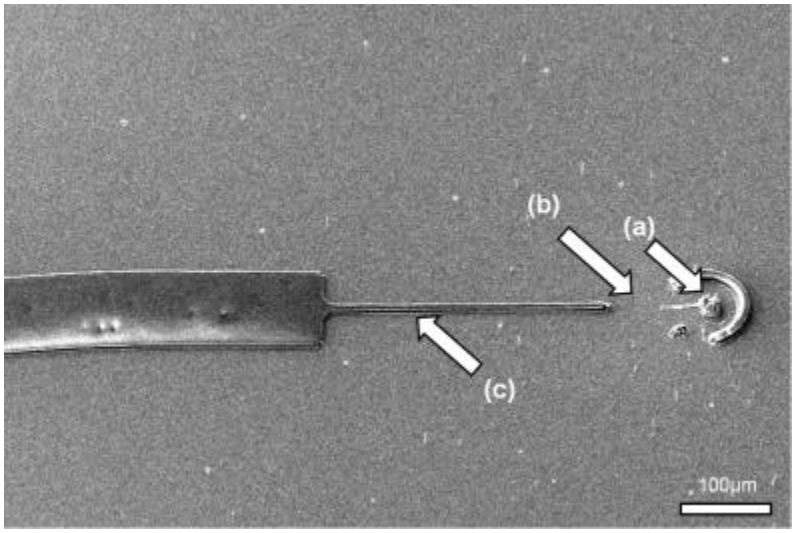

Figure 2.11: Electron micrograph of photoresist after development defining electrical contacts to VACNF electrodes in the center (a). The leads are interrupted (b) due to nonuniformity of photoresist height caused by presence of VACNFs during spinning of photoresist.

Chapter 3 - Vertically Aligned Carbon Nanofibers for Biointerfacing

This work has previously appeared in Pearce, R.C.; McKnight, T.E.; Melechko, A.V. "Biosensors Based on Nanomaterials and Nanodevices" Ch. 12 edited by Jun Li and Nick Wu.

VACNFs are quasi-one-dimensional nanostructures with unique physical and electrical properties, owing to their unique morphology, separate from carbon nanotubes. These properties, such as chemical robustness, high electrical conductivity, and high mechanical strength make VACNFs ideal for interfacing with living systems. VACNFs have been used for a variety of biological applications such as cellular transfection, neuronal interfacing, and biosensing. A key aspect of VACNF viability for biointerfacing and biosensing is control of the placement, morphology, and alignment of the fibers. This chapter will cover VACNF synthesis, explore integration with live systems, and discuss challenges and future prospects for VACNF applications.

3.1 Introduction

Vertically aligned carbon nanofibers, stacked cylinders of graphitic carbon, possess many properties that make them attractive structures for implementation as interfaces to biological systems on a cellular level or subcellular level. Their geometric dimensions, from tens to hundreds of nanometers in diameter, and from a few hundred nanometers to a hundred micrometers long, along with their mechanical properties facilitates their use as nanoneedles, suitable for insertion into tissue or single cells. Their electrical conductivity renders them suitable as nanoelectrodes. The electron transfer rates at the sidewall surfaces makes VACNFs suitable for electrochemical probes. The exposed graphitic edge planes of VACNFs have been shown to exhibit ~30 times better capacitance and orders of magnitude better electron transfer rates than carbon basal planes, which are present in CNTs.[1, 2] Finally, the surface of VACNFs is amenable to a range of chemistries that allow their functionalization with desirable chemical- or biochemical- species.

In biosensing both selectivity, i.e. the ability to distinguish between molecular species, and sensitivity, i.e. the signal amplitude, are important for signal detection. The selectivity of graphitic carbon can be achieved in two ways. The first is two use carbon nanostructures as electrochemical probes where selectivity is achieved via observation of a distinct signature in electrochemical spectra (redox). The second route is to utilize surface chemistry of graphitic carbon in enhancing sensitivity via attachment of biomolecules. Utilization of nanostructures can directly enhance sensitivity via increase in surface area. However, this route typically involves use of large numbers of nanostructures, such as a

forest of carbon nanofibers [3]. If individual nanostructures are used, signals can be very small. However, this drawback is traded for another advantage of using nanostructures as highly localized probes. In this case each individual nanostructure is connected to one channel of the measurement system. When interfacing to a single cell with a carbon nanofiber, such a local probe can provide access to one billionth of a volume of a cell. In this chapter we explore another modality of using carbon nanofibers in biointerfacing, i.e. via mechanical properties. Since VACNFs are extremely sharp needles with subcellular dimensions they can be inserted inside a cell. With proper insulation a nanofiber can serve as an intracellular electrochemical probe. Alternatively it can serve as a delivery vehicle of biochemical functionality if its surface is coated with biomolecules. One particular application of such biointerfacing is gene delivery. In this case, DNA coding for a particular exogenous gene is attached to a nanofiber surface and then inserted inside a cell nucleus.

3.2 Biochemical Functionalization of VACNFs

The ability to attach biologically-active molecules to VACNFs in a controlled fashion is critical to many of their biological applications. In this section, the attachment chemistry for DNA, proteins, and antibodies will be discussed. The fibers frequently undergo some form of surface treatment prior to any attachment. One example of a common pretreatment for VACNFs is a wet etch or an oxygen plasma etch, the result of which is production of COO^- groups on the surface, which can then be further modified with carbodiimide chemistry. The presence of native H groups on the fiber surfaces allows for electrochemical or photochemical reactions to produce COO^- or amine terminated surfaces which can be

useful with various crosslinking or adsorption strategies. The biochemicals that fibers are most commonly functionalized with are DNA, proteins, and antibodies. A few functionalization strategies that have been previously used will be discussed for each of these biochemicals.

3.2.1 DNA Functionalization

There are a number of strategies for attachment of DNA to VACNFs. Baker et al have two methods of attachment that they have compared.[4] The first relies on a photochemical reaction between the nanofibers and linker molecules that have terminal olefin groups in addition to a protected amine group. A subsequent reaction results in a free primary amine which is then attached to a thio-terminated oligonucleotide. In the second approach, a reaction between an aryldiazonium salt with the fibers is followed by an electrochemical reduction to the primary amine which is linked to thio-terminated DNA oligonucleotides. Comparatively, the diazonium approach links amino groups to nanofibers via an aromatic ring, while the photochemical method generally links through an alkyl chain. The diazonium functionalization also allows for electrically addressable functionalization by selectively reducing the nitro group to an amino under electrochemical control.

After amino group attachment, thio-modified DNA can be linked covalently to the fibers. This addressable functionalization has been demonstrated by modifying discrete VACNF forest electrodes with two separate DNA probe sequences. The selectivity of hybridization that resulted from the different implementation methods was established through hybridization studies using complementary and non-complementary DNA.

Quantitative measurements of the amount of DNA that hybridized to DNA attached to VACNFs were done using fluorescence measurements and fluorescence wash-off methods. Baker *et al* found an eightfold increase in DNA attachment to VACNFs as opposed to the underlying planar footprint.[4] Other DNA attachment schemes have also been developed.[5, 6]

3.2.2 Protein and Antibody Functionalization

Several attachment chemistries have been used for protein functionalization of VACNFs. The simplest of these methods relies on biotin/avidin affinity. In one study, Baker *et al* had avidin (50Å diameter) bind to biotin (1 nm) which was then attached to VACNFs via a disulfide bond-bearing linker.[4] McKnight *et al* used a slightly different biotin/avidin attachment chemistry, starting with a carboiimide cross-linking reaction to covalently bond gold-conjugated streptavidin to VACNFs.[7] Baker *et al* have also functionalized VACNFs with the protein cytochrome c (cyt c).[8] **Figure 3.1** shows their approach schematically. The results of this study suggest that proteins can retain their functionality, post-functionalization. It has also been shown by Naguib *et al* that phycoerythrin conjugated anti-CD3 antibodies can be adsorped onto pyrolitically stripped CNFs and that protein adsorption can be drastically increased through pretreatment with poly-L-lysine.[9]

It should be noted that the VACNF surface does not remain unchanged over time. It is speculated that the atoms on the edge planes of the fibers are hydrogen terminated immediately after growth in a highly reducing hydrogen environment, but that over time in ambient conditions these sites may degrade. This information is relevant to functionalization

as Baker *et al* reported that the functionalization yield of VACNFs exposed to ambient for extended periods is decreased.

Functionalization of VACNFs extends beyond DNA, proteins, and antibodies. There are many molecules of biological relevance that can be attached to VACNF surfaces through traditional carbon chemistry strategies. It has also been demonstrated that click chemistry can applied to VACNFs, with large potential for biological applications.[10]

3.3 Cellular Interfacing of VACNFs for Gene/Material Delivery

Gene delivery to individual mammalian cells via a physical impalement process was one of the earliest demonstrations of VACNF utility in biointerfacing [11]. The aspect ratio of a VACNF is similar to the extreme tip of conventional, pulled-glass microcapillaries, with a 10-20 micron long nanofiber having a submicron base diameter and a tip diameter typically less than 100 nm. As with microinjection pipettes, the sharp tip and high aspect ratio enables the nanofiber to penetrate into the interior of a eukaryotic cell using a variety of techniques, and to deliver either physisorbed or covalently linked cargo during the penetration event (**Figure 3.2**). One of the earliest demonstrations achieved cellular penetration and delivery of an impermeant dye via a centrifugation process, whereby a VACNF array was positioned within a microcentrifuge tube such that the nanofibers were positioned to impale cells as they were pelleted from suspension. Subsequent developments have simplified the approach, whereby small chips of nanofiber arrays are first modified with molecular cargo and then pressed into pellets of suspended cells, fragments of intact tissue, and even directly into intact tissue [12]. As with microinjection, a sharp, impulsive process is typically required to achieve

intracellular/intranuclear penetration. Unlike microinjection, however, arrays of nanofibers alleviate the necessity of microscopic visualization of the process, as the array density can be such that every cell encounters one or several nanofiber spikes (**Figure 3.2**).

Gene delivery via this impalement process has been demonstrated with both physisorbed- and covalently linked DNA immobilization strategies. For the former, DNA is suspended in water, or stabilizing buffer solutions at very low concentration, and dispensed and dried onto small 'chips' of VACNF arrays, typically at coverages of between 1-20 ng/um^2 . Choice of solvent is important, as conventional DNA stabilizing solutions such as 1X tris-edta (TE) will produce solid crystals during the drying process, the presence of which diminishes the ability of the deployed chip to effectively interact with individual cells and to achieve nanofiber intracellular residence. DNA modified chips are then prewetted immediately before cellular interfacing and pressed into pellets of cells or tissue.

Covalent strategies have also been demonstrated for effective gene delivery. Here, DNA is tethered to the nanofiber using a variety of strategies as outlined above. Early examples used a carbodiimide coupling to link plasmid DNA to nanofibers putatively via DNA-guanine amines and carboxylic acid sites native or generated upon the nanofiber surface. Subsequent methods have demonstrated effective gene expression from linear fragments of DNA generated using either restriction digest or PCR with high fidelity polymerases and primers chosen to provide coupling affinity to the nanofiber surface [6, 13]. This includes amine-terminated primers, for carbodiimide coupling, biotin-terminated fragments for binding to streptavidin-modified nanofibers, and the incorporation of disulfide

linkages to promote intracellular release of the bound DNA fragment via reduction of the disulfide bridge.

Chip planarity is an important consideration for cellular and tissue interfacing. Conventionally, nanofibers are grown on a Silicon wafer as vertical elements upon an otherwise planar, solid substrate. To promote handling, the silicon wafer is diced into small chips with a single, 100-mm diameter wafer yielding hundreds to thousands of millimeter scale gene delivery devices. The size of these chips is arbitrary, but the planarity of the resultant structure must be considered as the nanofibers only extend tens of microns from the surface. The target surface of tissue or a pellet of cells must therefore be very compliant, such that the nanofiber elements across the expanse of the chip can extend into the tissue across the expanse of tissue in order to deliver their cargo intracellularly. The surface of the chip must also be clear of debris and micro-/macroscopic contaminants. Dust particles, debris remaining from the dicing process, and other solid particulates can keep large regions of the chip from interacting with targeted tissue. Previous efforts have typically been conducted with chips diced to a size of 2-5 mm on a side. Protective coatings of photoresist can be used during the dicing process such that any debris generated from the process can be lifted off using conventional photoresist solvents, such as acetone/isopropanol/water or n-methyl pyrrolidone/water washes. The protective layer of photoresist may be patterned such that DNA solutions placed on the chips prior to photoresist liftoff are adsorbed or covalently attached only in localized regions of the chip [7] . Post-liftoff handling of the chips must be conducted in a way that minimizes accumulation of solid particulates prior to the cellular

interfacing event. For example, as mentioned above, the solvent of DNA spotting solutions must be chosen to avoid the formation of large solid crystals of the solvent solution during the drying process. For this reason, conventional strength DNA buffering solutions such as 1x tris-edta (TE), should be avoided. Lower concentrations of TE can be used, as can pure water, with the recognition that these solutions should not be used for long term storage of the DNA prior to experimentation, as they will result in hydrolytic decomposition of the DNA and reduced expression efficiency. By contrasting argument, it should be noted that once DNA is dried onto the array, it can remain active and intact for long periods of time provided it remains dark and dry, similar to long term storage of DNA as dried spots on blotter paper. DNA-modified nanofiber arrays thus provide a unique opportunity as a 'reagentless' gene delivery method. All that is required for transgene expression is removal of the DNA-spotted array from dry storage and integration of the array with targeted cells or tissue.

One of the more effective methods for interfacing cultured cells onto nanofiber arrays employs a solid pellet of a cellular suspension as the interfacing target. Here, adherent cells are passed using conventional trypsination or chelation methods to release the adherent cell layer, and the resultant cell suspension is spun in a swinging bucket centrifuge to form a pellet. This pellet is then carefully dislodged from the centrifuge tube, and dispensed onto a concavity slide under a small volume of media. DNA-modified nanofiber arrays can be pressed directly into the pellet to achieve cellular penetration and gene delivery. When using planar, silicon-based nanofiber arrays, the concavity slide presents a surface which does not

allow the cell pellet to be completely sandwiched beneath the nanofiber array. Rather, cells within the pellet are impaled and loose enough with respect to one another to come away with the chip when the chip is withdrawn from the pellet. A subsequent wash step, whereby the chip is agitated in fresh media serves to remove the bulk of unpenetrated cells, leaving behind a monolayer of cells impaled upon the chip surface. Subsequent culture of the chip results in very rapid transgene expression, due to a high potential for nuclear penetration of the nanofiber and its DNA cargo during the penetration event. Using timelapse fluorescent microscopy of cells impaled upon a nanofiber array spotted with the pd2eYFP-n1 plasmid, Hensley reported visual fluorescence of transgene yellow fluorescent protein within 55 minutes of the impalement event [14].

Flexible films of nanofiber arrays have been developed as an interface capable of interacting with large areas of non-planar tissue. By embedding the nanofibers in a thin film of ultraviolet crosslinked epoxy, Fletcher demonstrated that intact arrays of vertically-aligned nanofibers could be peeled from their silicon growth substrate and remained freestanding and vertical within the flexible epoxy film [15]. Further development of this approach, using a variety of spun-cast, vapor-deposited, or dimerization deposition techniques is anticipated to provide flexible films of nanofibers with tailored mechanical properties for a variety of tissue interfacing applications.

While it is not too surprising that carbon nanofibers are capable of penetrating soft mammalian tissues or cells in a cell matrix, it has been recently shown that they are sufficiently resilient to cross dermal tissue as well. **Figure 3.3** shows results of impaling pig

skin which has been stripped of stratum corneum. This opens up a possibility of using carbon nanofibers for construction of transdermal sensors.

3.4 VACNF Biosensors

This section will contain case studies of VACNFs that have been implemented as biosensors, combining information from the previous sections to discuss how the fibers were grown, how the device was made, the fibers functionalized, etc.

3.4.1 Ricin Detector

Meyyappan et al recently used a nanoelectrode array (NEA) consisting of VACNFs to detect the protein ricin.[16] Ricin detection is of interest due to its potential use as a bio-warfare agent. The authors bound ricin-A antibody or ricin aptamer to the NEAs to detect the presence of ricin. To create the array, a silicon wafer was coated with 200nm of chromium with 500nm thick thermal oxides, and a 30nm nickel catalyst layer. The fibers were grown as a "forest" using a dc-PECVD system with 125sccm acetylene and 444sccm of ammonia at 4.73 Torr and 180W of power. This recipe resulted in ~3μm tall fibers after a growth time of 15min. This forest of fibers was then completely encapsulated by CVD deposition of SiO_2. Chemical mechanical polishing left a smooth SiO_2 layer and only the tips of the VACNFs protruding from the surface.

After fabrication the chips were chemically activated by a HNO_3 soak followed by a wash with sterile water, which served to introduce –COOH groups for covalent binding of the antibody or aptamer probe for the biosensor. Functionalization with the antibody was

carried out by combining 5µl of ricin-A antibody in 50µl phosphate buffered saline containing 1mM MgCl mixed with a coupling reagent of 0.5 g N-(3-dimethylaminopropyl-N'-ethylcarbodiimide hydrochloride (EDC) and 0.25 mg N-hydroxysulfosuccinimide sodium salt (NHS). This mixture was then placed on the VACNF NEA and incubated at room temperature for two hours. During incubation, the primary amine groups of the Ricin A antibody formed amide bonds with the carboxyl-groups on the VACNF tips. To remove any non-specific binding, the authors performed a stringent wash. The antibody binding and functional activity was evaluated by cyclic voltammetry (CV) and electrochemical impedance spectroscopy (EIS). The capture binding was performed by first incubating the antibody-functionalized chip in ricin protein or collagen, which served as a control protein, mixed with PBS buffer for one hour. The incubation was followed by another rinsing phase. Target capture binding was determined with CV and EIS as well.

To detect the protein using ricin aptamer, an anti-ricin RNA aptamer with a specific sequence in a PBS buffer which contained magnesium chloride was mixed with a coupling reagent consisting of EDC and NHS. This solution was allowed to incubate on the VACNF chip for two hours at 40°C. A stringent wash procedure was followed again to remove the possibility of nonspecific binding. Target binding was performed by incubation of the chip in ricin protein-PBS buffer solution. The control was a nonspecific DNA aptamer. The authors found that the ricin-A antibody probe did not bind sufficiently to the VACNFs, but the aptamer probe was stable and could be regenerated multiple times for a reusable biosensor.

3.4.2 Glucose Biosensor

Glucose is considered to be one of the most important biosignatures due to its use in identifying some bacteria, eukaryotes, and archaea. VACNFs could potentially replace CNTs for glucose biosensors, since VACNFs have better sensitivity and responsiveness to CNTs.[17] Islam et al have created a mediator free amperometric bienzymatic glucose biosensor made with VACNFs that can detect concentrations as low as 0.4μM.[18] The authors use an enzyme wiring technique, which improves the electrical contact between the electrode surfaces and the glucose oxidase, with VACNFs used as the working electrode. Their amperometric bienzymatic glucose biosensor is based on glucose oxidase (GO_x) and horseradish peroxidase (HRP).

Fabrication of the electrode began with creating a ~500nm thick silicon oxide layer on a silicon substrate followed by deposition and patterning of nickel catalyst arrays using photolithography. After growth of the VACNF clusters, a ~200nm thick chromium electrode layer was sputter deposited and patterned to create five individually addressable electrode pads. After fabrication, the wafer was sonicated in sulfuric acid to ensure the cleanliness of the fibers.

The next step is the chemical functionalization of the chips. To do this, the authors used the enzyme wiring technique where they carefully spread just enough HRP and Go_x to cover the entire surface area of the VACNF forest. When this sensor comes in contact with glucose, a reduction to gluconic acid occurs and the resulting current can be detected. HRP has the ability to react with other interfering molecules, but amperometric tests carried out by

the authors revealed that even in the presence of these other molecules glucose can be detected due to its significantly higher response. They conclude that their sensor has a sensitivity of 89.035μA/mM and has a dynamic range of 0.4-40μM.

3.4.3 Ethanol Biosensor

A VACNF biosensor has been made for the detection of ethanol by immobilizing yeast alcohol dehydrogenase (YADH) and its coenzyme on the fibers by Weeks et al.[19] YADH is an oxidoreductase enzyme which catalyzes the following redox reaction:

$$ethanol + NAD^+ \leftrightarrow acetaldehyde + NADH$$

YADH's coenzyme is the oxidized form of adenine dinucleotide NAD^+ which must be bound to the enzyme's active site in order for a reaction to occur. Thus, when ethanol is present to the biosensor, a reaction takes place.

The working electrode containing the nanofibers was created on silicon dioxide. Small regions of the wafer (0.5mm x 0.5mm) had catalyst deposited on them for growth of fiber forests. After dc-PECVD, the fibers were approximately 4 μm tall and 100 nm in diameter. A thin titanium wire lead was connected electrically to the electrode area. Following growth, the fibers were sonicated in sulfuric acid to clean the fibers.

Two different immobilization techniques were used to attach the enzyme and coenzyme to the nanofibers. The first method used was adsorption where the VACNF electrode was first immersed in the solution containing YADH followed by a rinse to remove excess enzyme. Afterwards, the electrode was immersed in a solution of NAD^+ followed by

another rinse. The second method used was covalent bonding through diimide-activated amidation. Reactive intermediates can be formed at the carboxylic acid sites on the nanofibers by 1-ethyl-3-(3-dimethylaminopropyl) carbodiimide (EDAC), which can then couple with amines to form amides. The subsequent reaction was stabilized by N-hydroxysuccinimide (NHS). The electrode was allowed to soak in a mixture of EDAC and NHS with a buffer. After this soak, the electrode was transferred to a solution of YADH, followed by rinsing. The electrode then underwent immersion in NAD^+ and a final rinse.

Drops of 0.1mL of ethanol were introduced into the electrochemical cell every 20s and amperometric measurements were made with both attachment schemes. The results were obtained from electrodes on which the enzyme is adsorbed and covalently attached. The initial current increase seen upon each injection of ethanol slightly overshoots and then approaches a steady state after ~5s. The linear concentration range for the adsorbed electrode was 1.75mM to 10mM while the covalent electrode was 2mM to 8mM. The electrodes were also tested after storage for 1-7 days and it was found that both electrodes only lost 1.5% of electrical current in amperometric analysis after a full week. Reusability tests also showed that after 10 tests the current decreased by 75% and 60% for 20 tests. The study concluded that both electrodes were effective after multiple uses and week-long storage periods.

3.4.4 Neuronal Interfacing

The ability to stimulate and record signals from multiple neurons simultaneously has the potential to increase our understanding of neuronal network physiology. In this section,

several studies using VACNF arrays to record and/or stimulate hippocampal slices will be reviewed.

Zhe Yu et al were the first to report the use of VACNFs for stimulation and extracellular recording of spontaneous and evoked neuroelectrical activity in hippocampal slices.[20] They created a 40-element linear array of VACNFs by insulating n-type silicon wafers with 1µm of silicon dioxide, after which metal buffer layers and 100µm thick, 2µm diameter nickel catalyst pucks with 15µm spacing were patterned and deposited. Each puck resulted in a cluster of nanofibers ~10µm tall after PECVD. Interconnects were then defined lithographically and generated by reactive ion refractory metal etch. A passivation layer was then deposited upon the entire wafer and then removed from the contact pads and the electrode tips. This step was followed by an HF buffered oxide etch to remove the exposed silicon oxide coating from the contact pads and the portion of the nanofibers above the passivation layer. **Figure 3.4** shows optical and SEM micrographs of the VACNF arrays that were used.

Before performing recordings, the VACNF chips were cleaned by an air plasma treatment for 30s before being coated with a poly-L-lysine and laminin in water mixture overnight followed by three water rinses. The hippocampal slices were obtained from a postnatal 8-11 day rat pup and were sectioned to be 400µm thick.

Spontaneous electrical activity of hippocampal slices was recorded by aligning the tissue with the electrode array crossing the hilus of the hippocampus, with electrode 1 of the linear array in the CA3 pyramidal cell layer and electrode 40 in the dentate gyrus (DG)

granule cell layer. Other measurements required various alignments of the slices with the fiber electrodes, which could be reused with multiple tissue slices and alignments. Spontaneous complex spikes were recorded and were easily distinguishable from the background noise of $25\mu V_{rms}$. Nanofibers could also be used to evoke responses by applying current through individual VACNF electrodes and then recording the responses at other electrodes in the linear array.

The authors conclude that the VACNF electrodes are capable of performing the same functions as other micro-electrode arrays (MEAs) despite being much smaller, including having sufficient charge injection capacity to stimulate the tissue. The electrodes were capable of a maximal stimulus of 100µA for 100µs, passing 10nC of charge to the tissue without damaging it. The theoretical maximum charge injection of the VACNF electrodes is $8mC/cm^2$. The VACNF electrodes also have an advantage over planar MEAs due to their ability to penetrate the tissue. Penetration of slices may provide improved means of interrogating the native condition of acute tissue slices rather than requiring extended culture periods required for tissue recovery at the surface of the slice.

In the second study, Nguyen-Vu et al compared the function of a plain VACNF electrode to one coated with polypyrrole. It has been shown that electrically conductive polymer coatings on CNFs can improve the biocompatibility of the electrodes and potentially prevent electrolysis from occurring.[21, 22, 23] The electrodes are fabricated by first defining and depositing the electrode pads and interconnects, followed by deposition of a 30nm thick catalyst layer on the electrode area. The nickel particles left at the tips of the VACNFs after

growth were then removed by a nitric acid etch. The authors then electrochemically deposited polypyrrole using an Autolab potentiostat. They found that the polypyrrole coated arrays were the only electrodes they tested capable of evoking a large amplitude, short duration field potential, with lower latency and able to function at lower voltage, preventing electrolysis. Additionally the polymer coated arrays did not induce a toxic extracellular pH change which were observed with metallic MEAs and unmodified VACNF electrodes.

A follow-up of the Yu study demonstrated VACNF neural interfaces being used to monitor the dynamic behavior of neuronal network activity.[24] Neuronal cells sat randomly on the electrode and some electrode tips were engulfed via endocytosis by the cells, which is thought to be minimally invasive or non-invasive. Paired-pulse facilitation and depression (PPF/D) ratios were generated in the cells by two successive stimuli of equal intensity with different inter-stimulus intervals. PPF/D is an example of short-term neuroplasticity that is thought to be involved with temporal cognitive abilities. These ratios were simultaneously recorded by all the electrodes.

VACNF electrodes are very promising for use in neuronal interfacing since they can record and stimulate signals in and around single cells without any apparent damage. Further the spatial characteristics of both individual nanofiber electrodes, and arrays of these electrodes can provide enhanced spatiotemporal information of tissue response.

3.4.5 Neurotransmitter Sensor

The ability to measure neural transmitter dynamics is critical to further develop our understanding of neural network physiology. Lamprecht et al measured dopamine concentrations in the nanomolar range using VACNF arrays coated with over-oxidized polypyrrole.[25] The dopamine concentration was measured by attaching a small well to a typical nanofiber array through which a constant flow of artificial cerebral spinal fluid was introduced for baseline measurements. After two minutes, artificial cerebral spinal fluid with a known concentration of dopamine was introduced and electrochemical measurements were recorded using a potentiostat and an Ag/AgCl electrode for both the reference and counter electrodes in 3-electrode amperometry mode. The over-oxidized polypyrrole was synthesized on the electrodes by filling the well with KCl and pyrrole and then cycled from 0-1V at 10V/s followed by another 10 cycles while placed in NaOH. This entire process was performed three times for three coats of over-oxidized polypyrrole. The purpose of this coating was to increase the limit of detection of the electrodes due to the high background capacitive current that resulted from the large surface area of the VACNF electrodes. This coating increased the limit of detection from 100nM to 10nM while simultaneously improving the sensitivity from 17.5pA/μM to 57.1pA/μM. It has also been shown in a similar manner that VACNF arrays are sensitive to other easily oxidized neurotransmitters such as norepinephrine and 5-hydroxytyramide.[26]

3.5 Future Challenges and Conclusions

The true potential of vertically aligned carbon nanofibers as elements in biosensor platforms is yet to be fully realized. There are several challenges that have to be overcome in order to make them attractive for large scale sensor manufacturing. The first is the high temperature of catalytic synthesis. Reduction of nanofiber synthesis temperature is essential for in situ growth of nanofibers on substrates that cannot withstand high thermal load, such as plastics and underlying electronics. Among strategies that have been proposed is selective heating of catalyst, for example. The second challenge is control of nanofiber structure and geometry by precisely tuning plasma properties. For example, controlling ion flux without significant power dissipation into the substrate could be of high interest. Further development of spatially controlled functionalization strategies is essential in creating multiplexed sensors in which combinations of signals could significantly enhance selectivity and sensitivity of the sensor. Further developments in integration of VACNFs as microelectrodes require improvements in insulating sheathing. One of the possible solutions lies in utilization of atomic layer deposition and it has yet to be used in formation of such coatings.

3.6 References

(1) Rice, R. J.; Mccreery, R. L. *Anal Chem* **1989,** *61,* 1637-1641.

(2) Robinson, R. S.; Sternitzke, K.; Mcdermott, M. T.; Mccreery, R. L. *J Electrochem Soc* **1991,** *138,* 2412-2418.

(3) McKnight, T. E.; Melechko, A. V.; Guillorn, M. A.; Merkulov, V. I.; Doktycz, M. J.; Culbertson, C. T.; Jacobson, S. C.; Lowndes, D. H.; Simpson, M. L. *Journal of Physical Chemistry B* **2003,** *107,* 10722-10728.

(4) Baker, S. E.; Tse, K. Y.; Hindin, E.; Nichols, B. M.; Clare, T. L.; Hamers, R. J. *Chemistry of Materials* **2005,** *17,* 4971-4978.

(5) Mann, D. G. J.; McKnight, T. E.; Melechko, A. V.; Simpson, M. L.; Sayler, G. S. *Biotechnology and Bioengineering* **2007,** *97,* 680-688.

(6) Peckys, D. B.; de Jonge, N.; Simpson, M. L.; McKnight, T. E. *Nanotechnology* **2008,** *19,* art. 435301.

(7) McKnight, T. E.; Peeraphatdit, C.; Jones, S. W.; Fowlkes, J. D.; Fletcher, B. L.; Klein, K. L.; Melechko, A. V.; Doktycz, M. J.; Simpson, M. L. *Chemistry of Materials* **2006,** *18,* 3203-3211.

(8) Baker, S. E.; Colavita, P. E.; Tse, K. Y.; Hamers, R. J. *Chem Mater* **2006,** *18,* 4415-4422.

(9) Naguib, N. N.; Mueller, Y. M.; Bojczuk, P. M.; Rossi, M. P.; Katsikis, P. D.; Gogotsi, Y. *Nanotechnology* **2005,** *16,* 567-571.

(10) Landis, E. C.; Hamers, R. J. *Chemistry of Materials* **2009,** *21,* 724-730.

(11) McKnight, T. E.; Melechko, A. V.; Griffin, G. D.; Guillorn, M. A.; Merkulov, V. I.; Serna, F.; Hensley, D. K.; Doktycz, M. J.; Lowndes, D. H.; Simpson, M. L. *Nanotechnology* **2003,** *14,* 551-556.

(12) McKnight, T. E.; Melechko, A. V.; Hensley, D. K.; Mann, D. G. J.; Griffin, G. D.; Simpson, M. L. *Nano Letters* **2004,** *4,* 1213-1219.

(13) Peckys, D. B.; Melechko, A. V.; Simpson, M. L.; McKnight, T. E. *Nanotechnology* **2009,** *20,* 145304.

(14) Hensley, D. K.; Melechko, A. V.; Ericson, M. N.; Simpson, M. L.; McKnight, T. E. In *Transparent microarrays of vertically aligned carbon nanofibers as a multimodal tissue interface*, Biomedical Sciences and Engineering Conference (BSEC), 2010, 2010; pp 1-4.

(15) Fletcher, B. L.; McKnight, T. E.; Melechko, A. V.; Hensley, D. K.; Thomas, D. K.; Ericson, M. N.; Simpson, M. L. *Advanced Materials* **2006,** *18,* 1689-+.

(16) Periyakaruppan, A.; Arumugam, P. U.; Meyyappan, M.; Koehne, J. E. *Biosensors and Bioelectronics* **2011,** *28,* 428-433.

(17) Jang, J.; Bae, J.; Choi, M.; Yoon, S. H. *Carbon* **2005,** *43,* 2730-2736.

(18) Islam, A. B.; Tulip, F. S.; Islam, S. K.; Rahman, T.; MacArthur, K. C. *IEEE Sens. J.* **2011,** *11,* 2798-2804.

(19) Weeks, M. L.; Rahman, T.; Frymier, P. D.; Islam, S. K.; McKnight, T. E. *Sensors and Actuators B: Chemical* **2008,** *133,* 53-59.

(20) Yu, Z.; McKnight, T. E.; Ericson, M. N.; Melechko, A. V.; Simpson, M. L.; Morrison, B. *Nano Letters* **2007,** *7,* 2188-2195.

(21) Nguyen-Vu, T. D. B.; Chen, H.; Cassell, A. M.; Andrews, R.; Meyyappan, M.; Li, J. *Small* **2006,** *2,* 89-94.

(22) Nguyen-Vu, T. D. B.; Hua, C.; Cassell, A. M.; Andrews, R. J.; Meyyappan, M.; Jun, L. *Biomedical Engineering, IEEE Transactions on* **2007,** *54,* 1121-1128.

(23) de Asis, E. D.; Nguyen-Vu, T. D. B.; Arumugam, P. U.; Chen, H.; Cassell, A. M.; Andrews, R. J.; Yang, C. Y.; Li, J. *Biomed. Microdevices* **2009,** *11,* 801-808.

(24) Yu, Z.; McKnight, T. E.; Ericson, M. N.; Melechko, A. V.; Simpson, M. L.; Morrison, B. *Nanomed-Nanotechnol* **2012,** *8,* 419-423.

(25) Lamprecht, M. R.; McKnight, T. E.; Ericson, M. N.; Morrison, B. *Northeast Bioengin C* **2010**.

(26) McKnight, T. E.; Melechko, A. V.; Fletcher, B. L.; Jones, S. W.; Hensley, D. K.; Peckys, D. B.; Griffin, G. D.; Simpson, M. L.; Ericson, M. N. *Journal of Physical Chemistry B* **2006,** *110,* 15317-15327.

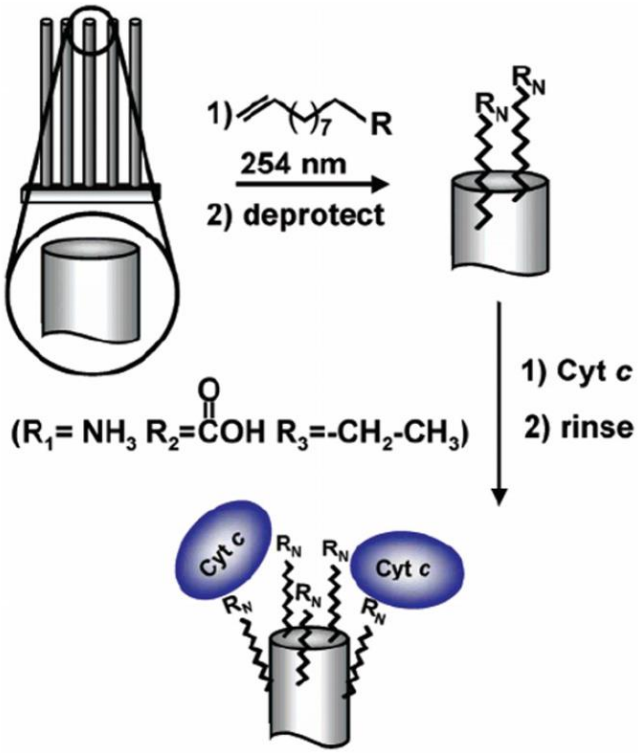

Figure 3.1: A schematic representation of VACNF functionalization with the protein cytochrome c. Adapted from [8]. Copyright 2006, American Chemical Society.

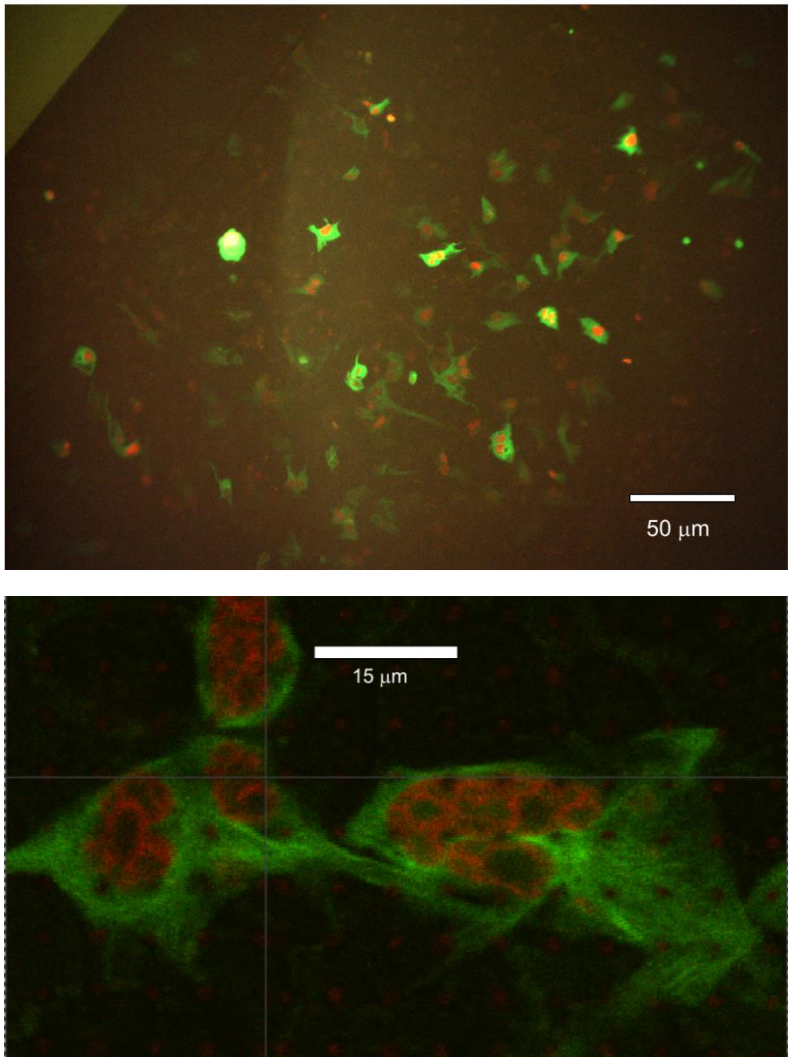

Figure 3.2: Images of impalefected U2OS osteosarcoma cells resident upon a 2.2 mm square VACNF array following multiplexed delivery of plasmids encoding GFP-tubulin and dsRed-monomer H2B. Top: widefield view (100X) with field of view approximately 1/4 of the VACNF array chip. Bottom: Laser scanning confocal micrograph of a 40 micron x 70 micron region showing individual nanofibers as a periodic array of red dots, and the interaction of cytoplasmic GFP-tubulin and nuclear dsRed-H2B with cell-penetrant nanofibers.

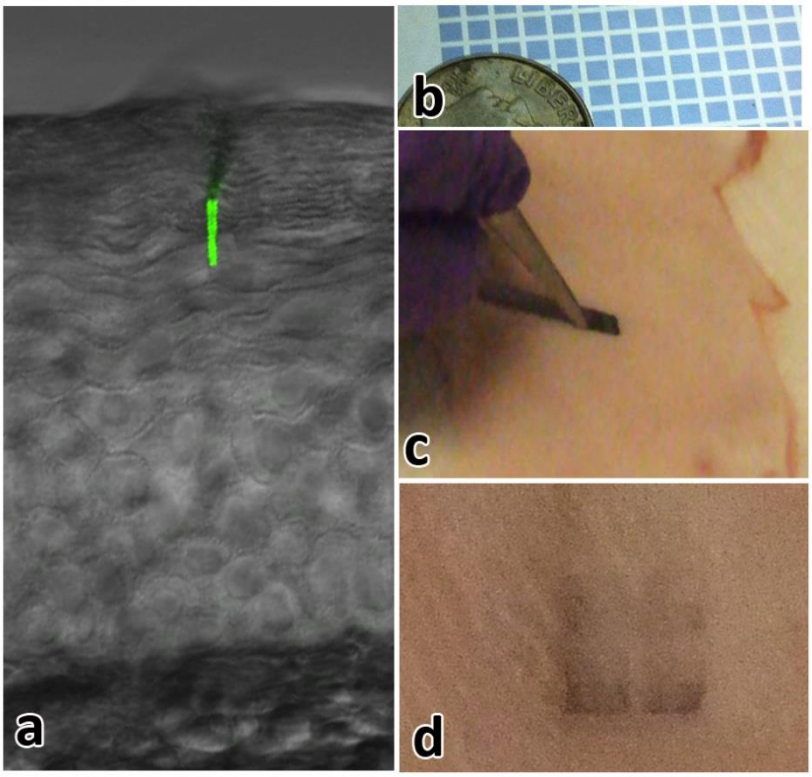

Figure 3.3: Application of an array of nanofibers to porcine skin for gene delivery. (a) A laser scanning confocal micrograph of a nanofiber spanning a portion of epidermis. This nanofiber is 32 um long tilted with respect to a scan slice (its tip pointing out of the plane). Si_3N_4 coating on a nanofiber provides fluorescent label. The tissue is unstained and imaged in DIC mode. The stratum corneum was reduced by tape stripping. (b) A photograph showing a portion of a silicon wafer with nanofiber arrays. (c) A chip with nanofibers (up to 50 um long) is laid down and then repeatedly pressed against a skin slice to insert and leave nanofibers in the tissue (d). The darkness of the squares corresponds to nanofiber density (5 um, 10, 20, and 50 um in periodicity from dark to light). The experiments were performed in collaboration with Dr. Monteiro-Riviere, NCSU.

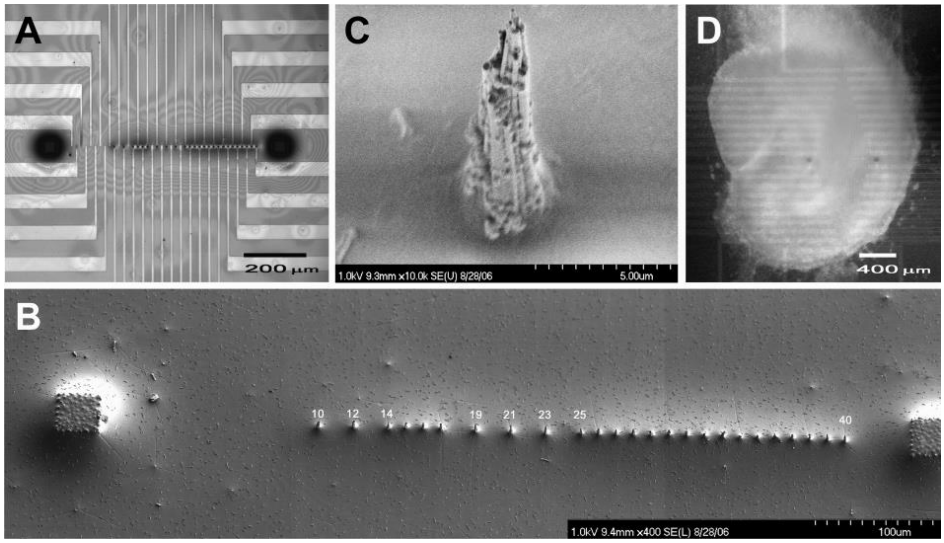

Figure 3.4: (a) Light microscopy image of the array prior to use. (b) SEM image of the VACNF array after several recordings had taken place. The missing electrodes (1-9, 11, 13, 18, 20, 22, 24) were absent before testing, as can be seen in (a), indicating that the fibers were not shorn from the mechanical stress of testing. (c) SEM image of a single electrode from (b). (d) Light micrograph of a hippocampal slice impaled upon the VACNF array chip. Adapted with permission from [20]. Copyright 2007 American Chemical Society.

Chapter 4 - Role of Ion Flux on Alignment of Carbon Nanofibers Synthesized by DC Plasma on Transparent Insulating Substrates

This work has previously appeared in Pearce, R.C., A.V. Vasenkov, D.K. Hensley, et al., *Role of Ion Flux on Alignment of Carbon Nanofibers Synthesized by DC Plasma on Transparent Insulating Substrates.* Acs Applied Materials & Interfaces, 2011. **3**(9): p. 3501-3507.

It was noted in **Chapter 1** that a key gap in the knowledge of VACNF synthesis was an alignment mechanism that took into account all the observed experimental data. A key factor to the implementation of devices with vertically aligned carbon nanofibers (VACNFs) is fundamental understanding of how to control fluctuations in the growth direction of the fibers. It has previously been established that the electric field at the substrate is the primary factor in determining the orientation of fibers grown catalytically using plasma enhanced chemical vapor deposition (PECVD) process. However, the hypotheses for the mechanism that correlates the processes at the catalyst nanoparticle with the nanofiber growth direction with electric field still await validation. Synthesis of carbon nanofibers on insulating substrates by continuous direct current (DC) plasma in the vicinity of grid electrodes provide observations important in elucidation of the role of electric field in alignment. To perform these observations, VACNFs were synthesized on a fused silica substrates using direct

current PECVD. To maintain continuous glow discharge above the substrate, a metal grid electrode layer (Cr) was deposited over silica with windows of exposed silica ranging in size from 200μm to 1mm. Observed trends in nanofiber alignment at the window-electrode interface suggests that the alignment is governed by the direction of the ion flux rather than the electric field at the substrate level. The proposed alignment mechanism is that ion sputtering of the carbon film on a catalyst particle defines the growth direction of the nanofibers. With this development, fiber growth direction can be better manipulated through changes in ionic flux direction, opening the possibility for growth of nanofibers on substrates with unique geometries.

4.1 Introduction

In thermal chemical vapor deposition, the growth direction is random for an isolated nanofiber. Helveg et al have reported *in situ* observations of carbon nanofiber growth in which nanoparticle growth direction randomly changes depending on the graphitic carbon configuration formed after each lurching step[1]. There is no preference in growth direction defined by nanoparticle crystallographic orientation and the shape of nanoparticle varies significantly during growth [2].

Aligned growth has been observed in the presence of DC bias in plasma. Ren et al. showed that by performing the catalytic synthesis in DC plasma, the direction of nanofiber growth can be maintained perpendicular to the substrate[3]. Such vertically aligned carbon nanofibers can be grown in sparse arrays either from nickel catalyst dots that are defined lithographically[4] or from a thin catalyst layer. With electrically conductive substrates (such

as Si), direct biasing has been used extensively. In response to observations that the direction of alignment correlates with electrical field lines, it has been suggested that the alignment mechanism involves the electrostatic forces on the nanofibers. One of the hypotheses stated that the electrostatic forces produce differential stresses on the nanoparticle/nanofiber interface that controls mass transport distribution and provides negative feedback to self-correct deviation from the direction of the electric field[5]. In a DC-PECVD chamber, the substrate acts as the cathode while the showerhead that introduces the process gases is the anode. Because of the need for an electric field to align the fibers, previously all substrates used for fiber growth in continuous DC plasma had to be conducting.

To sustain glow discharge at the catalyst location, the underlying electrically conductive substrate can be simply connected to the cathode. However, in fabrication of devices with VACNF elements it is often necessary to provide isolation between the nanofibers or their groups. Several methods exist to grow VACNFs on insulating substrates, such as SiO_2. In one approach, the whole surface of a wafer is coated by a metal layer, which is removed after growth at the areas outside of the nanofibers and the connecting electrodes[6]. The use of pulsed DC plasma does not require continuous conduction path and allowed growth on metal micropads that are patterned prior to growth of VACNFs[7, 8, 9, 10, 11, 12, 13]. Alternatively, radio frequency sources can be used to sustain plasma with generated self-bias to provide vertical alignment[14]. The term vertical alignment means that the structures are perpendicular to the plane of the substrate.

Modification of the growth direction of carbon nanofibers in plasma synthesis has been achieved by varying geometry of the cathode and relative position of catalyst sites with respect to the electrode edges[15]. By varying electrode geometry the nanofiber growth directed to create structures with curved geometries[16, 17]. Thus correlation between alignment of tip-type carbon nanofiber growth direction and the direction of the electric field in the vicinity of the substrate has been well established. However the exact coincidence of these directions, apart from a trivial case of growth on planar electrode far from the edge, has never been observed. Moreover, the calculated electrical fields were found to deviate from the measured nanofiber alignment directions[15].

In this chapter, the alignment of carbon nanofibers on regions of transparent, fully insulating substrate as well as grid electrodes is described. The width of the insulating window within a metalized grid was varied to determine its effect on the morphology of VACNFs grown by continuous DC plasma. We hypothesize that ion flux direction, rather than electric field defines the growth direction. This hypothesis stems from (i) observation of vertically aligned tip-type CNFs in at the center of insulating windows, (ii) observation of tilted CNFs on the metal electrodes, and (iii) strong pressure dependence of the nanofiber tilt.

4.2 Experimental Section

4.2.1 Substrate Preparation

Chromium strips were defined on two fused silica wafers with photolithography. First P-20 primer was allowed to spread across the wafer for 10 seconds before being spun at

6000 rpm for 45 seconds to enhance to the cohesion of photoresist. Negative tone NFR photoresist was then spun on the wafers at 6000 rpm for 45 seconds. The wafers were then baked at 115°C for 90 seconds. A mask resulting in a wafer with the pattern shown schematically in **Figure 4.1** was then exposed onto the wafers for 6 seconds at 9.45mJ/cm^2 intensity on a contact aligner using a vacuum contact. The wafers were then given a post exposure bake at 115°C for 90 seconds. Then, the two wafers were developed in CD-26 developer for 15 seconds before being rinsed with deionized water. Following development, the wafers were cleaned with oxygen plasma for 1 minute at 400W in a reactive ion etcher to remove excess photoresist before having 1000Å of chromium deposited via electron beam evaporation. Liftoff was done in an acetone bath with assistance from an ultrasonic cleaner before being rinsed with IPA and dried. The wafers then had SPR 955 CM 0.7 photoresist spun on them at 3000 rpm for 45 seconds before being baked at 115°C for 90 seconds. A second mask was then used to create 2μm diameter dots on the wafers. This mask was exposed with the same parameters as the first and followed an identical post-exposure procedure. Following the post-exposure procedure, the wafers had 500Å of nickel deposited on them. Liftoff and cleaning was carried out as before. These steps resulted in two wafers with a grid of stripes underneath small nickel dots which act as a catalyst for nanofiber growth

4.2.2 Nanofiber Synthesis

Fibers were then grown on the wafers in a custom built PECVD chamber. The parameters for growth were as follows: 700°C, 200sccms of NH_3, 85sccms of C_2H_2, 1 Amp

with a ramp rate of 0.25 minutes, an etch on time of -10 seconds indicating that acetylene is allowed to run for 10 seconds before the plasma is sparked, and a growth time of 16 minutes. Processing parameters have been explored to a great extent in literature. One wafer was run at 15 Torr while the other was performed at 4 Torr.

4.2.3 Imaging

Scanning electron microscopy of the fibers was done on a Zeiss Merlin FE-SEM at 5kV. A nitrogen charge compensator was used for imaging of the insulating areas on the wafer. Optical microscopy was performed on a Nikon LV150 automated microscopy imaging system.

4.2.4 Simulation

We considered a 2-D model of a dc glow discharge cell with a powered electrode being connected to the resistor-capacitor (RC) circuit. The system of equations of a dc glow discharge was solved using the CFD-ACE software[18], and the RC circuit was modeled using SPICE software[19]. The plasma modeling and RC circuit simulations were coupled using an interface module. This module updates on- the-fly plasma current for the SPICE modeling and voltage at the powered electrode for the CFD-ACE simulations using CFD-ACE and SPICE output data, respectively. Chemical reactions and gas flow in a dc glow discharge are known to have a strong influence on gas temperature and neutral species spatial profiles in a Torr pressure range[20]. The effect of these processes on plasma density is not dominant and was neglected in the present simulations. This allows us to obtain a rapid steady state

solution after approximately 10^5 time iterations. The time step in plasma simulations was controlled by the SPICE module and varied from 10^{-8} s to 10^{-9} s. The details of the model are given in [20, 21].

4.2.5 Cell Culture and Imaging

U2OS, human osteosarcoma cells were cultured in DMEM/F12K supplemented with 10% fetal bovine serum and routinely passed at approximately 80% confluency. At passage, 1 mL of a suspension of U2OS (~10^6 cells/mL) were plated upon a 100-mm VACNF wafer (as described) placed within a 125 mm dish containing 15 mL of supplemented media. Cells were imaged at 24 hr intervals for a period of 4 days on a Nikon Diaphot 200 inverted phase contrast microscope at 200× magnification.

4.3 Results and Discussion

Vertically aligned carbon nanofibers have been synthesized directly on regions of transparent, insulating substrate in a DC plasma. **Figure 4.1** shows VACNF fibers that were grown by catalytic DC-PECVD on fused silica with a 100 nm thick chromium layer covering the wafer, except for "windows" of fused silica that were left uncovered. Fibers shown in Fig. 1a and 1b were grown at 15 Torr. The fibers in Fig. 1a were grown on fused silica 100 μm from a chrome electrode on either side (i.e., in a "window"), while those in Fig. 1b were grown directly on a chrome electrode. All of these VACNFs feature a catalyst nanoparticle (NP) at the tip, indicating a tip-type growth mode. In tip-type growth, a nanoparticle, which serves the location for carbon deposition, is immersed in the anisotropic plasma environment

where ion bombardment plays a significant role in governing surface decomposition, diffusion, and even particle temperature[22, 23]. Base-type growth, where the NP remains at the substrate, has been observed to result in non-aligned nanofibers[5]. Such a scenario is likely to occur without an electrode grid on the substrate. Also, we expect that base-type growth may occur if the width of the bare fused silica windows were sufficiently large. Since the glow discharge cannot be maintained in a continuous DC plasma far away from grid electrodes, it becomes equivalent to thermal CVD conditions that produced base-type growth in this environment as has been reported in [5] . However in the range of window sizes from 0.2 to 1mm, we only observed tip-type growth.

A schematic of the reactor geometry is shown in **Figure 4.2a**. The window (E) width was varied from 0.2mm to 1mm across a 100mm wafer in increments of 100μm to establish the correlation between nanofiber morphology and distance from a window. The glow was observed to cover the whole wafer including the fused silica windows. **Figure 4.3** shows the variation of fiber growth as a function of distance from an electrode. The fibers on the interface have discernible tilt which straightens as the distance from the interface increases. The fibers also shorten further from the electrode. There is a significant, in case of **Figure 4.1** an order of magnitude, difference in growth rate between nanofibers grown on the electrode and the window. Such difference can be attributed to at least two factors: (i) the number of excited neutral radicals drops down away from electrode due to lowering of plasma density or (ii) the balance between etching and deposition of carbon on catalyst surface shifts away from optimum[24].

The influence of electrical field on alignment of carbon nanofibers can be most prominently observed at the edge of the thin film electrode where it strongly varies. **Figure 4.4** compares the fibers grown at 4 Torr and 15 Torr at the boundary between the fused silica windows and the Cr electrode strips. At 4 Torr, the fibers on the interface between chrome and fused silica are perpendicular to the substrate, whereas the fibers on the 15 Torr sample are extremely tilted in the same area. The only parameter that was changed between the two is the pressure. Maintaining the bias the same change in this pressure range (4 - 15 Torr) the electric field direction does not change significantly within a few microns from the substrate. The increase in pressure leads to decrease in dark field size, where most of the voltage drop occurs, thus increasing the magnitude of the electric field. Since the alignment of nanofibers at these two pressures is drastically different, the electric field cannot be the alignment vector. Even at the base of the nanofibers indicated by an arrow in **Figure 4.4b**, located 3 μm from the edge of the electrode and only a few nanometers from the electrode surface the tilt angle is significantly different from 90° with respect to the surface and it is the same as at the tip. A calculated direction of the electric field at such position over a flat metal surface is negligibly different from 90° with respect to the surface. This also serves as a strong indication that something else rather than electric field defines the growth direction.

Ion flux, on the other hand, can significantly vary depending on pressure. The estimated mean free path of ions changes from 14 to 4 μm when pressure changes from 4 to 15 Torr. Assuming that the balance between carbon deposition at the catalyst surface and its removal must be maintained in order for tip-type growth to occur[5], the anisotropy vector of

etch by ion bombardment can be such defining direction. The direction of the ion flux is the factor that controls the removal of carbon film build up on a nanoparticle surface thus defining the nanoparticle motion. Others have measured the ion current density and found that below 15 ions/nm^2/s the carbon nanofibers follow the base-type growth regime, and that above 370 ions/nm^2/s the fibers were over-etched[25]. The insets in **Figure 4.4** indicate the differences in the electric field and ionic flux, deduced from the nanofiber alignment, at the two pressures. 'The angle of the fibers is determined by the ionic flux vector in the vicinity of its catalyst particle as is demonstrated in **Figure 4.4** where the vector is normal to the substrate at 4 Torr in the area near a chrome strip, but angled at 15 Torr in the same area. The electric field at the interface is likely to be nearly horizontal, but this edge effect would only occur within a fraction of a micron from the interface[26].

Figure 4.5 shows the 2D profile of electrical potential a few microns above the surface calculated for a 4 Torr of total pressure (a), the profiles of electric potential and ion current density just above the wafer as a function of position in the x axis on the wafer (b), and the ***vector of ion current*** density a few microns above the surface (c). The potential has minimums and the ionic flux peaks at the chromium strips due to the ***ion acceleration in the sheath*** between the plasma and the grounded chromium strips. The ionic flux is non-zero in the fused silica areas because of the surface charge accumulation in these areas.

To explain variation of alignment and fiber height as a function of position with relation to the edge of the metal, we present the following model. Ion flux controls both the alignment and the growth rate of the fibers. The etch rate, which affects the growth rate, is

determined by reactive etching and physical etching in the form of ion bombardment. The dependence of the alignment and growth rate can be explained by the directionality and rate of removal of carbon species on the catalyst particle. Carbon can interact with the catalyst nanoparticle in several ways. It can diffuse through the particle to form a graphene layer under the particle or it can adhere to the surface. The nanoparticle tip quickly becomes covered with a carbon layer during growth if there are few or no ions bombarding and volatilizing the deposited carbon. This carbon layer will halt growth, which is controlled by the amount of carbon which diffuses through the particle, unless it is removed. Therefore, there exists a maximum growth rate for a given process gas ratio and current, where etch regime does not outpace the carbon deposition and vice versa. Furthermore, the nanofiber will only grow in the direction from which the carbon is removed through a phenomenon called anisotropic etching. The ionic flux close to the edge of the chromium strips and fused silica is not perpendicular to the substrate, which leads to tilted fibers close to the interface which become straighter the further they are from the interface. In reactive ion etching, ion bombardment is responsible for directional etching[27]. The anisotropy of distribution of chemical potential across the catalyst nanoparticle is believed to control the direction of catalyst motion[28]. Fiber height is controlled by etch rate which is a function of current and pressure[29].

Ultimately, the ability to grow VACNF on transparent substrates and control of their geometry (alignment) at the nanoscale are essential to the application of VACNF arrays for cellular and tissue interfacing[30, 31, 32, 33, 34]. Transparent substrates enable the use of

transmission (and specifically phase-contrast) microscopy thereby promoting visualization of the spatial relationship and dynamic interaction of the cellular matrix with VACNF elements[35]. **Figure 4.6a** presents a phase contrast image of human osteosarcoma cells (U2OS) cultured upon the optically transparent window of a VACNF array grown as specified in this report, and provides clear visualization of subcellular organelles and individual VACNF elements. The ability to maintain nanofiber alignment normal to the substrate is necessary for efficient use of such arrays in impalefection, a gene delivery process in which nanofibers are pressed into cellular matrix or tissue[36]. **Figure 4.6b** shows variation of nanofiber alignment across an electrode strip in an SEM image of the same cell covered substrate as in **Figure 4.6a**. The nanofiber geometry is crucial in performing cellular impalement, i.e. it should be oriented with the direction of insertion. Thus nanofibers tilted with respect to the substrate would be undesirable. This study shows that growth at lower pressures (i.e. 4 Torr) is required to reduce the variation on the nanofiber deviation from the normal. This requirement puts limitation on the synthesis process leading to significantly longer growth times necessary to achieve desired nanofiber length of a few tens of micrometers.[37] Engineering rector/substrate geometries that provide ion flux uniformity at large pressure ranges are required for large-scale control of nanofiber alignment.

4.4 Conclusion

We have performed synthesis of vertically aligned carbon nanofibers in a DC plasma on an insulating substrate with a grid of electrodes. The alignment of the fibers has been observed to vary as a function of distance from the electrode grids. The pressures under

which the fibers grow also play a large role in the tilt. It's been previously proposed that electrical fields on the surface of the substrate define the direction of the nanofiber growth. If that were the case the nanofibers at lower pressure (4 Torr) would be as tilted as nanofibers at high pressure (15 Torr), contrary to our observations. Theoretical calculations show that direction of ion flux diverges from the directions of electrical field vectors at the substrate level near the electrode edges. The trends in the calculated ion flux direction fit better the trends of nanofiber alignment. While observations provided here along with computational modeling support the hypothesis that ion flux controls the direction of nanofiber growth, it still remains to establish this correlation in direct experimental measurement of ion flux direction. These observations also help to choose the growth regime in implementation of nanofiber-based structures where function depends on the alignment (i.e. cellular impalement for gene delivery). A compromise between high growth rate (and large nanofibers) at high pressure and high normal alignment at low pressure needs to be made depending on critical need for chosen functionality. With further understanding of how ionic flux determines morphology and alignment the possibility of a single reactor capable of synthesizing fibers customized geometry is closer to a reality.

4.5 References

(1) Helveg, S.; Lopez-Cartes, C.; Sehested, J.; Hansen, P. L.; Clausen, B. S.; Rostrup-Nielsen, J. R.; Abild-Pedersen, F.; Norskov, J. K. *Nature* **2004,** *427,* 426-429.

(2) Behr, M. J.; Mkhoyan, K. A.; Aydil, E. S. *ACS Nano* **2010,** *4,* 5087-5094.

(3) Ren, Z. F.; Huang, Z. P.; Xu, J. W.; Wang, J. H.; Bush, P.; Siegal, M. P.; Provencio, P. N. *Science* **1998,** *282,* 1105-1107.

(4) Merkulov, V. I.; Lowndes, D. H.; Wei, Y. Y.; Eres, G.; Voelkl, E. *Applied Physics Letters* **2000,** *76,* 3555-3557.

(5) Merkulov, V. I.; Melechko, A. V.; Guillorn, M. A.; Lowndes, D. H.; Simpson, M. L. *Applied Physics Letters* **2001,** *79,* 2970-2972.

(6) Guillorn, M. A.; McKnight, T. E.; Melechko, A.; Merkulov, V. I.; Britt, P. F.; Austin, D. W.; Lowndes, D. H.; Simpson, M. L. *J. Appl. Phys.* **2002,** *91,* 3824-3828.

(7) Teo, K. B. K., Rupesinghe NL Equipment Innovations for Nanotechnology Equipment, Especially for Plasma Growth Chambers of Carbon Nanotube and Nanowire. 7842135, 2010.

(8) Arumugam, P. U.; Chen, H.; Siddiqui, S.; Weinrich, J. A. P.; Jejelowo, A.; Li, J.; Meyyappan, M. *Biosensors and Bioelectronics* **2009,** *24,* 2818-2824.

(9) Siddiqui, S.; Arumugam, P. U.; Chen, H.; Li, J.; Meyyappan, M. *ACS Nano* **2010,** *4,* 955-961.

(10) Li, J.; Ng, H. T.; Cassell, A.; Fan, W.; Chen, H.; Ye, Q.; Koehne, J.; Han, J.; Meyyappan, M. *Nano Letters* **2003,** *3,* 597-602.

(11) Koehne, J. E.; Chen, H.; Cassell, A. M.; Ye, Q.; Han, J.; Meyyappan, M.; Li, J. *Clin Chem* **2004,** *50,* 1886-1893.

(12) Cassell, A. M.; Li, J.; Stevens, R. M. D.; Koehne, J. E.; Delzeit, L.; Ng, H. T.; Ye, Q.; Han, J.; Meyyappan, M. *Appl. Phys. Lett.* **2004,** *85,* 2364-2366.

(13) de Asis, E.; Nguyen-Vu, T.; Arumugam, P.; Chen, H.; Cassell, A.; Andrews, R.; Yang, C.; Li, J. *Biomedical Microdevices* **2009,** *11,* 801-808.

(14) Caughman, J. B. O.; Baylor, L. R.; Guillorn, M. A.; Merkulov, V. I.; Lowndes, D. H.; Allard, L. F. *Applied Physics Letters* **2003,** *83,* 1207-1209.

(15) Merkulov, V. I.; Melechko, A. V.; Guillorn, M. A.; Simpson, M. L.; Lowndes, D. H.; Whealton, J. H.; Raridon, R. J. *Applied Physics Letters* **2002,** *80,* 4816-4818.

(16) AuBuchon, J. F.; Chen, L. H.; Gapin, A. I.; Jin, S. H. *Chem. Vap. Deposition* **2006,** *12,* 370-374.

(17) AuBuchon, J. F.; Chen, L. H.; Gapin, A. I.; Kim, D. W.; Daraio, C.; Jin, S. H. *Nano Lett.* **2004,** *4,* 1781-1784.

(18) Kolobov, V. I. *Comput. Mater. Sci.* **2003,** *28,* 302-320.

(19) Thorpe, T. W., *Computerized circuit analysis with SPICE : a complete guide to SPICE, with applications*. Wiley: New York, 1992; p xix, 339 p.

(20) Vasenkov, A. V. *Journal of Computational and Theoretical Nanoscience* **2008,** *5,* 48-55.

(21) Vasenkov, A. V., Modeling Nanotube Synthesis: The Multiscale Approach. In *the Encyclopedia of Nanoscience and Nanotechnology* (2nd edition) ed.; Nalwa, H. S., Ed. 2011; Vol. V. 16, pp pp.281-302.

(22) Denysenko, I.; Ostrikov, K. *Appl. Phys. Lett.* **2007,** *90*.

(23) Denysenko, I.; Ostrikov, K. *J. Phys. D-Appl. Phys.* **2009,** *42,* 12.

(24) Merkulov, V.; Melechko, A. V.; Guillorn, M. A.; Lowndes, D. H.; Simpson, M. L. *Chemical Physics Letters* **2002,** *361,* 492-498.

(25) Mauger, M.; Binh, V. T. *Journal of Vacuum Science & Technology B* **2006,** *24,* 997-1003.

(26) Yoo, M. J.; Fulton, T. A.; Hess, H. F.; Willett, R. L.; Dunkleberger, L. N.; Chichester, R. J.; Pfeiffer, L. N.; West, K. W. *Science* **1997,** *276,* 579-582.

(27) Coburn, J. W.; Winters, H. F. *Annu. Rev. Mater. Sci.* **1983,** *13,* 91-116.

(28) Merkulov, I. A.; Klein, K. L.; Simpson, M. L. *J. Appl. Phys.* **2009,** *105,* -.

(29) Merkulov, I. A.; Merkulov, V. I.; Melechko, A. V.; Klein, K. L.; Lowndes, D. H.; Simpson, M. L. *Phys. Rev. B: Condens. Matter Mater. Phys.* **2007,** *76,* -.

(30) McKnight, T. E.; Melechko, A. V.; Griffin, G. D.; Guillorn, M. A.; Merkulov, V. I.; Serna, F.; Hensley, D. K.; Doktycz, M. J.; Lowndes, D. H.; Simpson, M. L. *Nanotechnology* **2003,** *14,* 551-556.

(31) McKnight, T. E.; Melechko, A. V.; Hensley, D. K.; Mann, D. G. J.; Griffin, G. D.; Simpson, M. L. *Nano Letters* **2004,** *4,* 1213-1219.

(32) McKnight, T. E.; Mann, D. G. J.; McPherson, J. T.; Hoyt, P. R.; Melechko, A. V.; Simpson, M. L.; Sayler, G. S. *ACS Nano* **2008,** *2,* 69-76.

(33) Yu, Z.; McKnight, T. E.; Ericson, M. N.; Melechko, A. V.; Simpson, M. L.; Morrison, B. *J Neurotraum* **2007,** *24,* 1235-1235.

(34) McKnight, T. E.; Melechko, A. V.; Griffin, G. D.; Simpson, M. L. *In Vitro Cell. Dev. Biol.: Anim.* **2006,** *42,* 17a-17a.

(35) Hensley, D. K.; Melechko, A. V.; Ericson, M. N.; Simpson, M. L.; McKnight, T. E. In *Transparent microarrays of vertically aligned carbon nanofibers as a multimodal tissue interface*, Biomedical Sciences and Engineering Conference (BSEC), 2010, 2010; pp 1-4.

(36) Mann, D. G. J.; McKnight, T. E.; McPherson, J. T.; Hoyt, P. R.; Melechko, A. V.; Simpson, M. L.; Sayler, G. S. *ACS Nano* **2008,** *2*, 69-76.

(37) Melechko, A. V.; Klein, K. L.; Fowlkes, J. D.; Hensley, D. K.; Merkulov, I. A.; McKnight, T. E.; Rack, P. D.; Horton, J. A.; Simpson, M. L. *Journal of Applied Physics* **2007,** *102*, 074314-7.

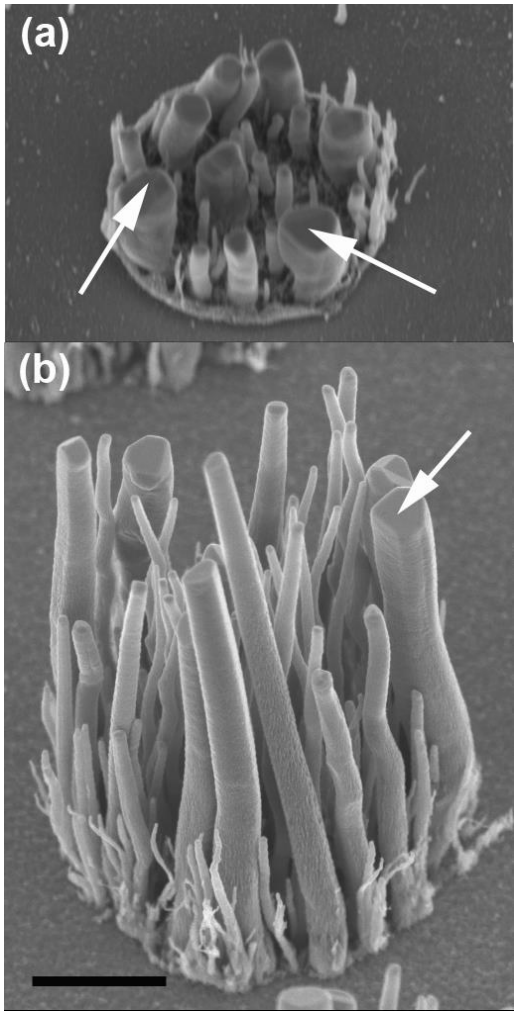

Figure 4.1: (a) An SEM image of tip-type vertically aligned carbon nanofibers grown on fused silica in DC plasma. The arrows indicate the Ni catalyst nanoparticles. This VACNF cluster is ~200μm away from a grounded 100 nm thick chromium strip on the left and right. These fibers were grown at 15 Torr, 1A, and 550V with 200 sccm NH_3 and 85 sccm C_2H_2.

(b) SEM image of VACNFs on the same wafer as the one seen in a) but grown on 100nm thick chromium 400μm away on each side from fused silica.

The scale bar represents 1μm for both (a) and (b).

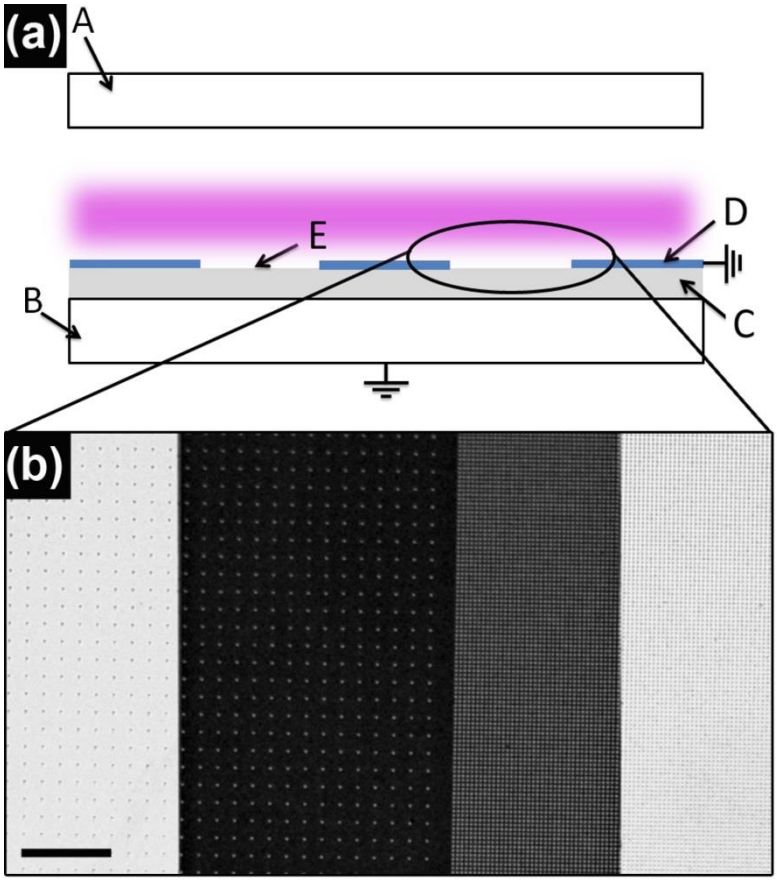

Figure 4.2: (a) A schematic of the reactor, electrode geometry, and wafer design: A- The anode which also acts as the showerhead where the process gases originate, B- The cathode which doubles as the substrate heater, C- The fused silica wafer, D- 100nm thick Cr "strips," E- "Windows" of fused silica left uncovered by Cr

(b) An optical micrograph of a fused silica window in between two Cr strips with the nickel catalyst dot pattern overlayed. The distance between Cr electrodes is 500μm. The scale bar corresponds to 100μm.

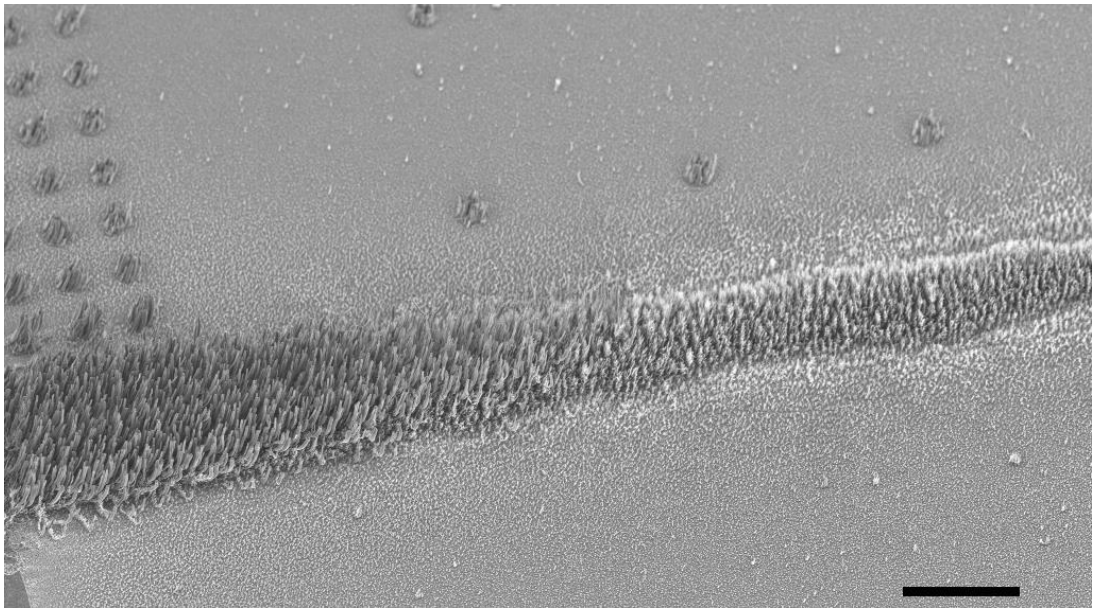

Figure 4.3: The transition across the Cr-fused silica interface can be seen clearly. The majority of the picture shows fused silica, while the interface can be seen in the bottom left corner of the image. The growth conditions cannot be optimal for such a strong difference in the substrate, explaining the difference in the character of the fibers. The scale bar represents 10μm.

Figure 4.4: SEM images of the boundary between the electrode layer and insulating window. The images were taken at a 30° tilt. The fibers in Fig. 3a were grown at 4 Torr while those in Fig. 3b were grown at 15 Torr. At 4 Torr the fibers at the interface are nearly perpendicular with the substrate, while at 15 Torr there is significant tilt. The insets indicate the approximate directions of the electric field (E) and ionic flux (J) determined from simulations. The electric field should remain nearly identical between the two, though the ionic flux will likely differ drastically as a function of pressure. At a pressure of 4 Torr the ionic flux must be perpendicular to the substrate, resulting in vertical fibers, whereas at 15 Torr the ionic flux is not perpendicular to the substrate, resulting in tilted fibers. This explanation is only true directly at the interface. Further into the electrode strip, the electric field will likely be more perpendicular to the substrate, though it is seen clearly in (b) that the fibers are tilted a few microns into the strip. The only cause for the fibers to remain tilted so far into the strip is that the ionic flux not being perpendicular. In each image, the distance between Cr electrodes is 600μm. The scale bar corresponds to 1μm.

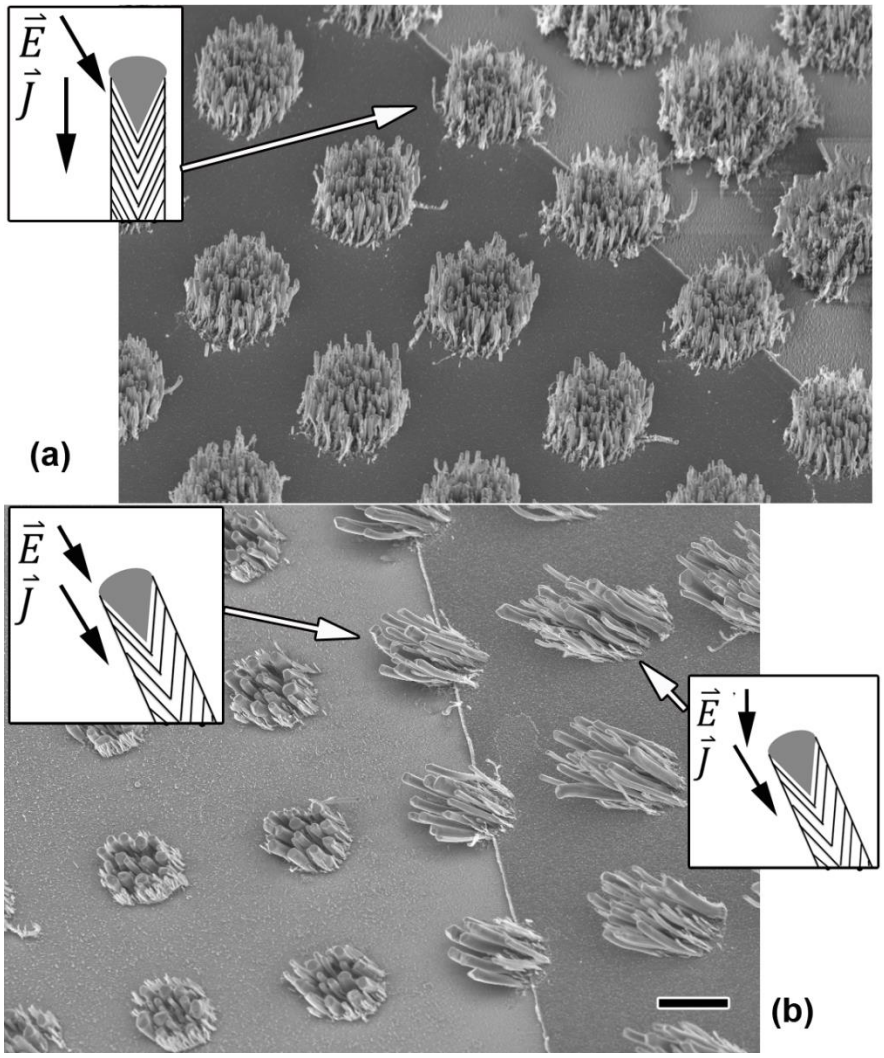
$\vec{E}$
$\vec{J}$
(a)
$\vec{E}$
$\vec{J}$
$\vec{E}$
$\vec{J}$
(b)

Figure 4.5: Graphs generated using the results of a CFD-ACE plasma modeling coupled with a SPICE circuit simulation at 4 Torr of total pressure. (a) 2D profile of electrical potential a few microns above the surface of the substrate. The electric potential reaches its minima at the grounded chromium strips, the conducting paths, while the minima for the ion flux are on the fused silica windows. (b) Profiles of electric potential and ion current density just above the wafer. (c) Vector of ion current density a few microns above the surface of the substrate. The ions are coulombically attracted to the grounded chromium strips which are in the locations of highest flux. The inertia of the ions, however, prevents them from precisely following the electric field lines and a fraction of them still bombard the surfaces that are nonconducting. (d) Electric field lines a few microns above the substrate surface.

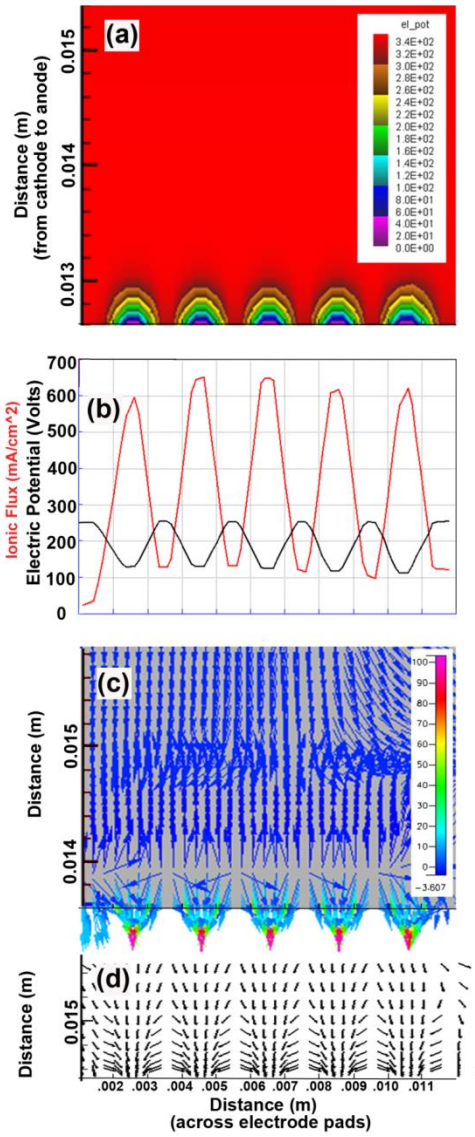
(a)
el_pot
3.4E+02
3.2E+02
3.0E+02
2.8E+02
2.6E+02
2.4E+02
2.2E+02
2.0E+02
1.8E+02
1.6E+02
1.4E+02
1.2E+02
1.0E+02
8.0E+01
6.0E+01
4.0E+01
2.0E+01
0.0E+00
Distance (m)
(from cathode to anode)
0.015
0.014
0.013
(b)
Ionic Flux (mA/cm^2)
Electric Potential (Volts)
700
600
500
400
300
200
100
0
(c)
Distance (m)
0.015
0.014
100
90
80
70
60
50
40
30
20
10
0
-3.607
(d)
Distance (m)
0.015
.002 .003 .004 .005 .006 .007 .008 .009 .010 .011
Distance (m)
(across electrode pads)

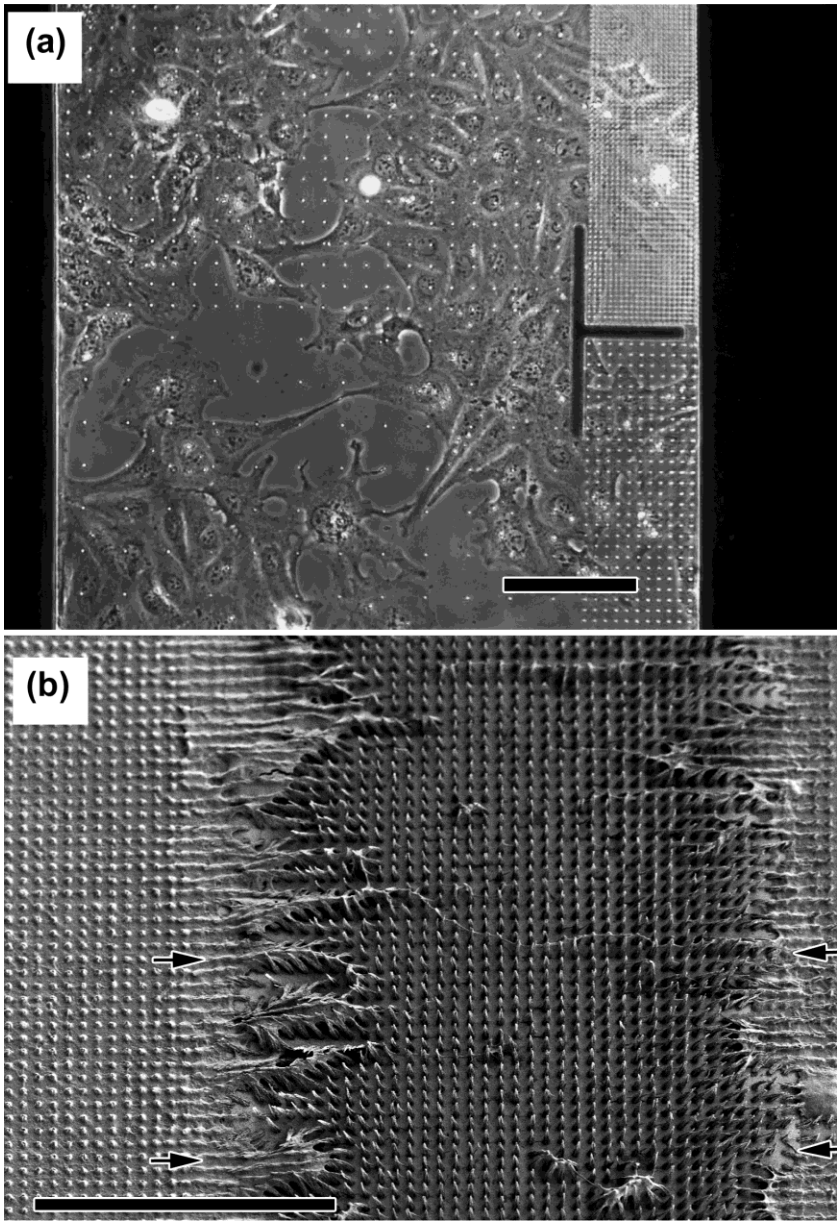

Figure 4.6: Phase contrast optical micrograph (a) and scanning electron micrograph (b) of human osteosarcoma cells (U2OS) cultured upon a VACNF array synthesized upon a transparent window on fused silica. The scale bar represents 100 μm. The arrows in (b) show the edge of Cr strip.

Chapter 5 - Fluorescence of SiN_x coated VACNFs from Si clusters

5.1 Introduction

It has long been known that under some synthesis parameters a silicon nitride coating forms on the sidewalls and at the base of vertically aligned carbon nanofibers (VACNFs) during plasma enhanced chemical vapor deposition (PECVD) synthesis.[1, 2, 3, 4, 5] **Figure 5.1** shows electron microscopy images of fibers with a SiNx sheath. This coating has proven useful for enhancing mechanical properties and biocompatibility.[6] The increased mechanical properties stems from changing the fiber structure to a more conical shape than its usual cylindrical shape. Some of the benefits of this coating include the ability to be pressed into tissue many times without mechanical degradation,[3] and enough rigidity to undergo many post-processing steps such as photoresist or other polymer spinning without collapsing.[3, 6, 7] In one study, the source of the silicon was a thin sacrificial Si layer.[2] A different study used dropcast Si microparticles which were redeposited onto the VACNFs during synthesis.[6] However, in all of these instances, the only source of silicon was either the substrate or added to the substrate, it was never as a silicon bearing gas such as silane. VACNFs are typically grown from a combination of two gases, a carbon source and an etchant, most typically acetylene and ammonia respectively. The coating forms during PECVD synthesis through redeposition of any present silicon in combination with nitrogen from ammonia. The coating can also be fluorescent in the visible spectrum, making it potentially useful for biomarking in cellular impalefection studies. This chapter will propose a deposition mechanism for the

SiN_x coating to the VACNF sidewalls as well as exploration of the photoluminescent properties of the coating.

5.2 Experimental

5.2.1 VACNF Synthesis

Vertically aligned carbon nanofibers were synthesized on n-type <100> Si wafers. Dots 2μm in diameter were photo-lithographically patterned onto the wafers. A 50nm thick nickel catalyst layer was then deposited via electron beam evaporation and liftoff was performed to remove the nickel everywhere except for the previously defined dot pattern. The nanofibers were grown in a custom-built dc-PECVD chamber. The growth parameters for the VACNFs that were used for the fluorescence measurements were 70sccm C_2H_2, 110sccm NH_3, 8 Torr, 700°C, and 0.7A for 1 hour. The fibers that underwent Auger depth profiling were grown at 700°C with 80sccm NH_3, 40sccm C_2H_2, 3 Torr, 350mA, for 1 hour. In depth explanation of VACNF synthesis can be found elsewhere.[8, 9, 10, 11]

A PECVD deposited SiN_x reference film was deposited on a separate p-type <100> Si wafer using an Oxford Instruments Plasmalab 100 PECVD system. The growth parameters were 400sccm of 5% SiH_4/Ar, 20sccm of NH_3, and 600sccm of N_2 at 650mT and 350°C for 17 minutes, resulting in a film 115nm thick.

5.2.2 Characterization

Characterization of the resultant fibers included optical measurements, imaging, and elemental analysis. Photoluminescence mapping was performed using a Spex Flurolog 2 at

room temperature over an excitation range of 300-500nm and an emission range of 350-700nm. Additionally fluorescence microscopy in Leica TCS SP2 MP laser scanning confocal system was used to assess the photobleaching time. EDX was used extensively along with auger electron spectroscopy (AES) depth profiling to determine chemical composition. EDX and SEM imaging was done using a Zeiss Merlin SEM with a Bruker EDX system. AES was performed using a PHI 680 Scanning Auger Nanoprobe.

5.3 Results and Discussion

5.3.1 Deposition Mechanism

There are two primary mechanisms as to how the SiN_x coating forms. Either the silicon is sputtered from the substrate to the sidewalls of the fiber, or hydrogen volatilizes silicon from the substrate creating silane and other compounds in the plasma whereupon it further reacts with nitrogen from the ammonia and is redeposited through CVD processes. It has been shown that it is possible to form SiN_x films using rf magnetron sputtering by using a silicon target with argon and ammonia process gases.[12] However, the amount of power supplied to the system is much greater than in a PECVD chamber. Additionally the deposition pressures are usually lower, meaning the particles in the system experience fewer collisions and retain more of their energy before impacting the substrate or target. It seems unlikely that in a PECVD chamber the ions and gas molecules would acquire the energy necessary to physically knock out many Si atoms from the substrate.

PECVD deposition of silicon nitride is also well established as previously mentioned. However, films deposited in this way use a silicon bearing gas, such as silane, as a silicon source, instead of the substrate itself. The silane decomposes and combines with nitrogen (usually from ammonia) on the surface of the substrate.

The films formed on VACNFs differ from both of these techniques in some regards. The largest difference between all three of them is the films formed on VACNFs are being formed on three dimensional structures that are continuously growing during deposition instead of on a planar surface that exists before deposition begins. Additionally, for the work presented here, the source of silicon is only from the substrate, as opposed to sputtering and PECVD SiN_x films which use a target or a silicon bearing gas respectively. **Figure 5.2** shows the possible mechanisms of deposition. It is important to note that sputtering usually occurs at very low pressures, around 10^{-5} Pa which correlates to a mean free path of ~10^{4}m. The synthesis of VACNFs however, takes place at hundreds to thousands of Pa. A growth at 4 Torr has a mean free path of roughly 100μm. A significantly lower mean free path indicates that it is likely that any sputtered Si atom would undergo collisions with the other process gases and react with it, leading to a more CVD-like deposition. Alternatively, excited hydrogen molecules could react with the substrate and become subsequently volatilized, further reacting with the process gases and resulting in the SiN_x film. It is possible that a combination of these two processes is what is occurring to deposit the film.

5.3.2 Photoluminescence properties of SiN_x-coated VACNFs

In the literature there is a large ongoing debate on the origin of the photoluminescence observed in SiN_x films. There is a substantial body of work indicating the presence of Si nanoclusters (NCs) in Si-rich SiN_x films.[13, 14, 15, 16, 17, 18, 19, 20, 21, 22, 23] Many of these studies attribute the photoluminescence of the films to quantum confinement effects (QCE).[19, 23, 24, 25, 26] According to the QCE model, the photoluminescence (PL) peak is inversely proportional to the square of the average size of the Si-NCs, while intensity increases with NC density and improved passivation.[13] Others attribute the PL to the presence of defect-related states, such as nitrogen defects or Si dangling bonds.[27] Another study surmised that the blue, green, and red components of the PL were due to defects, bandtail recombination, and QCE respectively.[28] SiN_x films without any Si-NCs have also been studied, with the PL in those samples being attributed to bandtail recombination.[20] It seems that the Si-NCs do not spontaneously form spontaneously during co-sputtering of Si and Si_3N_4 targets or with some PECVD parameters and require annealing of more than 1000°C to form the nanostructures.[20, 23] Yet, it appears that growths that encourage an *a*-SiN_x:H matrix yield *in-situ* formatting of Si-NCs.

We observe a strong PL response from SiN_x coated VACNFs as shown in **Figure 5.3**. There appear to be two emission peaks at 416nm and 432nm for both the PECVD SiN_x coating and the VACNF coating with an excitation wavelength of 380nm. **Figure 5.4** shows the PL spectra for 380nm excitation for both samples. It is possible that this dual peak stems from the presence of a bimodal size distribution of Si-NCs. From **Figure 5.4** it can be

observed that the intensity of the sample with VACNFs coated with SiN_x has nearly twice the intensity of the flat PECVD SiN_x film, though this could be due to there simply being a greater amount of material present on the VACNFs, which seems unlikely. Here we will make the argument that this PL response is due to the presence of Si-NCs. First it is important to show the plausibility of Si-NCs forming. As was previously mentioned, both annealing and high hydrogen content have shown the ability to yield Si-NCs. Since the samples are grown at 700°C in the presence of C_2H_2 and NH_3, both of these conditions are met. Another key factor is that for the synthesis of Si-NCs, the film must be Si-rich. That is, the Si/N ratio is greater than stoichiometric Si_3N_4. **Table 5.1** shows that the coating is in fact Si-rich, lending further credibility to the presence of Si-NCs.

Figure 5.5 shows an EDS line scan of a broken VACNF with a SiN_x coating. From this line scan it can be seen that many nitrogen troughs are accompanied by silicon peaks, while the inverse is never true. It can be inferred then, that these Si peaks are areas where Si-NCs are present. The lack of nitrogen peaks accompanied by silicon troughs is expected, since nitrogen does not have a crystallographic structure at room temperature. The evidence for Si-NCs is further corroborated by the EDS maps shown in **Figure 5.6**. From the EDS maps, it can be seen that there are areas where there are bright Si clusters.

Perhaps the most convincing proof of the presence of Si-NCs is shown in **Figure 5.7**. Auger electron spectroscopy not only reveals elemental composition, but also bonding state of atoms. Combined with ion milling, AES is a very powerful tool for elemental analysis of samples. From **Figure 5.7** it can be seen that there is a significant amount Si that is bonded

to either O or N, and that after ~1000μm there is only Si bonded Si, indicating that the substrate has been reached by the probe. It is critical to note that Si bonded Si is in abundance throughout the area probed, well above the substrate, alongside the O and N bonded Si. Some of this Si is probably bonded to the carbon that is present to form SiC, since AES only shows bonding states of atoms with significantly different electronegativities. However, there is a much greater amount of "unbonded" Si than C, so even if full amount of present C is used to form SiC, there is still a large amount of Si that must be bonded to Si. These Si-Si bonds must invariably lead to small Si-NCs.

Now that the presence of Si-NCs and strong fluorescence of SiN_x coated fibers has been established, it will be shown that these fibers are extremely useful as registry markers for fluorescent cellular studies. **Figure 5.8** shows a cell undergoing mitosis at two different wavelengths of emission. The cell is dyed with both GFP-tubulin and H2B-DsRed, while the emission from the SiN_x coated VACNFs stems solely from the fluorescent SiN_x coating. Since the VACNFs emit over such a broad spectrum, they can be used as positional markers or "registry" markers. **Figure 5.9** shows a plot of the emission intensity across two emission ranges (same as **Figure 5.8**) as a function of time. It is observed that the emission from the dyed cell decreases over time, but the intensity of the emission from VACNFs seems to remain stable over the time period tested. Therefore, in addition to emitting over a broad range, the fluorescence of the VACNFs does not seem to undergo photobleaching, wherein the intensity of emission decreases over time due to the presence of intermediate energy levels with long half-lives.

5.4 Conclusions

Here we have proposed a potential mechanism for the deposition of SiN_x coatings that on the sidewalls of VACNFs during PECVD synthesis in addition to exploring the origin of the coatings photoluminescence. It seems most likely that the substrate reacts with the process gases through both processes similar to reactive sputtering and CVD to form silane and other silicon bearing compounds before being deposited isotropically as a SiN_x coating onto the VACNFs. The case for the presence of Si-NCs is made strong through a combination of the strong fluorescence and elemental analysis of the samples. These broadly luminescent fibers can prove useful as registry markers in fluorescent cellular studies.

5.5 References

(1) McKnight, T. E.; Melechko, A. V.; Griffin, G. D.; Guillorn, M. A.; Merkulov, V. I.; Serna, F.; Hensley, D. K.; Doktycz, M. J.; Lowndes, D. H.; Simpson, M. L. *Nanotechnology* **2003,** *14,* 551-556.

(2) Guillorn, M. A.; Melechko, A. V.; Merkulov, V. I.; Ellis, E. D.; Britton, C. L.; Simpson, M. L.; Lowndes, D. H.; Baylor, L. R. *Applied Physics Letters* **2001,** *79,* 3506-3508.

(3) Melechko, A. V.; McKnight, T. E.; Hensley, D. K.; Guillorn, M. A.; Borisevich, A. Y.; Merkulov, V. I.; Lowndes, D. H.; Simpson, M. L. *Nanotechnology* **2003,** *14,* 1029-1035.

(4) Teo, K. B. K.; Chhowalla, M.; Amaratunga, G. A. J.; Milne, W. I.; Pirio, G.; Legagneux, P.; Wyczisk, F.; Olivier, J.; Pribat, D. *Journal of Vacuum Science & Technology B* **2002,** *20,* 116-121.

(5) Yang, X.; Guillorn, M. A.; Austin, D.; Melechko, A. V.; Cui, H.; Meyer, H. M.; Merkulov, V. I.; Caughman, J. B. O.; Lowndes, D. H.; Simpson, M. L. *Nano Letters* **2003,** *3,* 1751-1755.

(6) Pearce, R. C.; Railsback, J. G.; Anderson, B. D.; Sarac, M. F.; McKnight, T. E.; Tracy, J. B.; Melechko, A. V. *ACS Appl. Mater. Interfaces* **2013**.

(7) McKnight, T. E.; Melechko, A. V.; Austin, D. W.; Sims, T.; Guillorn, M. A.; Simpson, M. L. *Journal of Physical Chemistry B* **2004,** *108,* 7115-7125.

(8) Melechko, A. V.; Desikan, R.; McKnight, T. E.; Klein, K. L.; Rack, P. D. *Journal of Physics D: Applied Physics* **2009,** *42,* 193001.

(9) Melechko, A. V.; Klein, K. L.; Fowlkes, J. D.; Hensley, D. K.; Merkulov, I. A.; McKnight, T. E.; Rack, P. D.; Horton, J. A.; Simpson, M. L. *Journal of Applied Physics* **2007,** *102,* 074314-7.

(10) Chhowalla, M.; Teo, K. B. K.; Ducati, C.; Rupesinghe, N. L.; Amaratunga, G. A. J.; Ferrari, A. C.; Roy, D.; Robertson, J.; Milne, W. I. *Journal of Applied Physics* **2001,** *90,* 5308-5317.

(11) Arumugam, P. U.; Chen, H.; Siddiqui, S.; Weinrich, J. A. P.; Jejelowo, A.; Li, J.; Meyyappan, M. *Biosens. Bioelectron.* **2009,** *24,* 2818-2824.

(12) Serikawa, T.; Okamoto, A. *Journal of The Electrochemical Society* **1984,** *131,* 2928-2933.

(13) Benami, A.; Santana, G.; Monroy, B. M.; Ortiz, A.; Alonso, J. C.; Fandiño, J.; Aguilar-Hernández, J.; Contreras-Puente, G. *Physica E: Low-dimensional Systems and Nanostructures* **2007,** *38,* 148-151.

(14) Benami, A.; Santana, G.; Ortiz, A.; Ponce, A.; Romeu, D.; Aguilar-Hernández, J.; Contreras-Puente, G.; Alonso, J. C. *Nanotechnology* **2007,** *18,* 155704.

(15) Bommali, R. K.; Singh, S. P.; Rai, S.; Mishra, P.; Sekhar, B. R.; Prakash, G. V.; Srivastava, P. *Journal of Applied Physics* **2012,** *112*.

(16) Brewer, A.; von Haeften, K. *Applied Physics Letters* **2009,** *94,* -.

(17) Chopra, S.; Gupta, R. P.; Joshi, B. C.; Eranna, G.; Banerjee, S. *Mater Sci-Poland* **2009,** *27,* 559-568.

(18) Kim, B. H.; Cho, C. H.; Kim, T. W.; Parka, N. M.; Sung, G. Y.; Park, S. J. *Applied Physics Letters* **2005,** *86,* -.

(19) Kim, T. Y.; Park, N. M.; Kim, K. H.; Sung, G. Y.; Ok, Y. W.; Seong, T. Y.; Choi, C. J. *Applied Physics Letters* **2004,** *85,* 5355-5357.

(20) Kistner, J.; Chen, X.; Weng, Y.; Strunk, H. P.; Schubert, M. B.; Werner, J. H. *Journal of Applied Physics* **2011,** *110*.

(21) Lopez-Suarez, A.; Fandino, J.; Monroy, B. M.; Santana, G.; Alonso, J. C. *Physica E* **2008,** *40*, 3141-3146.

(22) Ma, K.; Feng, J. Y.; Zhang, Z. J. *Nanotechnology* **2006,** *17*, 4650.

(23) Nguyen, P. D.; Kepaptsoglou, D. M.; Ramasse, Q. M.; Olsen, A. *Physical Review B* **2012,** *85*.

(24) Cho, C. H.; Kim, B. H.; Kim, T. W.; Park, S. J.; Park, N. M.; Sung, G. Y. *Applied Physics Letters* **2005,** *86*.

(25) Pei, Z.; Hwang, H. L. *Applied Surface Science* **2003,** *212–213*, 760-764.

(26) Santana, G.; Monroy, B. M.; Ortiz, A.; Huerta, L.; Alonso, J. C.; Fandino, J.; Aguilar-Hernandez, J.; Hoyos, E.; Cruz-Gandarilla, F.; Contreras-Puentes, G. *Applied Physics Letters* **2006,** *88*.

(27) Wang, M. H.; Li, D. S.; Yuan, Z.; Yang, D. R.; Que, D. L. *Applied Physics Letters* **2007,** *90*.

(28) Hao, H. L.; Wu, L. K.; Shen, W. Z.; Dekkers, H. F. W. *Applied Physics Letters* **2007,** *91*.

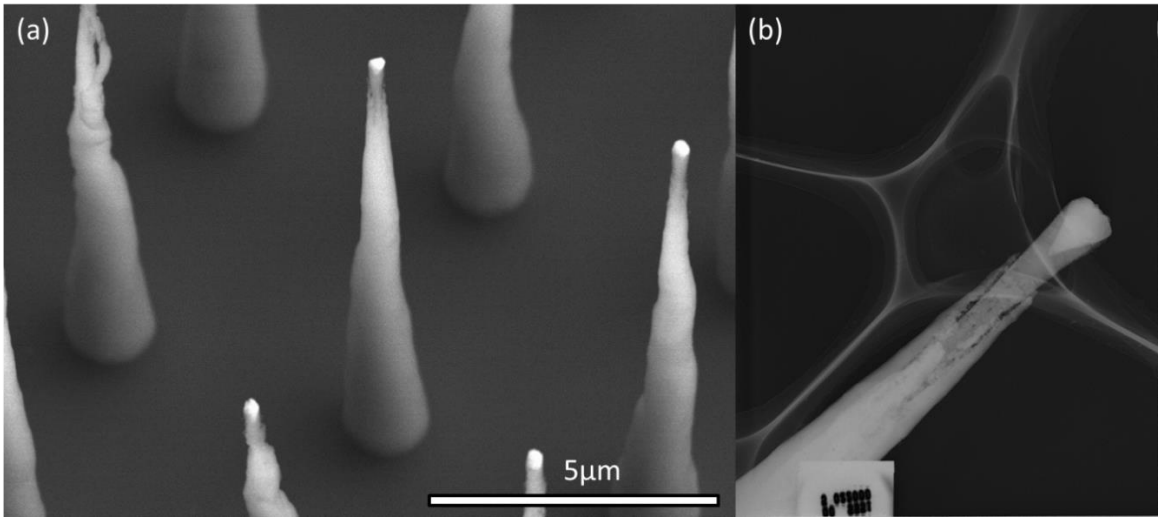

Figure 5.1: a) SEM image of an array of vertically aligned carbon nanofibers synthesized on Si with SiNx coating. A portion of an uncoated carbon nanofiber is extending from SiNx sheath by about 500 nm. b) TEM image of a VACNF coated with SiNx. The initial stages of the film growth at the frieshly form carbon nanofiber surface can be observed near the tip.

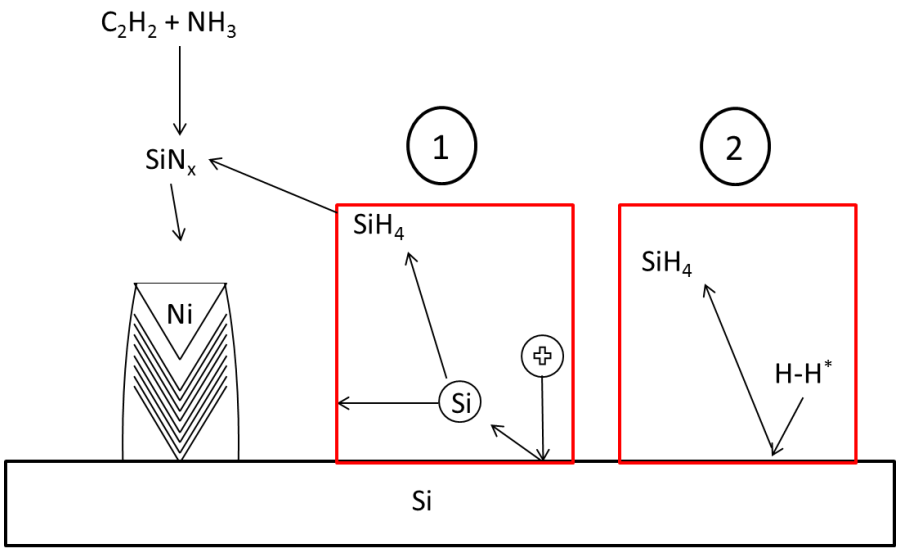

Figure 5.2: Illustration of possible deposition mechanisms of SiN_x coating to VACNF sidewalls (1) Reactive sputtering where ions eject Si atoms from the substrate which go on to react with the gas or (2) Excited hydrogen chemically reacts with the substrate and then volatilizes to further react through CVD processes.

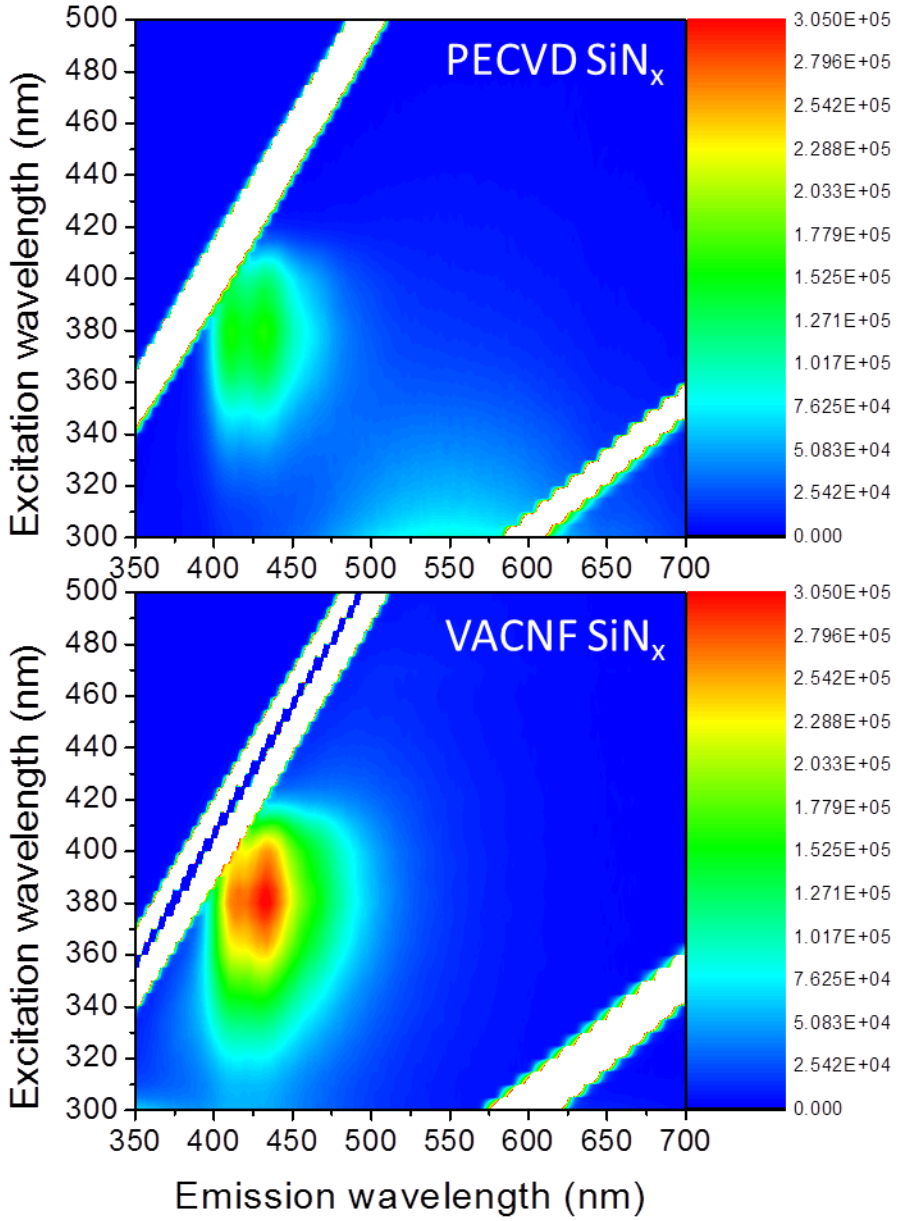

Figure 5.3: Fluorescent response from a PECVD SiN_x coating (top) and from a SiN_x coated VACNF array (bottom).

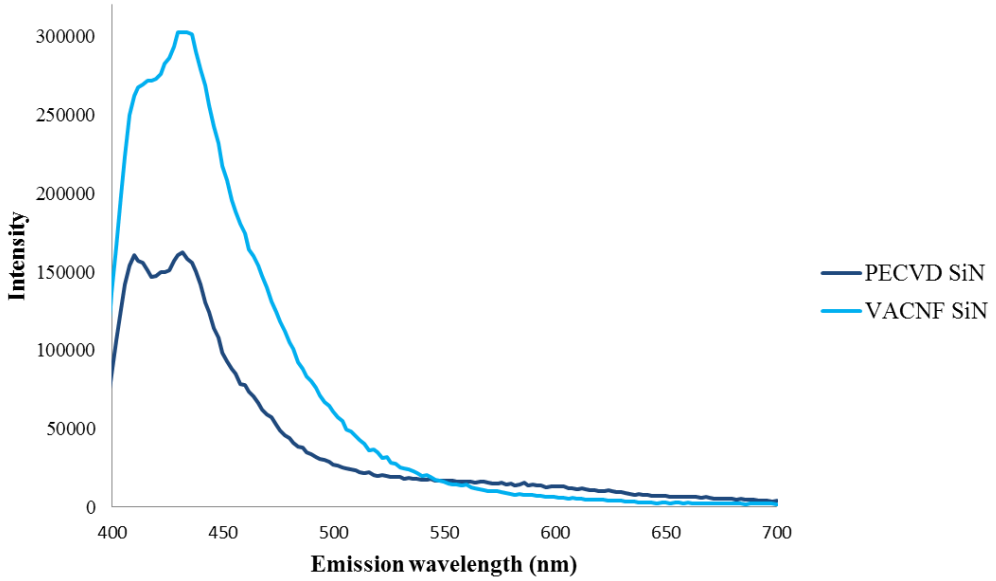

Figure 5.4: PL spectra at 380nm excitation for VACNF SiN_x and PECVD SiN_x

Table 5.1: Relative atomic concentrations in VACNF SiN_x coating

Element	Atomic %
Si	41.07
N	45.75
C	7.86
O	5.33

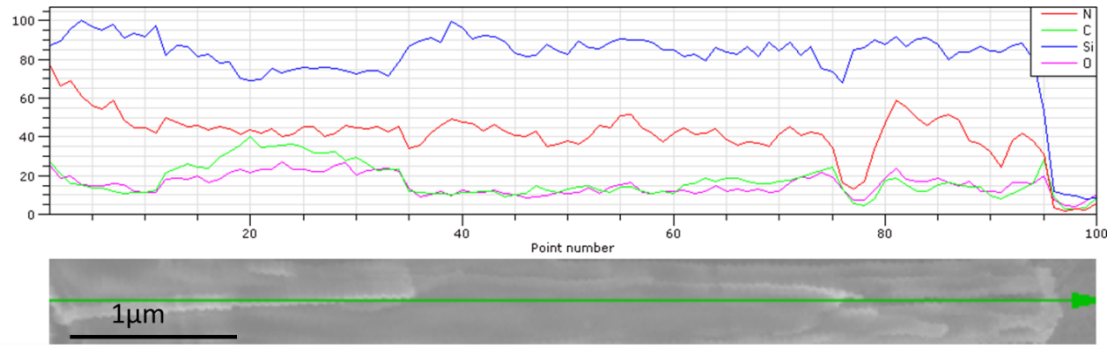

Figure 5.5: EDS line scan of a broken VACNF coated with SiN_x (top) with positionally accurate SEM image of broken VACNF (bottom).

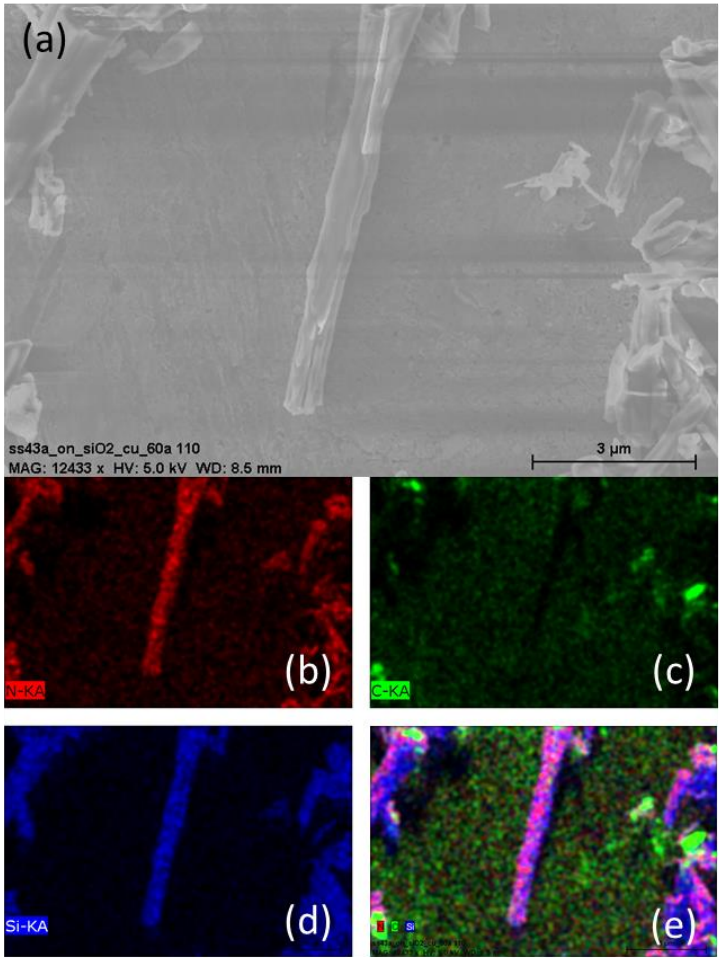

Figure 5.6: (a) SEM image of broken VACNFs with SiN_x coatings on an aluminum viewing platform. EDS maps were made of this area showing location of (b) Nitrogen (c) Carbon (d) Silicon and (e) Composite of all three.

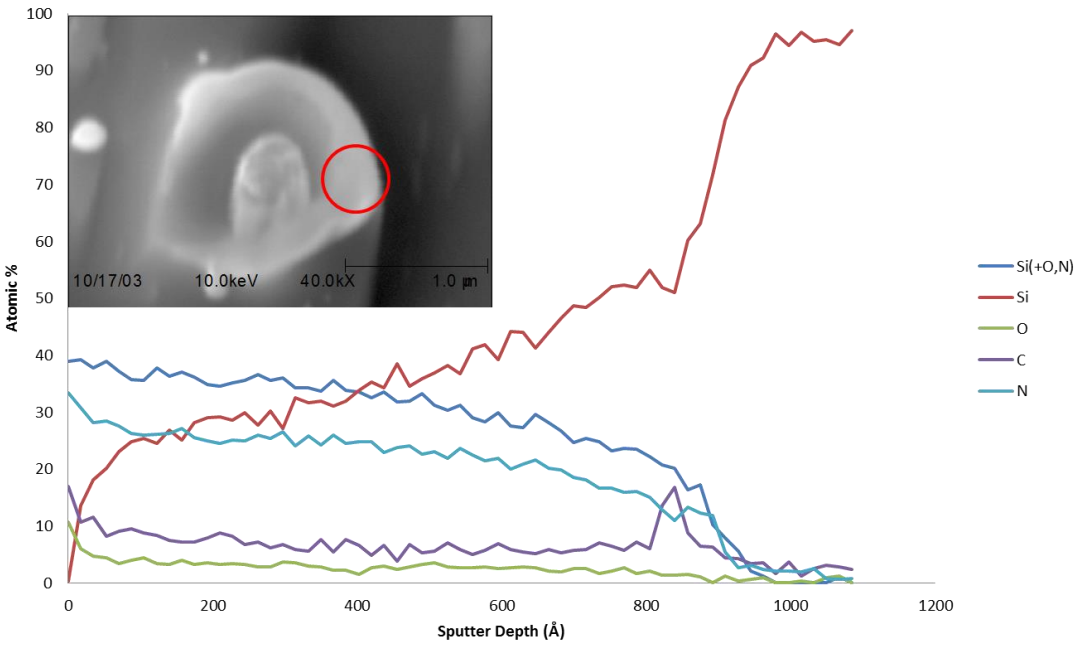

Figure 5.7: AES depth profile showing the composition of the SiN_x coating on a VACNF as a function of depth. The inset shows the region that was probed.

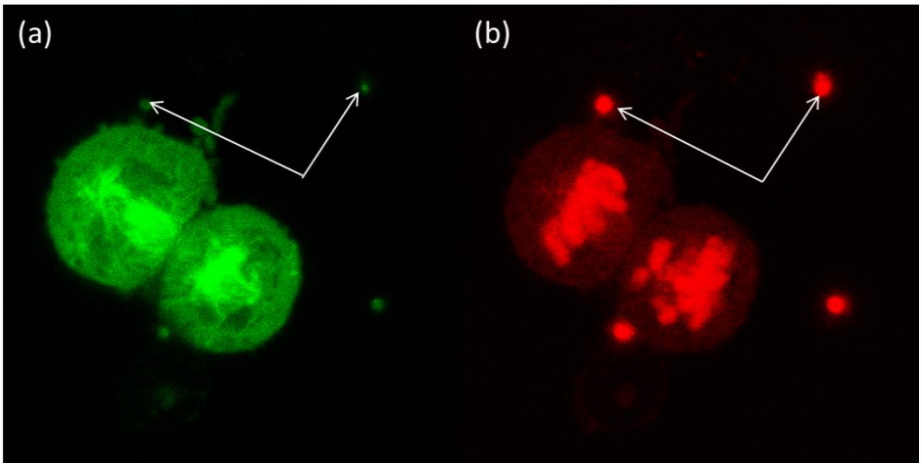

Figure 5.8: Fluorescent optical micrographs of a cell undergoing mitosis looking at different emission wavelengths. (a) Emission of 505nm-520nm from GFP-tubulin (b) Emission of 610nm-650nm from H2B-DsRed. Arrows indicate location of SiN_x coated VACNFs from a top-down view. The VACNFs are not dyed.

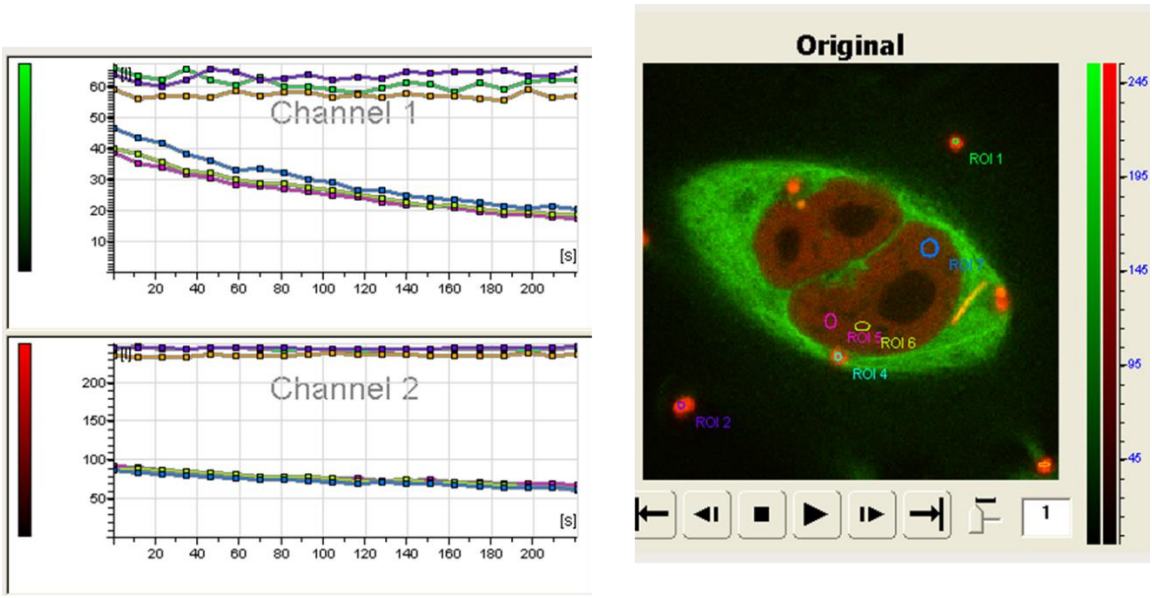

Figure 5.9: Fluorescent optical micrograph (right) showing a cell impaled on a SiN_x coated VACNF array. ROI 1, 2, and 4 indicate VACNFs. Two channels of emission are being collected as depicted in the graphs (left). The graphs show change in emission intensity of the ROIs as a function of time.

Chapter 6 - Transfer of Vertically Aligned Carbon Nanofibers to Polydimethylsiloxane (PDMS) while Maintaining their Alignment and Impalefection Functionality

This work appeared in: Pearce, R.C., J.G. Railsback, B.D. Anderson, et al., *Transfer of Vertically Aligned Carbon Nanofibers to Polydimethylsiloxane (PDMS) While Maintaining their Alignment and Impalefection Functionality.* Acs Applied Materials & Interfaces, 2013.

As mentioned previously in **Chapter 2**, one of the challenges with VACNF device integration is the ability to reliably transfer the fibers from one substrate to another. This chapter will present a method to transfer fibers to flexible PDMS while maintaining their functionality and morphology. Vertically aligned carbon nanofibers (VACNFs) are synthesized on Al 3003 alloy substrates by direct current plasma-enhanced chemical vapor deposition. Chemically synthesized Ni nanoparticles were used as the catalyst for growth. The Si-containing coating (SiN_x) typically created when VACNFs are grown on silicon was produced by adding Si microparticles prior to growth. The fiber arrays were transferred to PDMS by spin coating a layer on the grown substrates, curing the PDMS, and etching away the Al in KOH. The fiber arrays contain many fibers over 15 μm (long enough to protrude from the PDMS film and penetrate cell membranes) and SiN_x coatings as observed by SEM, EDX, and fluorescence microscopy. The free standing array in PDMS was loaded with

pVENUS-C1 plasmid and human brain microcapillary endothelial (HBMEC) cells and was successfully impalefected.

6.1 Introduction

Vertically-aligned carbon nanofibers (VACNFs) have shown great utility for chemically and electrically addressing tissues and cells.[1, 2, 3] VACNFs are structurally different from carbon nanotubes (CNTs), though the two are often conflated in the literature due to similarities in their morphology and graphitic nature. In carbon nanofibers graphene layers are arranged in stacked cone or cup structure while in nanotubes graphene layers are rolled into cylinders that span the whole length of a nanotube. Such structural differences result in diverging physical and chemical properties. Carbon nanofibers are more amenable to chemical and biochemical functionalization as well as posessing much higher electron transfer rates at the graphene edges on the sidewalls than CNTS.[4, 5, 6, 7, 8, 9, 10] Vertically aligned carbon nanofibers can be synthesized in a deterministic process which is compatible with most of the microfabrication techniques, with alignment controlled by the plasma environment.[11, 12, 13, 14, 15, 16, 17] It has been shown that VACNFs can be grown as an array of free standing structures.[18] In contrast, vertically aligned carbon nanotubes require a presence of supporting neighbors to maintain alignment perpendicular to a substrate.[19] Second, it has been shown that VACNFs can withstand a variety of post-synthesis processing steps such as silicon dioxide and silicon nitride film deposition, electroplating, photoresist spinning (of various viscosities from S1813 to SU-8) as well as resist removal, and dry/wet etching.[20, 21] This made them an attractive structure for integration into microfabricated devices such as

electron field emission arrays, scanning probe tips, electrochemical probes and neuronal multielectrodes arrays, and cell mimic microfluidic devices.[22, 23, 24, 25, 26, 27, 28, 29, 30, 31, 32] Thirdly, VACNFs have been shown to withstand mechanical interfaces with live tissues and cells arrays. For example, hippocampal tissues slices could be pressed onto VACNF multielectrode array and then removed many times without loss of functionality, though it should be noted that a silicon nitride conical side coating was added to enhance the mechanical strength of the freestanding fibers.[33] Even when VACNFs are grown on metal substrates a thin sacrificial layer of Si was used to add robustness to freestanding nanofibers.[34] In this work Si microparticles were used for Si source. VACNF arrays have been used in laboratory demonstrations of transfection by cell impalement, resulting in viable cells expressing proteins encoded on DNA physically inserted into their nuclei.[2] The insertion of genetic material into a cell for the purpose of generating desired proteins, by using a physical structure to impale the cell is termed "impalefection."[35] Impalefection is useful for *in vitro* experiments[23, 35, 36, 37] associated with exploring gene therapy, but has yet to be used in a therapeutic or diagnostic technology. VACNFs can be grown as free standing, sparse arrays, similar to a bed of nails making them ideal for impalefection, as opposed to CNTs which can be thought of as a carpet and therefore less useful for impalefection.[7]

VACNF arrays are limited in their utility in part by the expensive, inflexible Si substrate that they are typically grown upon. Replacing the Si is a non-trivial task because the substrate must satisfy requirements for chemical compatibility with the catalyst nanoparticles

(NPs) and VANCFs, as well as remain intact throughout the VACNF growth process, which typically involves temperatures of ~700 °C and plasma processing. Perhaps the most important role of the Si substrate is providing a silicon source for the SiN_x coating that is formed on the fibers during plasma-enhanced chemical vapor deposition (PECVD) growth. This SiN_x coating imparts fluorescence properties in the visible spectrum, which allows the fibers to be easily imaged by fluorescence microscopy. The coating is also thought to improve the mechanical properties of the fibers as seen by the ability of coated fibers to remain vertically aligned even after spin coating polymer solutions such as photoresist, in addition to possibly reducing the cytotoxicity compared to other uncoated carbon structures.[38, 39, 40] Work has also been performed on CNTs, which reveals that CNTs usually deform upon solution coating.[41, 42] VACNF arrays on flexible substrates have been attempted previously[43] and, if the substrate is biocompatible, may be particularly useful for biomedical applications.[44] Another attraction to flexible substrates for VACNFs is for impalefection of tissues.

The primary goal of this research is to lay the groundwork for an angioplasty balloon with VACNFs, so that upon inflation the blood-brain barrier will be penetrated and genetic material or drugs can be delivered. Current schemes for transferring VACNF arrays to flexible substrates rely on non-biocompatible materials and processing conditions that are difficult to reproduce.[43] Here, we demonstrate a process that expands the utility of VACNFs toward impalefection schemes by replacing the typical Si substrate with inexpensive Al and replacing the e-beam evaporated catalyst deposition step with air-brushed Ni nanoparticles

(NiNPs). Furthermore, we show that the fiber array may be transferred to a free-standing polydimethylsiloxane (PDMS) film (following chemical etching of the Al substrate) and the array will maintain the ability to transfect cells.

6.2 Experimental Section

An overview of the fabrication process from catalyst synthesis to a free-standing PDMS film containing the VACNF array is depicted in **Figure 6.1**.

6.2.1 Nickel Nanoparticle Synthesis

100 nm NiNPs (**Figure 6.2a**) were synthesized according to a modified procedure developed by Wang et. al.[45] A mixture of, 5.0 mL 1-octadecene (90 %, Sigma Aldrich), 5 mL oleylamine (80-90%, Acros), and 0.50 g nickel(II) acetylacetonate hydrate (98%, TCI America) was mixed and allowed to degas under vacuum in a three-necked round-bottomed flash for 120 min at 60°C. The solution was then backfilled with N_2 and heated at a rate of 10 °C/min to 240 °C, where the temperature was held for 30 min. The Ni NPs were then flocculated by adding ethanol, and the supernatant was discarded following centrifugation at 5000 rpm. The NPs were then redispersed in hexanes. After centrifuging the solution a second time, the supernatant was discarded, and the NPs were redispersed in heptane for airbrushing.

6.22 Airbrushing

The heptane solution containing the Ni NPs was airbrushed onto sections of 0.016”-thick 3003 Al (McMaster Carr) using an Iwata Eclipse HP-CS airbrush operating at 50 psi.

Prior to airbrushing, the Al sections were sonicated in acetone and rinsed with methanol to remove any contaminants. The NPs were deposited in short (0.5-2 s) bursts at a 0.3 m distance from the substrate. Heptane was chosen because it gave a more uniform pattern of deposited NPs than other solvents (results not shown).

6.2.3 Silicon Deposition

Si serves an important role in the synthesis of VACNFs for impalefection. During synthesis, Si sputtered by the plasma reacts with ammonia to form a SiN_x coating on the VACNFs. This coating is thought to enhance the mechanical stability of the VACNFs which is important for cell impalement. In order to achieve this same coating when using an Al substrate, small, surfactant-free Si microparticles ranging from 1-3 μm in size (Atlantic Equipment Engineers) were dispersed in acetone (~0.5 g Si to 10 mL acetone) for deposition onto the substrate. The dispersion was sonicated for 20 s and 50 μL were immediately dropcast onto each substrate.

6.2.4 VACNF Synthesis

VACNFs were synthesized by direct-current PECVD in a custom built system. The catalyst-coated substrate was heated to 600 °C under a 0.05 Torr vacuum, and then the chamber was backfilled with 4 Torr NH_3. Acetylene was then introduced to the chamber for 10 s prior to striking the plasma. The NH_3/C_2H_2 flow ratio was 85 sccm/45 sccm, and the pressure was maintained at 4 Torr throughout the remainder of the process. The growth took place for 2 hours at a current of 0.5 A, and temperature of 600 °C. The chamber was

evacuated after the growth, and the substrate was allowed to cool to room temperature under vacuum.

6.2.5 PDMS Deposition

PDMS was mixed with crosslinker (Sylgard 184 kit) according to the standard procedure, in a 10:1 ratio. For deposition onto the Al substrates, a drop of the PDMS mixture was placed on the substrate and spun at 5000 rpm for 3 min, followed by curing on a hotplate at 150 °C for one hour.

6.2.6 Aluminum Etch

To release the PDMS film and the VACNF array, KOH was used to dissolve the Al substrate. A KOH solution (30% by mass) was heated to 80 °C, and the substrate was submerged for 20-30 minutes with continuous stirring, which dissolved it completely. The free-standing PDMS film was removed from the solution and rinsed with deionized water. Changing the etch time and fraction of the substrate immersed can yield a PDMS film with no metal attached or a film with only some areas supported by metal, effectively making windows in the substrate below.

6.2.7 Cell Transfection

A 5 mm × 5 mm section of the Al substrate with VACNFs embedded in the PDMS film was back-etched for 3 hours in 1 *M* KOH at room temperature, yielding a substrate with some portion of thin Al and free-standing PDMS film. The conventional cell pellet on concavity slide method (pellet of cells, prewet DNA functionalized chip, press chip against

cell pellet) was used to integrate the VACNFs with the cells, as previously described.[2] HBMEC cells and the plasmid pVENUS-C1 were used. The PDMS side of the chip was etched with a water plasma for about 15 s to promote wetting and cell adhesion prior to wetting with DNA solution. This initial experiment yielded low transfection rates. Only a small number of cells on the DNA-spotted region of the 5 mm × 5 mm chip were successfully transfected. However, none of the impalefected cells adhered to the substrate as previously described using Si substrates.[2] The transgene-expressing cells appeared pierced, but were elevated above the substrate. Thus, a larger number of cells may have been transfected, but not retained on the device during overnight imaging due to poor adhesion. **Figure 6.4** shows a transfection, and an internalized nanofiber (visible with TRITC green/red filter).

6.3 Results and Discussion

VACNFs were grown by direct-current PECVD on Al foil using solution-processed NiNPs as the catalyst material (**Figure 6.1**).[46] 100 nm NiNPs were synthesized by previously reported methods,[45] then suspended in heptane and airbrushed onto sections of Al 3003 alloy foil. Al was chosen because it is inexpensive and can be easily dissolved in KOH. The substrates were heated to 600° C under vacuum and subjected to an acetylene and ammonia plasma at 4 Torr for 2 hours. Initial growths without a Si source resulted in small fibers that were over-etched by ammonia during synthesis (results not shown). Depositing Si microparticles by dropcasting prior to VACNF growth results in the formation of SiN_x coatings on the fibers that are comparable to growth on Si substrates, where the Si is

sputtered and reacts with ammonia ions (**Figure 6.1**). Energy dispersive X-ray spectroscopy (EDX) mapping indicates that Si is present on the VACNFs but not on the Al substrate between the fibers, except for the Si microparticles added prior to growth.[46] Given the combination of green luminescence and EDX signal for Si (**Figure 6.2**), it is likely that a SiN_x species forms preferentially on the sidewalls of the fibers. Dangling Si, C, and N bonds can account for the green emission.[47]

Transferring VACNFs to a flexible membrane while leaving enough of the fibers protruding for cell impalement requires control over the film thickness. Spin-casting is universally used in the semiconductor industry to produce polymer films of photoresist on flat substrates with well-defined thickness and uniformity. Spin-casting was used here to produce a PDMS film thin enough to allow for many VACNFs to protrude, while remaining thick enough to have the mechanical robustness to be free standing. PDMS was chosen because it is biocompatible, flexible, and chemically inert. The Al substrates have a roughness (standard deviation of height measurements) of about 3 μm, as measured by profilometry (results not shown), which determines the lower limit for PDMS film thickness in order to obtain a continuous film. After growth, the VACNFs varied in height between ~4-20 μm due to agglomeration of the catalyst NPs. Fibers grown from smaller, non-agglomerated catalyst particles run out of catalyst more quickly due to sputtering, which subsequently leads to etching back of the fiber over the long growth time.[48] Therefore we chose to produce PDMS films 7-10 μm thick, in order to sufficiently exceed the surface roughness of the substrate. This thickness is close to that of LDPE plastic wrap commonly

used for food storage (12.7 μm). The films were deposited by spin coating a standard Sylgard 184 PDMS mixture according to methods reported for PDMS on Si.[49] Capillary action of the PDMS solution on the sidewalls of the VACNFs during spin coating causes the film to be thicker near the fiber base but still leaves much of the fibers exposed (**Figure 6.3a**).

Release of the film from the Al substrate is performed by KOH etching at elevated temperature (80 °C). PDMS is largely resistant to KOH etching and no noticeable damage or swelling occurred during release. The free-standing arrays (**Figure 6.3**) contain a sparse population of fibers with the mechanical robustness and length necessary to impale and transfect cells.

After the KOH etch, a UV-ozone plasma treatment was performed to increase the hydrophilicity of the substrate and consequently increase cell adhesion. 100 ng of pVENUS-C1 plasmid was suspended in one μL of nuclease-free water and dried onto the surface of a small region of the VACNF-PDMS film**.** The side of the film with the exposed VACNFs was then pressed into a pellet of human capillary endothelial cells (HBMEC) and incubated overnight using methods described elsewhere.[2] The sparse density of long, robust fibers in the DNA-spotted region of the array resulted in a small number of transfections, evident by the expression of the Venus fluorescent protein in the localized spotted region (**Figure 6.4**). The low transfection rate could stem from the low-density of emergent fibers from the PDMS, allowing cells to roll off the nanofiber tip and down to the substrate. Future efforts to provide higher density of emergent nanofibers are anticipated to increase transfection rates by improving the penetration and retention of individual cells. This successful transfection

shows that our simple and inexpensive approach to conduct impalefection using flexible substrates is effective, which can be further optimized by controlling the density of VACNFs protruding through the PDMS film.

6.4 Conclusions

We have demonstrated the ability to grow VACNFs on Al substrates by PECVD using chemically-synthesized Ni NP catalysts. EDX and optical fluorescence measurements indicate that the SiN_x-containing coating observed in fibers grown on silicon can be reproduced for fibers grown on Al when Si microparticles are added to serve as a source of Si. The fibers can successfully be incorporated into PDMS films, while maintaining their alignment and impalefection functionality. These results demonstrate a simple and reliable method, by which we have brought the impalefection platform to flexible substrates. This development is a critical first step towards the creation of an angioplasty balloon with blood-brain barrier piercing capabilities for gene and drug delivery.

6.5 References

(1) de Asis, E. D.; Nguyen-Vu, T. D. B.; Arumugam, P. U.; Chen, H.; Cassell, A. M.; Andrews, R. J.; Yang, C. Y.; Li, J. *Biomed Microdevices* **2009,** *11,* 801-808.

(2) McKnight, T. E.; Melechko, A. V.; Hensley, D. K.; Mann, D. G. J.; Griffin, G. D.; Simpson, M. L. *Nano Letters* **2004,** *4,* 1213-1219.

(3) Paranjape, M.; Garra, J.; Brida, S.; Schneider, T.; White, R.; Currie, J. *Sensor Actuat a-Phys* **2003,** *104,* 195-204.

(4) Baker, S. E.; Colavita, P. E.; Tse, K. Y.; Hamers, R. J. *Chem Mater* **2006,** *18,* 4415-4422.

(5) Baker, S. E.; Tse, K. Y.; Lee, C. S.; Hamers, R. J. *Diam Relat Mater* **2006,** *15,* 433-439.

(6) Tse, K. Y.; Zhang, L. Z.; Baker, S. E.; Nichols, B. M.; West, R.; Hamers, R. J. *Chem Mater* **2007,** *19,* 5734-5741.

(7) Melechko, A. V.; Merkulov, V. I.; McKnight, T. E.; Guillorn, M. A.; Klein, K. L.; Lowndes, D. H.; Simpson, M. L. *Journal of Applied Physics* **2005,** *97,* Artn 041301.

(8) Landis, E. C.; Hamers, R. J. *Chem Mater* **2009,** *21,* 724-730.

(9) Landis, E. C.; Klein, K. L.; Liao, A.; Pop, E.; Hensley, D. K.; Melechko, A. V.; Hamers, R. J. *Chem Mater* **2010,** *22,* 2357-2366.

(10) Fletcher, B. L.; McKnight, T. E.; Melechko, A. V.; Simpson, M. L.; Doktycz, M. J. *Nanotechnology* **2006,** *17,* 2032-2039.

(11) Pearce, R. C.; Vasenkov, A. V.; Hensley, D. K.; Simpson, M. L.; McKnight, T. E.; Melechko, A. V. *ACS Appl. Mater. Interfaces* **2011,** *3,* 3501-3507.

(12) Merkulov, V.; Melechko, A. V.; Guillorn, M. A.; Lowndes, D. H.; Simpson, M. L. *Chemical Physics Letters* **2002,** *361,* 492-498.

(13) Merkulov, V. I.; Guillorn, M. A.; Lowndes, D. H.; Simpson, M. L.; Voelkl, E. *Applied Physics Letters* **2001,** *79,* 1178-1180.

(14) Merkulov, V. I.; Hensley, D. K.; Melechko, A. V.; Guillorn, M. A.; Lowndes, D. H.; Simpson, M. L. *Journal of Physical Chemistry B* **2002,** *106,* 10570-10577.

(15) Merkulov, V. I.; Melechko, A. V.; Guillorn, M. A.; Lowndes, D. H.; Simpson, M. L. *Applied Physics Letters* **2001,** *79,* 2970-2972.

(16) Merkulov, V. I.; Melechko, A. V.; Guillorn, M. A.; Simpson, M. L.; Lowndes, D. H.; Whealton, J. H.; Raridon, R. J. *Applied Physics Letters* **2002,** *80,* 4816-4818.

(17) Chhowalla, M.; Teo, K. B. K.; Ducati, C.; Rupesinghe, N. L.; Amaratunga, G. A. J.; Ferrari, A. C.; Roy, D.; Robertson, J.; Milne, W. I. *J Appl Phys* **2001,** *90,* 5308-5317.

(18) Merkulov, V. I.; Lowndes, D. H.; Wei, Y. Y.; Eres, G.; Voelkl, E. *Applied Physics Letters* **2000,** *76,* 3555-3557.

(19) Fan, S. S.; Chapline, M. G.; Franklin, N. R.; Tombler, T. W.; Cassell, A. M.; Dai, H. J. *Science* **1999,** *283,* 512-514.

(20) Guillorn, M. A.; Melechko, A. V.; Merkulov, V. I.; Ellis, E. D.; Britton, C. L.; Simpson, M. L.; Lowndes, D. H.; Baylor, L. R. *Appl Phys Lett* **2001,** *79,* 3506-3508.

(21) McKnight, T. E.; Melechko, A. V.; Guillorn, M. A.; Merkulov, V. I.; Doktycz, M. J.; Culbertson, C. T.; Jacobson, S. C.; Lowndes, D. H.; Simpson, M. L. *Journal of Physical Chemistry B* **2003,** *107,* 10722-10728.

(22) Ye, Q.; Cassell, A.; Liu, H.; Chao, K.-J.; Han, J.; Meyyappan, M. *Nano Lett* **2004,** *4,* 1301-1305.

(23) Yu, Z.; McKnight, T. E.; Ericson, M. N.; Melechko, A. V.; Simpson, M. L.; Morrison, B. *Nano Lett* **2007,** *7,* 2188-2195.

(24) Koehne, J.; Chen, H.; Li, J.; Cassell, A. M.; Ye, Q.; Ng, H. T.; Han, J.; Meyyappan, M. *Nanotechnology* **2003,** *14,* 1239-1245.

(25) Li, J.; Cassell, A.; Delzeit, L.; Han, J.; Meyyappan, M. *J Phys Chem B* **2002,** *106,* 9299-9305.

(26) Guillorn, M. A.; Yang, X.; Melechko, A. V.; Hensley, D. K.; Hale, M. D.; Merkulov, V. I.; Simpson, M. L.; Baylor, L. R.; Gardner, W. L.; Lowndes, D. H. *J Vac Sci Technol B* **2004,** *22,* 35-39.

(27) Fletcher, B. L.; Hullander, E. D.; Melechko, A. V.; McKnight, T. E.; Klein, K. L.; Hensley, D. K.; Morrell, J. L.; Simpson, M. L.; Doktycz, M. J. *Nano Letters* **2004,** *4,* 1809-1814.

(28) Fletcher, B. L.; McKnight, T. E.; Fowlkes, J. D.; Allison, D. P.; Simpson, M. L.; Doktycz, M. J. *Synthetic Metals* **2007,** *157,* 282-289.

(29) Fletcher, B. L.; McKnight, T. E.; Melechko, A. V.; Hensley, D. K.; Thomas, D. K.; Ericson, M. N.; Simpson, M. L. *Advanced Materials* **2006,** *18,* 1689-+.

(30) Fletcher, B. L.; Retterer, S. T.; McKnight, T. E.; Melechko, A. V.; Fowlkes, J. D.; Simpson, M. L.; Doktycz, M. J. *ACS Nano* **2008,** *2,* 247-254.

(31) Milne, W. I.; Teo, K. B. K.; Chhowalla, M.; Arnaratunga, G. A. J.; Pribat, D.; Legagneux, P.; Pirio, G.; Binh, V. T.; Semet, V. *Current Applied Physics* **2002,** *2,* 509-513.

(32) Teo, K. B. K.; Chhowalla, M.; Amaratunga, G. A. J.; Milne, W. I.; Legagneux, P.; Pirio, G.; Gangloff, L.; Pribat, D.; Semet, V.; Binh, V. T.; Bruenger, W. H.; Eichholz, J.; Hanssen, H.; Friedrich, D.; Lee, S. B.; Hasko, D. G.; Ahmed, H. *J Vac Sci Technol B* **2003,** *21,* 693-697.

(33) Melechko, A. V.; McKnight, T. E.; Hensley, D. K.; Guillorn, M. A.; Borisevich, A. Y.; Merkulov, V. I.; Lowndes, D. H.; Simpson, M. L. *Nanotechnology* **2003,** *14,* 1029-1035.

(34) McKnight, T. E.; Melechko, A. V.; Austin, D. W.; Sims, T.; Guillorn, M. A.; Simpson, M. L. *Journal of Physical Chemistry B* **2004,** *108,* 7115-7125.

(35) Mann, D. G. J.; McKnight, T. E.; Melechko, A. V.; Simpson, M. L.; Sayler, G. S. *Biotechnology and Bioengineering* **2007,** *97,* 680-688.

(36) Melechko, A. V.; Desikan, R.; McKnight, T. E.; Klein, K. L.; Rack, P. D. *Journal of Physics D: Applied Physics* **2009,** *42,* 193001.

(37) Mann, D. G. J.; McKnight, T. E.; McPherson, J. T.; Hoyt, P. R.; Melechko, A. V.; Simpson, M. L.; Sayler, G. S. *ACS Nano* **2008,** *2,* 69-76.

(38) Klein, K. L.; Melechko, A. V.; Rack, P. D.; Fowlkes, J. D.; Meyer, H. M.; Simpson, M. L. *Carbon* **2005,** *43,* 1857-1863.

(39) McKnight, T. E.; Melechko, A. V.; Griffin, G. D.; Guillorn, M. A.; Merkulov, V. I.; Serna, F.; Hensley, D. K.; Doktycz, M. J.; Lowndes, D. H.; Simpson, M. L. *Nanotechnology* **2003,** *14,* 551-556.

(40) Silva, C. C. G.; Higa, O. Z.; Bressiani, J. C. *Mat Sci Eng C-Bio S* **2004,** *24,* 643-646.

(41) Peng, H. S.; Sun, X. M. *Chem Commun* **2009,** 1058-1060.

(42) Peng, H. S.; Sun, X. M. *Chem Phys Lett* **2009,** *471,* 103-105.

(43) McKnight, T. E.; Melechko, A. V.; Fletcher, B. L.; Jones, S. W.; Hensley, D. K.; Peckys, D. B.; Griffin, G. D.; Simpson, M. L.; Ericson, M. N. *Journal of Physical Chemistry B* **2006,** *110,* 15317-15327.

(44) McKnight, T. E.; Ericson, M. N.; Jones, S. W.; Melechko, A. V.; Simpson, M. L. *P Ann Int Ieee Embs* **2007,** 5381-5383.

(45) Wang, J. W.; Johnston-Peck, A. C.; Tracy, J. B. *Chem Mater* **2009,** *21,* 4462-4467.

(46) Sarac, M. F.; Anderson, B. D.; Pearce, R. C.; Railsback, J. G.; Hensley, D. K.; Melechko, A. V.; Tracy, J. B. *Submitted* **2012**.

(47) Deshpande, S. V.; Gulari, E.; Brown, S. W.; Rand, S. C. *Journal of Applied Physics* **1995,** *77,* 6534-6541.

(48) Melechko, A. V.; Pearce, R. C.; Hensley, D. K.; Simpson, M. L.; McKnight, T. E. *J. Phys. D-Appl. Phys.* **2011,** *44*.

(49) Koschwanez, J. H.; Carlson, R. H.; Meldrum, D. R. *Plos One* **2009,** *4*.

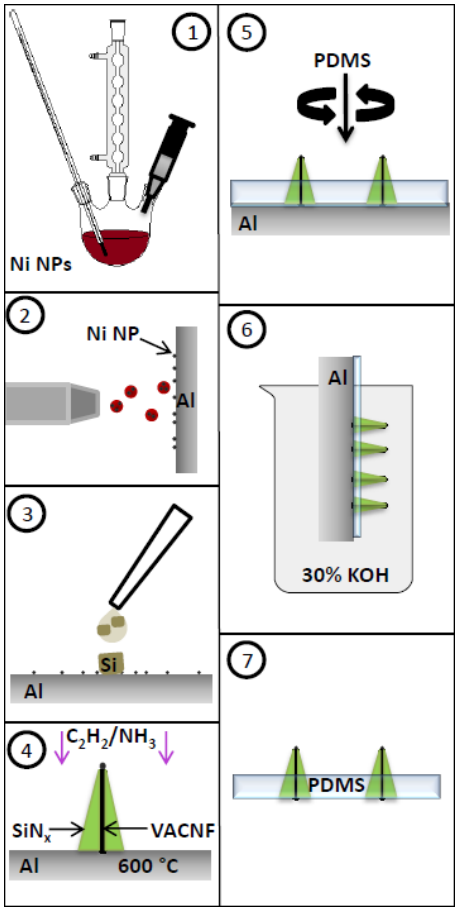

Figure 6.1: (1) Synthesis of 100 nm NiNPs. (2) Airbrushing of NiNPs dispersed in heptane onto an Al substrate followed by air drying. (3) Dropcasting of Si microparticles (1-3 μm in size) to provide a Si source for fiber coating. (4) VACNF growth by catalytic activity of the Ni NPs in PECVD from a mixture of acetylene and ammonia. A SiNx coating forms on the VACNFs as the Si is sputtered from the microparticles. (5) Spin casting of PDMS on top of the fiber array, followed by curing. (6) Dissolution of the Al substrate in 30% KOH at 80 °C. (7) The VACNF array remains aligned with the tips of the fibers exposed in a free-standing PDMS film.

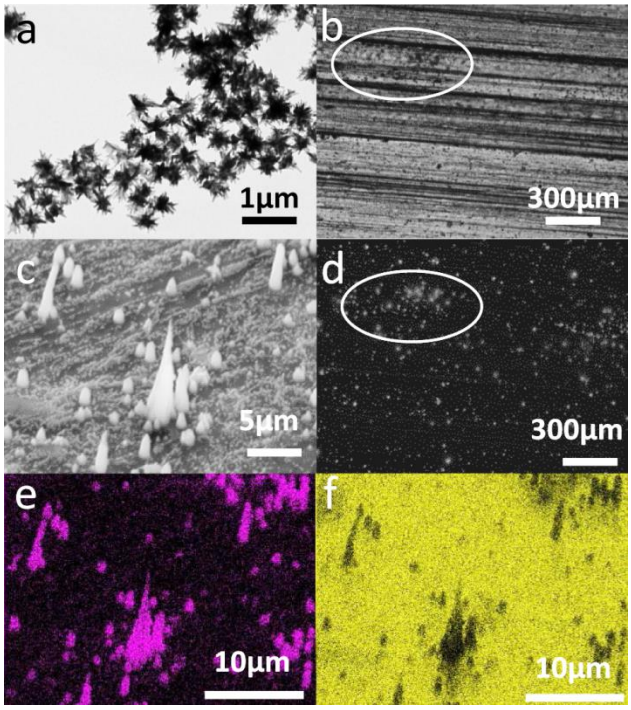

Figure 6.2: (a) Bright field TEM micrograph of chemically synthesized NiNPs; (b) optical micrograph of Al substrate after VACNF growth, circled area contains fibers; (c) secondary electron image of the substrate in (b); (d) fluorescence optical micrograph of the same area in (b) with a 360nm bandpass excitation filter cube and 410 nm illumination, circled area shows fiber fluorescence; (e) EDX map showing the location of silicon in the same region as panel (c); (f) EDX map showing aluminum in the same area as panel (c). Contrast has been enhanced for easier viewing

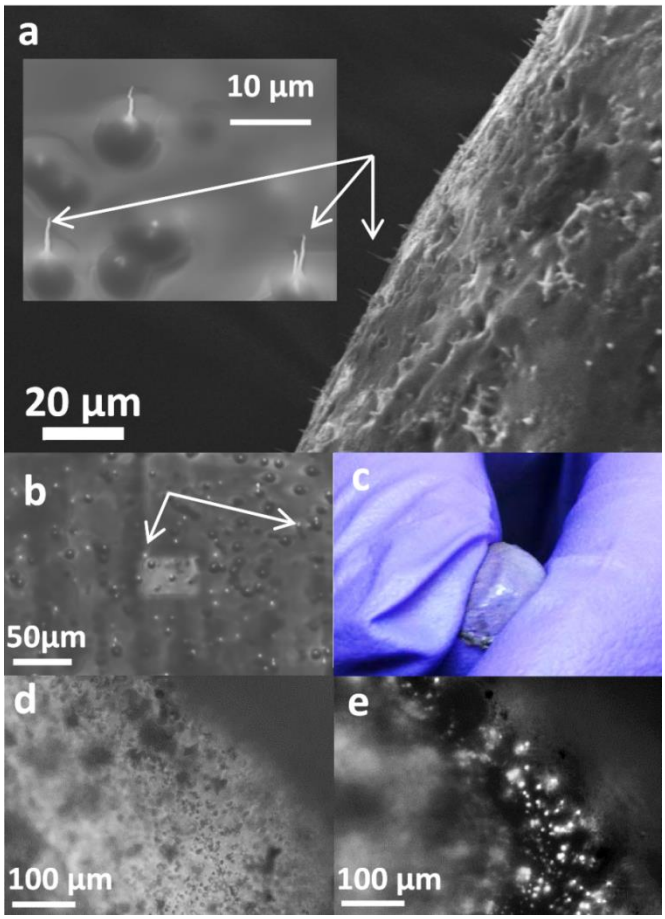

Figure 6.3: SEM micrographs of (a) of free standing PDMS film taken at a fold in the film showing protruding VACNFs, inset shows fibers on a planar area of the PDMS film, with a great deal of charging. Arrows denote fibers. (b) 30° tilted image of PDMS-coated VACNF array prior to KOH etch, arrows point to fibers protruding from PDMS film; (c) free-standing PDMS film with VACNF array stretched over a gloved finger; (d) transmission optical micrograph of free-standing PDMS film with an embedded VACNF array; (e) fluorescence optical micrograph of the same area of the film as in (d) under a 360nm bandpass excitation filter cube with 410 nm illumination.

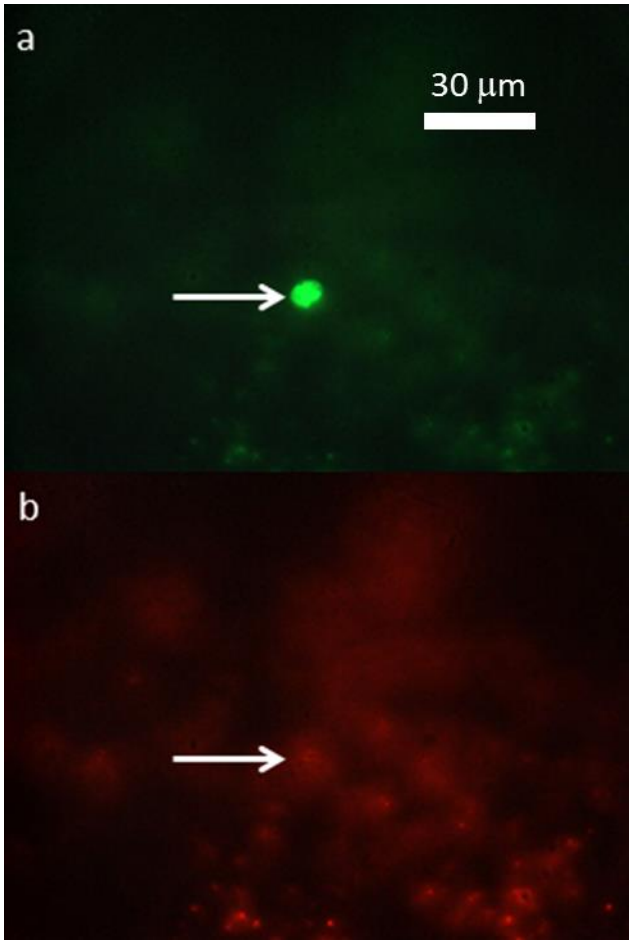

Figure 6.4: Fluorescence microscopy images of (a) a transfected cell expressing the Venus fluorescent protein using a YFP filter set that transmits fluorescence from both the Venus fluorescent protein and the VACNFs and (b) the same location with a TRITC filter, such that the Venus fluorescent protein is not excited, but the VACNFs emit red

Chapter 7 - Synthesizing Vertically Aligned Carbon Nanofibers from Air and Acetone

7.1 Introduction

One of the major roadblocks holding back development of many nanostructured devices is the prohibitive costs involved in their production. Vertically aligned carbon nanofibers (VACNFs) are of particular interest due to their extremely high aspect ratio, ease of chemical functionalization, electron transport characteristics, and ability to be deterministically synthesized.[1, 2, 3, 4] These properties lend themselves very well to VACNF coatings for various purposes such as anti-icing. However, limitations in VACNF synthesis make large scale coatings impractical. VACNF synthesis requires two process gases during dc plasma enhanced chemical vapor deposition (PECVD): a carbon source and an etchant source. Acetylene is most frequently used as the carbon gas, while ammonia is the most common etchant. These gases are expensive as well as hazardous. Due to the nature of these process gases, any synthesis of VACNFs must be performed in a contained system, which naturally limits the ability to cost effectively coat large surface areas with fibers. This chapter presents a feasibility study of using air and acetone (C_3H_6O) as the process gases for VACNF synthesis. In this work we replaced these two gases for the much cheaper and far less hazardous combination of acetone and air. In addition to being economically more viable, using this gas combination opens up the possibility of performing synthesis in atmosphere.

7.2 Experimental

The VACNFs were grown in a custom dc-PECVD chamber. The chamber is usually set up for growth using acetylene and ammonia for growth. For growth using air and ammonia some simple modifications were made. First, the mass flow controller (MFC) for ammonia was disconnected from the ammonia canister and opened to air. The MFC for acetylene was also disconnected from its canister and connected to a small cylinder containing acetone. Synthesis was carried out with 38sccm of acetone, 86sccm of air, at 0.4A, 4 Torr, and 700°C for 30 minutes.

Following growth, fibers were analyzed using a Zeiss Merlin scanning electron microscope (SEM). Elemental analysis was performed using a Bruker QUANTAX energy dispersive x-ray spectroscopy (EDS) system.

7.3 Results and Discussion

Initially, growth was attempted using ethanol instead of acetylene, as ethanol is even more prevalent. However, a sufficient flow rate for growth was not obtained, due to ethanol's low vapor pressure at room temperature. Acetone, however, has roughly four times as great a vapor pressure at room temperature than ethanol.[5]

After a period of parameterization, the fibers shown in **Figure 7.1** were obtained. This image shows the feasibility of growing fibers using a simple air-acetone process gas mixture. These fibers appear similar in morphology to those grown with the traditional gas mixture. The primary concern when switching to the gas mixture used here was the balance

of etching to deposition. With acetylene and ammonia isotropic etching stems from hydrogen, which is easily cracked from the parent molecules, while anisotropic etching occurs largely through nitrogen ions. With air and acetone, not only do you have a great deal of available hydrogen, but atomic nitrogen. This system opposed to the relatively easily cracked nitrogen in ammonia. An even further difference from acetylene and ammonia is the presence of an oxidant in the form of oxygen from both atomic oxygen and acetone.

The role of the oxygen and nitrogen is elucidated by EDS, shown in **Figure 7.2**. With acetylene and ammonia, it is very common to see a SiN_x coating form on the sidewalls of the VACNFs during synthesis.[6, 7, 8] In the previous chapter we discuss the deposition mechanism of this coating and its fluorescent properties. However, nitrogen from ammonia is relatively easily cracked compared to atomic nitrogen present in air. Here, a SiN_x coating does not form, most likely due to very low amounts of chemically available nitrogen. Instead, a SiO_2 coating appears to form on the VACNFs. The optical properties of this film have not yet been explored, but it is possible that Si nanoclusters form in a SiO_2 matrix on the VACNF sidewall, like they do in a SiN_x matrix. Fluorescent Si nanoclusters have previously been observed in SiO_2 matrixes.[9, 10] The deposition mechanism for SiO_2 is likely very similar to that proposed in the previous chapter for SiN_x, with excited hydrogen or oxygen reacting with the silicon substrate, becoming volatilized, and then redeposited onto the growing VACNF sidewall.

7.4 Conclusion

This is the first demonstration of VACNF growth using air and acetone. This demonstration shows the feasibility of using gases that are more economically viable as well as being the first step towards in-air VACNF coatings.

7.5 References

(1) Baker, S. E.; Colavita, P. E.; Tse, K. Y.; Hamers, R. J. *Chem Mater* **2006,** *18,* 4415-4422.

(2) Baker, S. E.; Tse, K. Y.; Lee, C. S.; Hamers, R. J. *Diam Relat Mater* **2006,** *15,* 433-439.

(3) Melechko, A. V.; Desikan, R.; McKnight, T. E.; Klein, K. L.; Rack, P. D. *Journal of Physics D: Applied Physics* **2009,** *42,* 193001.

(4) Melechko, A. V.; Merkulov, V. I.; McKnight, T. E.; Guillorn, M. A.; Klein, K. L.; Lowndes, D. H.; Simpson, M. L. *Journal of Applied Physics* **2005,** *97,* Artn 041301.

(5) Dean, J. A., McGraw-Hill: 1999.

(6) Guillorn, M. A.; Melechko, A. V.; Merkulov, V. I.; Ellis, E. D.; Britton, C. L.; Simpson, M. L.; Lowndes, D. H.; Baylor, L. R. *Applied Physics Letters* **2001,** *79,* 3506-3508.

(7) McKnight, T. E.; Melechko, A. V.; Austin, D. W.; Sims, T.; Guillorn, M. A.; Simpson, M. L. *Journal of Physical Chemistry B* **2004,** *108,* 7115-7125.

(8) Melechko, A. V.; McKnight, T. E.; Hensley, D. K.; Guillorn, M. A.; Borisevich, A. Y.; Merkulov, V. I.; Lowndes, D. H.; Simpson, M. L. *Nanotechnology* **2003,** *14,* 1029-1035.

(9) Min, K.; Shcheglov, K.; Yang, C.; Atwater, H. A.; Brongersma, M.; Polman, A. *Applied Physics Letters* **1996,** *69,* 2033-2035.

(10) Shimizu-Iwayama, T.; Hole, D. E.; Boyd, I. W. *Journal of Physics: Condensed Matter* **1999,** *11,* 6595.

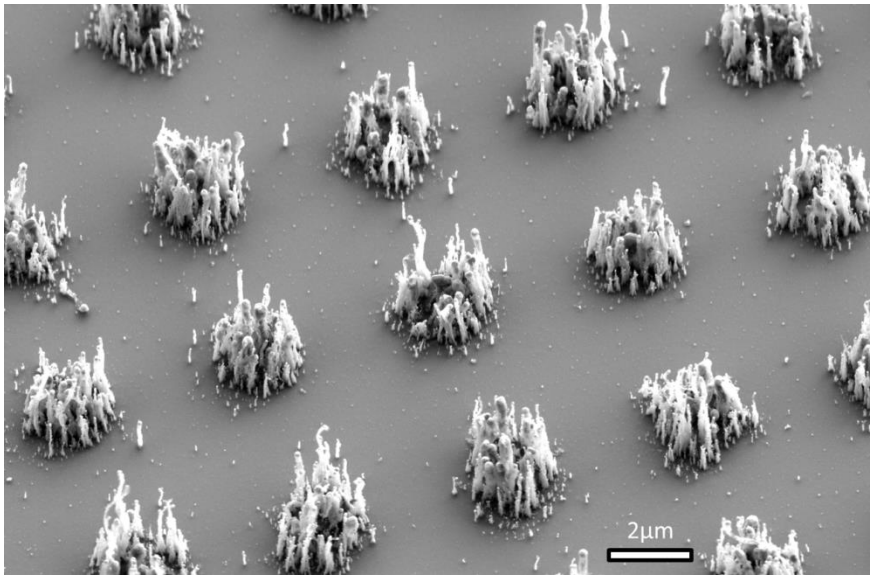

Figure 7.1: Scanning electron micrograph of VACNFs synthesized from nickel catalyst with an air and acetone gas mixture.

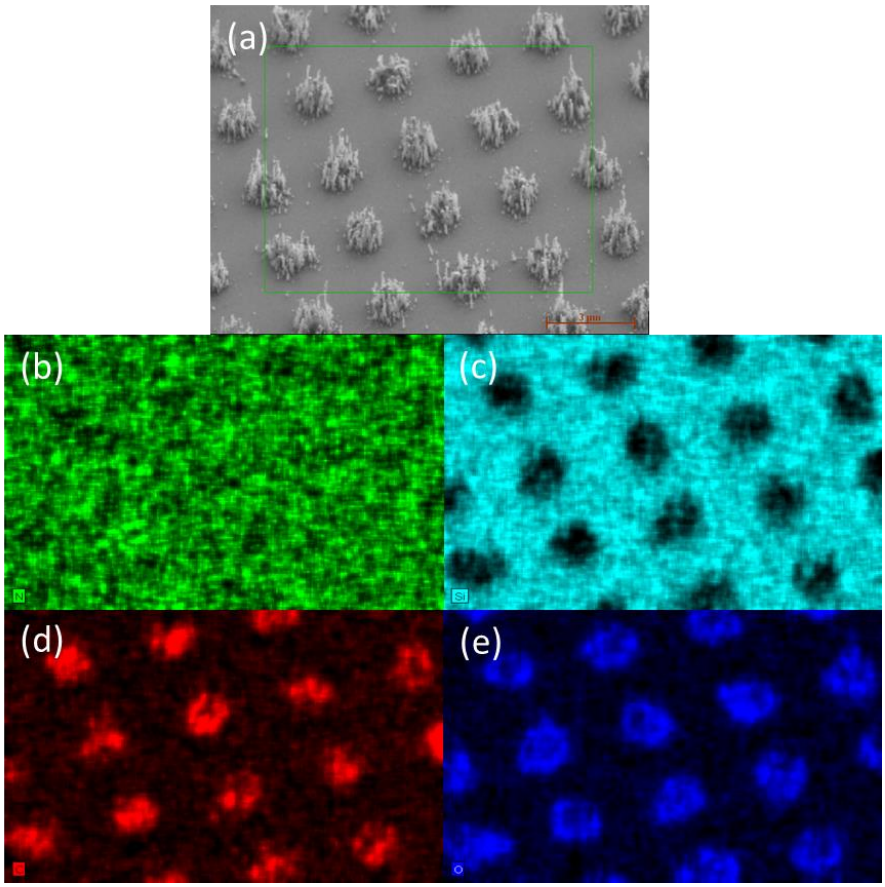

Figure 7.2: EDS maps of VACNFs grown from air an acetone process gases. (a) SEM image of VACNFs with green box indicating area that was scanned by EDS. (b) EDS map of nitrogen (c) Silicon (d) Carbon (e) Oxygen